Towards a demountable composite slab floor system

Alina Gritsenko

Towards a demountable composite slab floor system

by

Alina Gritsenko

in partial fulfillment of the requirements for the degree of

Master of Science
in Civil Engineering

at the Delft University of Technology,
to be defended publicly on Tuesday October 30, 2018 at 10:00 AM.

Supervisor:	Prof. dr.	M. Veljkovic	TU Delft
Thesis committee:	Dr. ir.	R. Abspoel	TU Delft
	Ir.	P. Lagendijk	TU Delft
	Ir.	M.P. Nijgh	TU Delft
	Ir.	J.P. den Hollander	Bouwen met Staal

An electronic version of this thesis is available at http://repository.tudelft.nl/.

TUDelft

Contents

List of Figures

List of Tables

Abstract

A composite slab consisting of in-situ casted reinforced concrete on profiled sheeting, which is connected to steel beams by shear connectors, is a common structural flooring system in office and multi-storey car park buildings. The headed welded studs, which are most widely used shear connectors, are inexpensive and easy to install because they can be welded to the steel beam through the profiled sheeting. A permanent link is created between the composite slab and steel beams leading to a time-consuming and expensive deconstruction process.

Various types of bolted shear connections, recently investigated by various researchers in Europe, Australia, and the USA, provide a demountable alternative for the flooring system. A part of this thesis describes the experimental study using a bolted shear connector consisting of an embedded bolt/coupler and external bolt, originally developed for a prefabricated solid concrete deck.

A full-scale composite beam was tested in two life cycles under total working loads up to 200kN in a 4-point bending set-up. In addition to bolted shear connectors, a timber joist was embedded in the composite slab over the web of the steel beam. After the first life cycle, the timber joist provides the cut edge of the slab. The experiment is used to model behavior of the composite beam in the first life cycle. The slab is then cut, demounted, re-assembled and tested again in the second life cycle. The load was applied up to 200kN and finally to failure. Multiple arrangements of shear connectors were investigated in second life cycle to analyze the performance of a prefabricated composite beam

Experience gained by the experiments on the composite beam in the first and the second life cycles is accompanied by FE analysis. Recommendations for practical use of the demountable composite floor system are proposed based on the experimental and numerical findings.

In addition, an investigation in the field of BIM (Building Information Modeling) functionality in the context of demountable structures was conducted. In order to identify the potential benefits of the BIM a case study of an in-situ casted car park was conducted. A number of software packages were used to conduct structural analysis, modeling and visualization of the construction sequence. As a result of this case study, valuable experience was gained on an application of BIM technologies for a design of demountable and reusable structures.

1

Preface

This thesis is submitted for the requirements of the Structural Engineering master track at the Faculty of Civil Engineering and Geo Sciences of the Delft University of Technology.

The assessment committee that supervised me during this research consists of prof. dr. M. Veljkovic, ir M.P. Nijgh, dr. ir. R. Abspoel, ir. P. Lagendijk from Delft University of Technology and ir. J.P. den Hollander from Bouwen met Staal. I would like to thank all committee members for their professional guidance, expertise and critical reviews that helped me to continuously improve my work.

I also would like to extend my gratitude to the TU Delft's steel laboratory staff for their professional work. Special thanks to Louis, John and Kevin.

Finally, I would like to thank my boyfriend and family for their support and encouragement. This journey would not have been possible without their patience.

<div align="right">

Alina Gritsenko
Delft, October 2018

</div>

<div align="right">

1

</div>

Introduction

1.1. Background

A composite slab consisting of in-situ casted reinforced concrete on profiled sheeting, which is connected to steel beams by shear connectors, is a common structural flooring system in office and multi-storey car park buildings. The steel decking can be either re-entrant or trapezoidal, as schematically represented on fig. 1.1. Composite profiled slabs have two major advantages. Firstly, the decking acts as a permanent and integral formwork during construction. Up to certain spans, depending on a type of sheeting and height of a slab, the construction loads, which consist mainly of wet concrete, can be supported without additional props. Moreover, because of small thickness of profiled sheeting, the shear studs can be welded directly though the decking to the flange of the beam. The second major advantage is that profiled sheeting acts as an external reinforcement at the final stage under live loading, thereby eliminating or greatly reducing the need for tensile reinforcement [32].

(a) Re-entrant decking   (b) Trapezoidal decking
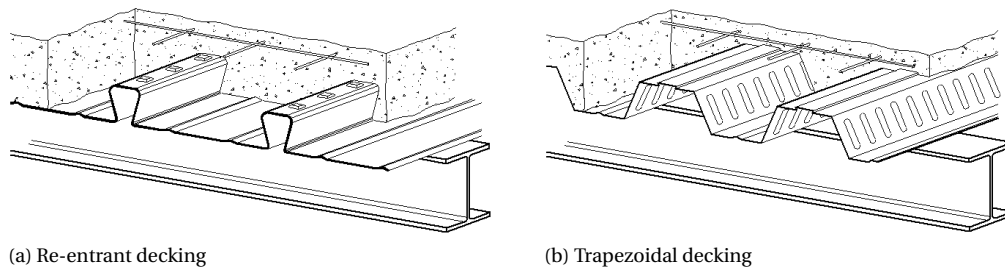
Figure 1.1: Composite profiled slab [1]

Composite slabs have a limited structural height and reduced weight compared to prismatic composite beams, which can reduce the foundation costs. The composite action, achieved by application of shear connectors, allows to efficiently use both steel and concrete and optimize the material usage.

The most widely used type of shear connector is the headed stud, because welded studs are inexpensive and rather easy to use in-situ because they can be welded to the steel beam through the metal sheeting. A permanent link is created between the composite slab and steel beams leading to rather time-consuming and expensive deconstruction process. Re-use of the whole structure or parts of it can greatly reduce material fabrication, disposal and as a result decrease energy consumption. Therefore, there is a need for a new type of shear connection system, which will allow demountable composite construction.

The design for de-construction should be addressed from different perspectives. It is of interest to promote and stimulate more structures which are designed for reuse, and therefore an appropriate platform or framework has to be developed to facilitate the design of such structures. A tool that looks promising for solving these issues is Building Information Modeling (BIM). BIM increasingly incorporates into nowadays design procedures of different type structures. There is a significant number of advantages that BIM can offer com-

pared to the conventional design practice. It allows BIM users to simplify such processes as design, fabrication, manufacturing, LCA analysis, construction scheduling, pricing and marketing and unify it into once single model.

In partnership with other universities, institutes and companies in the EU, a project called REDUCE (Reuse and demountability using steel structures and the circular economy) was carried out, which addresses the increasingly important requirements for design to facilitate reuse of structures, which is an important part of the circular economy initiative that underpins the sustainability and environmental impact of the built environment within the European Union.

1.2. Research questions

The aim of this thesis work is to investigate the load-deflection behavior of composite beams with demountable shear connectors in 4 point bending tests and investigate BIM capacity to provide practical tools which allow design of composite structures for deconstruction and reuse.

Following research question were defined in order to meet the goal of this research:

- What is the load-deflection behavior and initial stiffness of a composite beam tested in the experiments?

- What is the optimal degree of interaction and connector arrangement that lead to economic design of composite slab for office buildings?

- Is it possible to easily demount and successfully reuse composite decks with discontinuous reinforcement after 1st life cycle?

- How can BIM technology be used to facilitate and promote the design of structures ?

- How can BIM technology be used to create the construction simulation process?

1.3. Research methodology

Literature study is carried out to present theoretical background on composite slabs behavior and current state-of-art on demountable shear connectors.

Experimental test on a full scale beam are performed in order to assess the load-deflection behavior and initial stiffness of composite beams in first and second life cycles.

Finite Element models of beam tests are build, validated and calibrated with help of experimental results.

A parametric study is conducted in order to find an optimal number and arrangement of shear connectors for application in office buildings.

Review of BIM functionality is performed via literature review and personal testing of different software packages. Furthermore, the application of BIM capacity for construction visualization is demonstrated on an in-situ casted car park case study.

1.4. Outline of thesis

This thesis is organized in 7 chapters.

Chapter 1 provides a general introduction into the research objectives and methods.

Chapter 2 presents the current state-of-art for various demountable shear connectors, focuses on serviceability performance of composite beams and provides principles of Building Information Modeling.

Chapter 3 demonstrates in full the functionality of BIM on an example of an in-situ casted car park case study. This includes the concept design, verification of structural members and connections, modeling in BIM software and creation of construction sequence visualization.

Chapter 4 describes the experimental setups, testing program and presents the results of experimental work. The test results for bending moment resistance, mid-span deflections and initial stiffness are analyzed and compared with hand calculations.

Chapter 5 deals with the Finite Element (FE) modeling of beam tests. In this chapter the validation with analytical solutions as well as with experimental results is conducted.

In *Chapter 6* a parametric study is performed based on a developed FE model. An optimal number and arrangement of shear connectors is investigated.

Chapter 7 finalized the thesis by providing the main conclusions and recommendations for future work.

Literature review

2.1. Shear connectors

An essential component of a composite beam is the shear connection between the concrete slab and the steel beam. This connection is achieved by means of a mechanical shear connector, which transfers the forces between concrete and steel beam and also resists the vertical separation at the steel-concrete interface. A wide range of connectors has been developed in the past, however economic and ecological considerations keep motivating the development of new products.

2.1.1. Welded headed studs

The headed stud is the most widely used shear connector as it is inexpensive and rather easy to install using a welding gun, which is shown in a fig. 2.1. Numerous experimental and numerical studies conducted by various researchers [17, 18, 21, 34, 44] on performances of these shear connectors and well covered design rules in the design guides contribute to the wide application of these connector types in steel-concrete composite structures.

Figure 2.1: Welding of a stud connector using a welding gun

2.1.2. Bolted shear connectors

Comparing to the traditional welded headed studs connectors there is a limited research available in the field of demountable bolted connectors. This section provides an overview of various shear connections, namely, friction grip bolts, blind bolts, embedded shear connections with and without embedded nut(s) and bolted shear connection with coupler.

Friction grip bolts
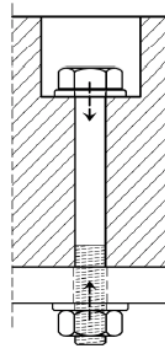
Figure 2.2: Bolted shear connector with friction grip bolt [37]

Friction grip bolts, shown in a figure 2.2, transfer shear forces through friction between concrete slab and steel beam flange interface. To accomplish the friction between concrete and steel a preloading of the bolts through the thickness of the concrete slab has to be made. This leads to high local compressive stresses in the concrete and as a result unfavorable loss of pretension due to trough thickness creep of concrete. Ataei et al. [9] conducted experiments in which precast concrete slabs were attached to a steel frame with semi-rigid bolted connections using high-strength friction grip bolts as the elements to provide the shear connection. This study showed that beams demonstrated very significant ductility and interface slips being developed and sustained during the testing. Similarly, Dallam [10] and Marshall et al. [23] investigated the behavior of high-strength grip bolts as composite shear connectors, however, an attempt to demount the shear connectors was not undertaken in any of above mentioned researches.

Blind bolts
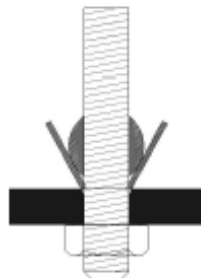
Figure 2.3: Blind bolt connection [43]

An application of blind bolts as shear connector in composite beams was investigated by Pathirana et al. [36] and Mirza et al. [24]. Full scale beam tests have shown that blind bolts exhibit comparable behavior to welded studs connectors in terms of stiffness, strength and ductility [36]. However, according to findings by Mirza et al. [24] blind bolts exhibit relatively brittle behavior compared to welded connectors.

Embedded bolted shear connectors with and without embedded nut(s)

Embedded bolted shear connectors are presented in figure 2.4. They transfer the shear force by bearing on the concrete and on the hole in the steel flange. Bolts without embedded nuts show lower initial stiffness compared to bolts with embedded nut. According to research conducted by Pavlović [37] experiments have shown that shear resistance and load-slip relation of welded headed studs and bolted shear connectors with

(a) without embed-ded nut

(b) with single em-bedded nut

(c) with double em-bedded nut
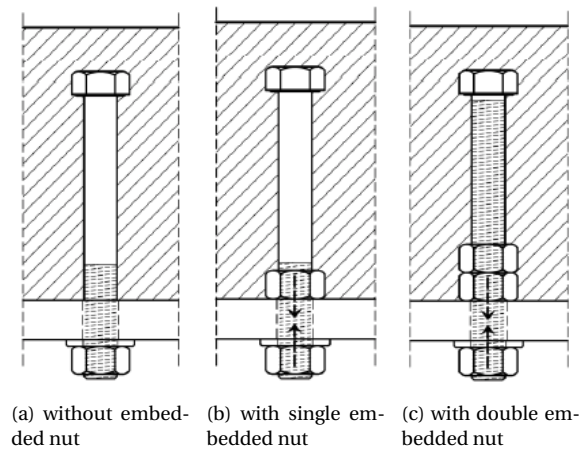
Figure 2.4: Bolted shear connector with embedded bolt [37]

single embedded nut are similar if they have the same dimensions. Moynihan and Allwood [25] tested 8.8 M20 bolted shear connector with embedded nut in composite beams tests with profiled sheeting. The experiments demonstrated that composite beam with bolted connectors performed in similar manner as beam with welded studs. Rehman et al. [40] conducted push-out and beam experiments using connectors machined from traditional studs with threads on a composite slab formed with profiled metal decking. The conclusion was that the behavior of demountable composite flooring system is very similar to conventional welded shear connector, additionally the composite beams were demounted and successfully reused after service load.

Bolted shear connector with coupler system

(a) Bolted shear connector with coupler [43]

(b) Novel bolted connector [45]
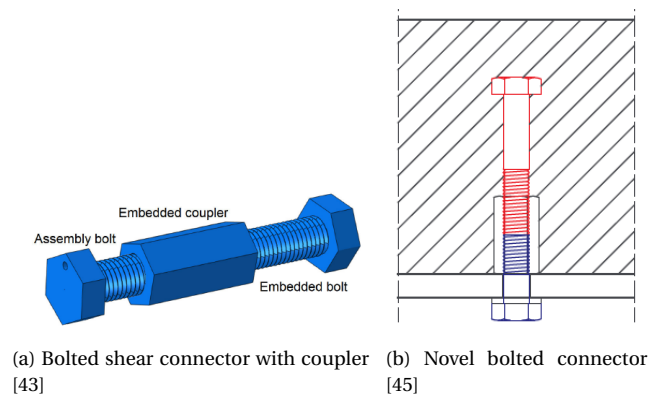
Figure 2.5: Demountable bolted shear connector

Bolted shear connector with embedded bolt, embedded coupler and external bolt is a novel demountable shear connector studied by von Arnim [43] and Nijgh et al. [30]. The advantage of this concept is that the dismantling process is facilitated and simplified by unscrewing the external bolt from underside of the steel flange.

Oversized holes
In order to facilitate the construction, deconstruction and re-assembly of demountable composite flooring systems oversized holes in the steel flange are required. However, the use of oversized holes results in initial slip between concrete deck and steel girder for shear connectors without structural pretension which leads to increased deflection and decreased vertical stiffness of the structure. In case of pretension of bolts, once the preloading and friction at the interface are overcome during the load, initial (residual) slip between the

components occurs. Results of experiments with bolted shear connectors in hole clearance of 1 mm showed that the ultimate shear resistance of the connectors is not influenced by the initial slip [38].

Injection bolts
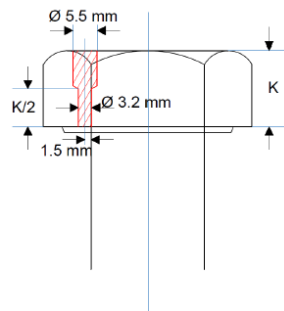
Figure 2.6: Injection bolt with injection nozzle according to Eurocode 3-1-1 [43]

Injection bolts can be used to obtain slip-resistant shear connections by injecting a two component epoxy resin into the free volume created by oversized holes within the connection, which was confirmed by Nijgh et al. [29] and Kozma et al. [20]. Injection bolts contain a small hole through the head as shown in a fig. 2.6. To ensure a complete filling of the bolt-to-hole clearance an escape path for air is required. When resin starts to come out of the air escape groove, it indicates a successful injection process. An excessive study was conducted by Nijgh [28] investigating the short- and long-term behaviour of injected bolted connections (IBCs) with oversize holes for various injection materials in context of demountable structures. Additionally, the epoxy resin can be reinforced with steel particles, which has shown to increase the connection stiffness and decrease the creep deformations. A hybrid homogenization method was applied to determine the mechanical properties of steel-reinforced resins by Nijgh et al. [31].

2.1.3. Other types of shear connectors

Apart from welded headed stud and bolted shear connector several other connection types were developed. Some of them are listed below:

- Channel shear connector
- Perfobond rib connector
- Shear connection by bonding and adherence
- Composite dowels

2.2. Serviceability performance of composite beams

The design of the beam for Serviceability Limit State (SLS) includes limitation of stresses, limitation of deflections, crack width control, vibrations and web breathing.

Deflections due to loading applied to the composite member should be calculated using elastic analysis taking into account effects from:

- cracking of concrete
- creep and shrinkage
- sequence of construction
- influence of local yielding of structural steel at internal supports
- influence of incomplete interaction

For composite beams with low degrees of shear connection, additional deflections occur due to slip in the shear connectors, which can be significant for beams with low degrees of shear connection.

2.2.1. Partial shear interaction in existing codes

Due to incomplete interaction, slip will occur between slab and beam which adds additional deflections at working load. The slip increases as the degree of shear connectors reduces. However, according to EN1994-1-1 [6], the effects of the incomplete interaction can be ignored given that following conditions are met:

- The design of the shear connection is in accordance with clause 6.6 of EN1994-1-1 [6]
- not less shear connectors are used than half the number for full shear connection
- the forces resulting from an elastic behavior and which act on the shear connectors in the serviceability limit state do not exceed P_{Rd}
- in case of a ribbed slab with ribs transverse to the beam, the height of the ribs does not exceed 80 mm.

Provided that the conditions mentioned above are fulfilled, the deflection of the composite beam can be calculated assuming rigid connection between steel beam and concrete slab as follows:

$$\delta = \frac{5 \cdot q \cdot L^4}{384 \cdot E_a I_{comp}} \tag{2.1}$$

$$I_{comp} = I_a + \frac{I_c}{n} + \frac{A_a A_c}{n A_a + A_c} \frac{(h + 2 h_p + h_c)^2}{4} \tag{2.2}$$

where:
  n = is the modular ratio of steel to concrete E_a / E_c
  h = is the elastic neutral axis depth of the steel section measured from the top of the steel section
  h_p = is the depth of the deck profile
  h_c = is the depth of the concrete over the deck profile

In clause 7.3.1(4) of the Dutch national annex to EN 1994-1-1 [7], a formula for the calculation of deflection in case of low degrees of shear interaction ($\eta < 0.5$) is provided.

For propped construction method:

$$\frac{\delta}{\delta_c} = 1 + 0.5(1 - \eta) \, (\frac{\delta_a}{\delta_c} - 1) \tag{2.3}$$

For un-propped construction method:

$$\frac{\delta}{\delta_c} = 1 + 0.3(1 - \eta) \, (\frac{\delta_a}{\delta_c} - 1) \tag{2.4}$$

where:
  δ_a = deflection of steel beam without concrete
  δ_c = deflection of composite beam assuming full composite action
  η = degree of shear interaction

Similarly, former BS 5950-3 [2] standard provides an approximative formula of additional deflection due to incomplete shear interaction.

For propped construction method:

$$w_{add} = 0.5 \cdot (1 - \eta) \cdot (w_s - w_c) \tag{2.5}$$

For un-propped construction method:

$$w_{add} = 0.3 \cdot (1 - \eta) \cdot (w_s - w_c) \tag{2.6}$$

where:
  w_s = deflection of steel beams at SLS
  w_c = deflection of composite beam assuming rigid connections (full composite action) at SLS

The ASCI Code [33] also offers a formula to modify second moment of area to take into account partial shear interaction, when determining the deflection of the beam.

$$I_{c,eff} = I_s + \eta^{0.5} \cdot (I_c - I_s) \tag{2.7}$$

where:

I_s = second moment of area of steel section

I_c = second moment of area of composite section assuming rigid connections (full composite action)

2.2.2. Analytical models for partial shear interaction

The first theory for the effects of partial shear connection on the design of composite beams was developed by Newmark et al. [27], in which a solution to a differential equation linking slip and deflection for beams with a single point load was presented. More study on behavior of composite beams with partial shear interaction was conducted by numerous researchers [16, 19, 35, 39]. In this section, two analytical models for the load-deflection behavior of a composite beam are presented:

Partial shear interaction: approach Girhammar

Girhammar [16] has proposed simplified analysis method for composite beams with interlayer slip. The analytical model of partially composite beam is based on Euler-Bernoulli beam theory, which neglects the effect of shear deformation. The beams are subjected only to transverse loading. Following assumptions are adopted:

- Relative slip can occur at the interface
- Discretely located shear connectors are regarded as continuous
- Materials behave elastically
- Curvature of components are assumed the same

A detailed background for the differential equation and general solution can be found in [15]. When knowing a solution for a given set of boundary conditions various internal actions can be formulated. Based on these results, the effective bending stiffness for partially composite beam can be calculated as follows:

$$EI_{c,eff} \approx (1 + \frac{\frac{EI_{inf}}{EI_0} - 1}{1 + (\frac{\alpha L}{\pi})^2})^{-1} \cdot EI_{inf} \tag{2.8}$$

$$EI_0 = E_a I_a + E_c I_c \tag{2.9}$$

$$EI_{inf} = EI_0 + \frac{E_a A_a \cdot E_c A_c}{E_a A_a + E_c A_c} r \tag{2.10}$$

$$\alpha = \sqrt{\frac{K r^2}{EI_0 (1 - \frac{EI_0}{EI_{inf}})}} \tag{2.11}$$

The exact and approximative (effective) deflection for the simply supported beam loaded with uniformly distributed load q are expressed as follows:

$$w_{exact} = w_{inf,max} + \frac{q}{\alpha^4 EI_{inf}} (\frac{EI_{inf}}{EI_0} - 1) (\frac{1}{\cosh(\frac{\alpha L}{2})} + \frac{\alpha^2 L^2}{8} - 1) \approx \frac{5qL^4}{384 EI_{c,eff}} \tag{2.12}$$

where:

r = distance between centroids of sub-elements

$K = \frac{k_{sc}}{s_{sc}}$ = Slip modulus of shear connection

k_{sc} = initial shear connector stiffness per deck rib

s_{sc} = spacing between shear connectors

EI_0 = bending stiffness of non-composite section

EI_{inf} = bending stiffness of fully composite beam

EA = axial stiffness

The interlayer slip between two sub-elements is given as follows:

$$u = \frac{V_{s,eff}}{K} \tag{2.13}$$

$$V_{s,eff} = (1 - \frac{EI_0}{EI_{c,eff}}) \frac{V}{r} \tag{2.14}$$

where:
  V = internal shear force acting on the whole cross-section

Additionally, internal stresses in the partially composite beam can be determined when knowing the effective bending stiffness. The maximum effective normal stresses in the individual sub-component from bending moment are given by:

$$\sigma_{i,eff,max} = [\mp (1 - \frac{EI_0}{EI_{c,eff}}) \frac{1}{A_i r} + \frac{E_i z_{i,max}}{EI_{c,eff}}] M \tag{2.15}$$

where:
  A_i = Cross sectional area of the ith component
  $z_{i,max}$ = Distance to the extreme fiber of the ith component

Alternatively, the maximum stresses can be written in a following way:

$$\sigma_{i,eff,max} = \mp \frac{E_i h_{na,i,eff}}{EI_{c,eff}} M \tag{2.16}$$

$$h_{na,i,eff} = r_i + (1 - \frac{EI_0}{EI_{c,eff}}) \frac{EI_{c,eff}}{E_i A_i r} \tag{2.17}$$

Partial shear interaction: approach Leskelä

An analytical approach for the load-deflection behavior of a composite beam with partial interaction has been given by Leskelä [22], which is presented here. The approach assumes linear-elastic behavior of both the steel and the concrete. There are several ways to determine the bending stiffness of composite section with full interaction. Leskelä [22] introduces composite stiffness parameter α_i, which is written as follows:

$$\alpha_i = \frac{r^2}{E_a I_a + E_c I_c} \frac{E_a A_a \cdot E_c A_c}{E_a A_a + E_c A_c} \tag{2.18}$$

With this parameter the bending stiffness of composite cross-section is expressed in simple form:

$$EI_{inf} = (1 + \alpha_i)(E_a I_a + E_c I_c) \tag{2.19}$$

Similarly to the bending stiffness of a fully composite beam, the effective bending stiffness of a beam with flexible shear connections can be written as follows:

$$EI_{c,eff} = (1 + \alpha_{i,eff})(E_a I_a + E_c I_c) \tag{2.20}$$

The composite stiffness parameter $\alpha_{i,eff}$ is dependent on the flexibility parameter r_δ :

$$\alpha_{i,eff} = \frac{1 - r_\delta}{1 + \alpha_i r_\delta} \alpha_i \tag{2.21}$$

For the situation of simply supported beam, where the loading is symmetrical with respect to the center of the span the following presentation of the flexibility parameter is valid:

$$r_\delta = \frac{\alpha_i (E_a I_a + E_c I_c)}{\alpha_i (E_a I_a + E_c I_c) + \mu_m K L^2 r^2 (\alpha_i + 1)} \tag{2.22}$$

The value of μ_m depends on a form of bending moment diagram :

- For uniformly distributed load $\mu_m = \frac{5}{16*3} \approx 0.104$
- For point load at midspan $\mu_m = \frac{1}{4*3} \approx 0.083$

Depending on the form of the bending moment diagram $1/12 = 0.083 < \mu_m < 5/48 = 0.104$, that means that the variability is rather limited and therefore all forms of load distributions may be approximated by $\mu_m \approx 0.1$.

The flexibility parameter r_δ is defined as the ratio between the end-slip with flexible shear connection and the maximum end slip without shear connection. Therefore, the end slip with flexible shear connection then can be described according to equation 2.23.

$$r_\delta = \frac{s_e}{s_{e,max}} \qquad (2.23)$$

where:
s_e = end slip with flexible shear connection
$s_{e,max}$ = maximum end slip without shear connection

The maximum end slip without shear connection is defined according to the equation 2.24.

$$s_{e,max} = \frac{A_m \cdot r}{E_a I_a + E_c I_c} \qquad (2.24)$$

Where A_m is the area under the bending moment diagram between maximum moment and the point of zero moment, as shown in a fig. 2.7.
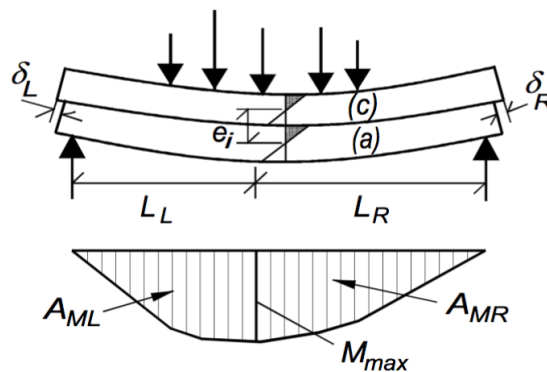
Figure 2.7: End slip in a member without shear connection [22]

Therefore the end slip between two components for the beam of length L with uniformly distributed load q can be expressed as follows:

$$s_e = \frac{qL^3}{24} \frac{r \cdot \alpha_i}{\alpha_i(E_a I_a + E_c I_c) + \mu_m K L^2 r^2(\alpha_i + 1)} \qquad (2.25)$$

Whereas for the beam with two point loads P at the distance a from the supports the expression for the end slip becomes as follows:

$$s_e = P \cdot a \cdot (L/2 - a/2) \cdot \frac{r \cdot \alpha_i}{\alpha_i(E_a I_a + E_c I_c) + \mu_m K L^2 r^2(\alpha_i + 1)} \qquad (2.26)$$

2.3. Plastic bending moment resistance of composite beams

The plastic design of composite beams is based on the development of idealized rectangular stress blocks in the steel section and in the concrete slab. It is simple and efficient structural analysis in terms of large resistances. In order to apply the rigid plastic design to composite beams a number of requirements has to be

fulfilled. The effective composite cross-section must be of Class 1 or 2 according to EN1994-1-1 clause 6.2.1.1. Shear connectors have to be classified as ductile, with characteristic displacement capacity larger than 6mm. Requirements for minimum degree of shear connection have to be satisfied in order to avoid brittle failure behavior.

The plastic bending resistance depends on the degree of shear connection. Full shear connection is achieved when the increase of the number of studs does not further increase the bending resistance. The bending resistance is then calculated from the plastic stress distribution as shown in a figure 2.8.
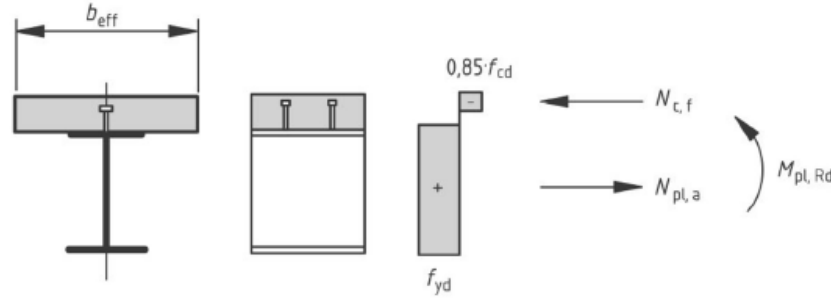
Figure 2.8: Plastic stress distributions in a composite beam for full shear connection [6]

However, for the composite slabs, typically a partial shear interaction is accomplished due to a limited number of ribs provided by a metal decking. In this case, the compression force in the concrete is determined by the shear resistance of the studs. The corresponding plastic stress distribution in the steel section is obtained from the equilibrium of axial forces. Two cases for the bending resistance can be distinguished based on a position of a plastic neutral axis as shown below:

Neutral axis in the steel flange

The stress distribution in a composite beam for partial interaction with neutral axis in steel flange is shown in a figure 2.9.

Neutral plastic axis is located in the steel flange i following condition is satisfied: $n \cdot P_{Rd} > h_w t_w f_{yd}$
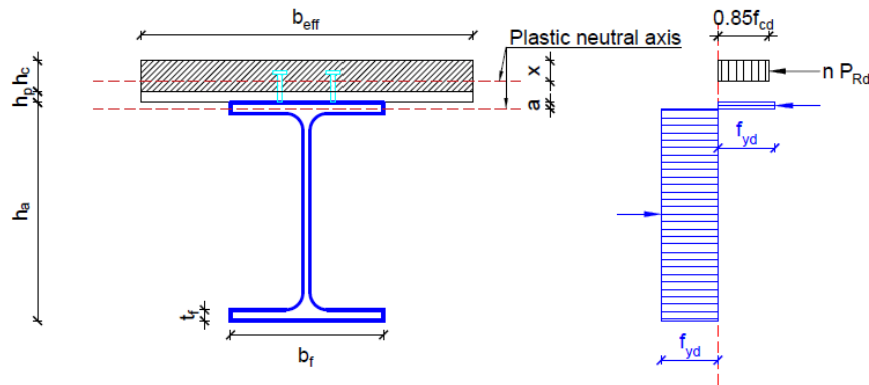
Figure 2.9: Neutral axis in steel flange for partial shear interaction [13]

$$x_c = \frac{n \cdot P_{Rd}}{0.85 \cdot b_{eff} \cdot f_{cd}} \qquad (2.27)$$

$$a = \frac{A_a \cdot f_{yd} - n \cdot P_{Rd}}{2 \cdot b_f \cdot f_{yd}} \qquad (2.28)$$

$$M_{Red,Rd} = n \cdot P_{Rd} \left(\frac{h_a}{2} + h_p + h_c - \frac{x_c}{2} \right) + \frac{N_a - n \cdot P_{Rd}}{2} (h_a - a) \tag{2.29}$$

Neutral axis in the steel web

Otherwise, if $n \cdot P_{Rd} < h_w t_w f_{yd}$, the neutral plastic axis is located in the steel web and the stress distribution is shown on the figure 2.10.
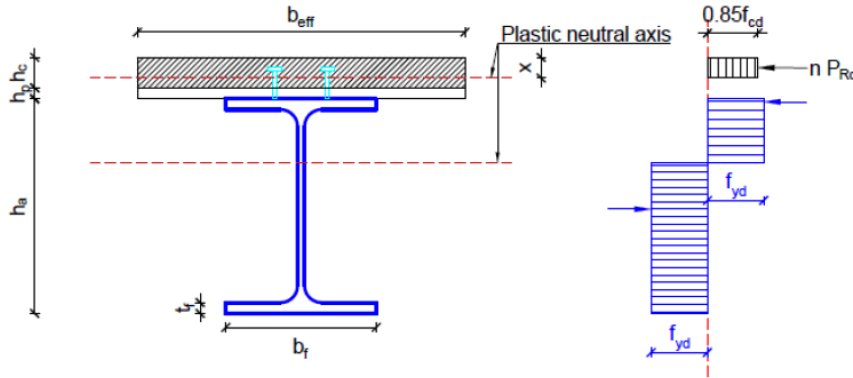
Figure 2.10: Neutral axis in steel web for partial shear interaction [13]

$$M_{Red,Rd} = n \cdot P_{Rd} \left(\frac{h_a}{2} + h_p + h_c - \frac{x_c}{2} \right) + W_{a,pl} f_{yd} - \frac{(n \cdot P_{Rd})^2}{4 t_w f_{yd}} \tag{2.30}$$

The dependency of bending resistance in terms of degree of shear connection can be described the convex curve ABC depicted in a figure 2.11.
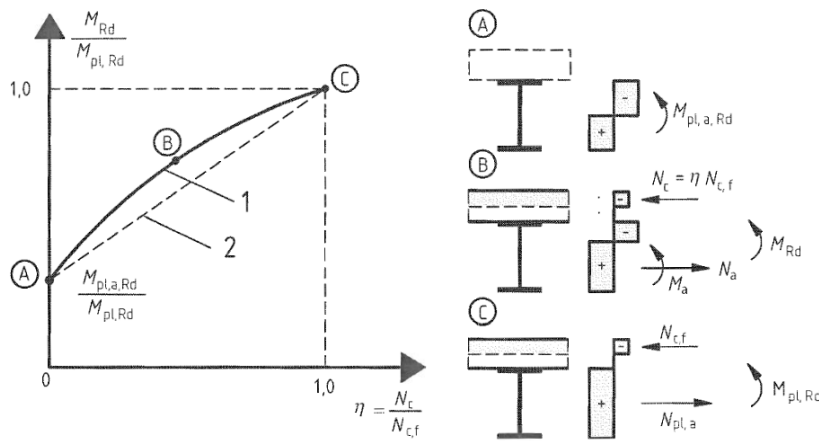
Key

1 plastic theory

2 simplified method

Figure 2.11: Relationship between M_{Rd} and N_c (for ductile connectors) [6]

Alternatively NEN 1994-1-1[6] allows a simplified conservative approach to determine the plastic bending resistance with partial shear interaction based on linear interpolation, as shown with line 2 on figure 2.11.

$$M_{Rd} = M_{pl.a.Rd} + (M_{pl.Rd} - M_{pl.a.Rd}) \cdot \eta \tag{2.31}$$

2.4. Building Information Modeling

2.4.1. BIM definitions and principles

BIM or Building Information Modeling aims to simplify the design, execution and operation of a building or renovation project. BIM is a "modeling technology and associated set of processes to produce, communicate and analyze building models"[11]. According to ISO [12] it is defined as follows: "use of a shared digital representation of a built object to facilitate design, construction and operation processes to form a reliable basis for decisions". In principle that means that BIM is a process of modeling and visualizing a structure in 3D as a catalog of objects positioned in space and described by their properties.

Created digital model should support following functionalities:

- automatic creation of scale drawings (plans, cross sections, facades etc.) and views without any "re-drawing"
- the automatic production of various measurements and the generation of bills of quantities
- the capability of combining different models (e.g. the combination of architecture and engineering models)

It is possible to add additional information, which can be regarded as a "adding new dimensions" to the 3D model:

- 4D (time-related information) to assist with planning
- 5D (prices and costs) to manage information about bills of quantities and associated costs
- 6D (project life cycle maintenance information) to manage facilities and assets

2.4.2. BIM roles

In order for the BIM concept to function efficiently, a particular organizational structure of different actors has to be established. As shown on fig. 2.12 client and design-construction teams are distinguished.
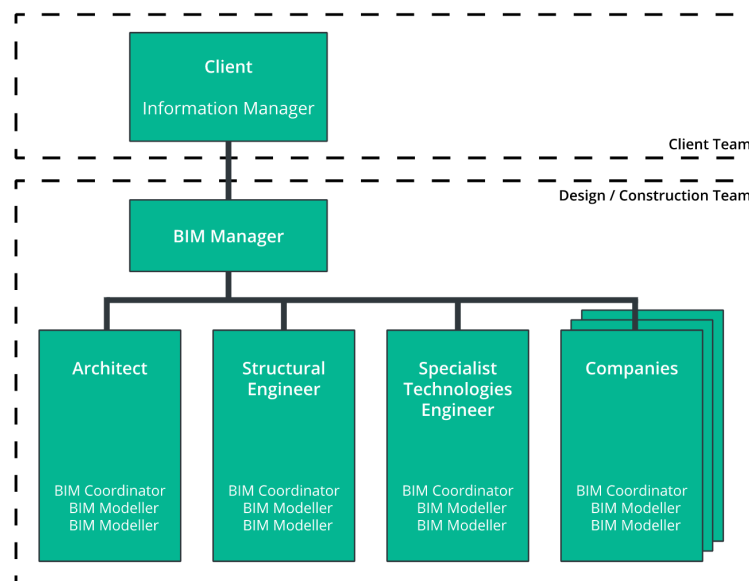
Figure 2.12: Standard organization chart

On the clients side, **information manager** is responsible for formalization of requirements.

On the design-construction side, **BIM modeler** is responsible for creation of a geometrically accurate model, modeler is fully trained to use 3D design software tools such as Revit, Archicad, Allplan, etc.

The **BIM coordinator** is responsible for supervising the BIM modelers in their work, checking the accuracy of models. This role combines both technical and managerial skills.

The **BIM manager** compiles the project's "BIM Execution Plan" which governs the project while complying with the client's requirements. When obtaining the deliverables from the various BIM coordinators, manager has to control that they comply with the plan. The BIM manager's role is different from that of project manager: this is not a decision-making role but rather one that involves audit and advice. However, BIM managers must have experience of building projects as a whole so that they understand how the different phases work and fit together.

2.4.3. Industry Foundation Classes

IFC (Industry Foundation Classes) format is an exchange format that aims to be universal so that it is possible to exchange and work on models, regardless which modeling software was used, it ensures interoperability between software packages, making it possible to universally describe the "elements".

2.4.4. Modeling and data processing software

In order to create a digital model, appropriate modeling software has to be used which not only produces 3D drawings, but which, most importantly, identifies and characterizes created objects. There are many software packages available on the market today, some of them are listed below:

- Autodesk Revit Structure
- Tekla Structures
- Nemetschek Allplan
- Nemetschek Scia

In general, they offer equivalent functionalities, however certain features might differ from one package to another. In addition to these modeling software packages, there are other tools in which BIM data can be manipulated, whether for clash detection, calculations, cost estimation, etc. One of the examples is Autodesk Navisworks. Using BIM does not rule out using 2D design, especially when creating special details. However, attention has to drawn to how is this 2D design is included into the 3D model. A link has to be maintained between BIM model and 2D drawing software, such that the alternation in drawing software would result in automatic changes in 3D model.

2.4.5. BIM in context of demountable structures

In the study conducted by Akinade et al. [8] BIM-based approaches were discussed in the context of Design for Deconstruction (DfD) tools. A number of interviews with professionals who have used BIM on their projects were conducted to identify the essential functionalities for a BIM-based deconstruction tool. The focus was given to the improved collaboration among stakeholders, visualization of deconstruction process, identification of recoverable materials, deconstruction plan development, performance analysis, improved building life cycle management and interoperability with existing BIM software.

BIM implementation provides more than a 3D computer modeling and visualization process, it gives a possibility to embed additional information from the early planning stage. This distinguishing feature of building life cycle information accumulation makes BIM applicable to construction for deconstruction concept. If stored properly, the information on building requirements, planning, design, construction, maintenance history and modifications can be collected and accessed at the end of life of buildings. However, inaccurate data, poor model update and maintenance may affect the quality of the model and lead to poor decision making process.

Another functionality of BIM that promotes its wide application is the ability to simulate building performances such as cost estimation and energy consumption. Despite the benefits of building performance analysis and the environmental/economic impacts, none of the existing BIM software has capabilities for end of life waste performance analysis.

2.5. Summary

The alternative to a headed welded stud shear connectors was discusses in this chapter. The main focus is given to the bolted shear connector and serviceability performance of the composite beams with flexible shear connectors as the main subject of this thesis. It has been demonstrated that a limited research is available in the field of demountable bolted connectors. Very few experimental studies were conducted on beam tests with bolted shear connectors to investigate the demountability and possibility of future reuse of the composite floor system.

Additionally an overview of Building Information Modeling principles is given. The available software packages and organization of the work flow between different actors is presented. A special attention is drawn to the application of the BIM functionalities in the context of demountable structures. It was shown that BIM has number of advantages that facilitate the design process of a structure. However, for a successful application of BIM tools for the design for deconstruction a number of issues has to be overcome, which involve improved collaboration among stakeholders, visualization of deconstruction process, identification of recoverable materials, deconstruction plan development, performance analysis, improved building life cycle management and interoperability with existing BIM software.

Case study cast in-situ multi-storey car park building

One of the goals of this thesis is to study the capability and functionality of BIM technology in the context of demountable structures, making a focus on the visualization of construction process. This chapter demonstrates the BIM visualization capacity on an example of case study.

3.1. Introduction

An in-situ casted car park is designed as a 3 story building, which is able to accommodate roughly 200 cars. An artistic impression is illustrated in the figure 3.1.
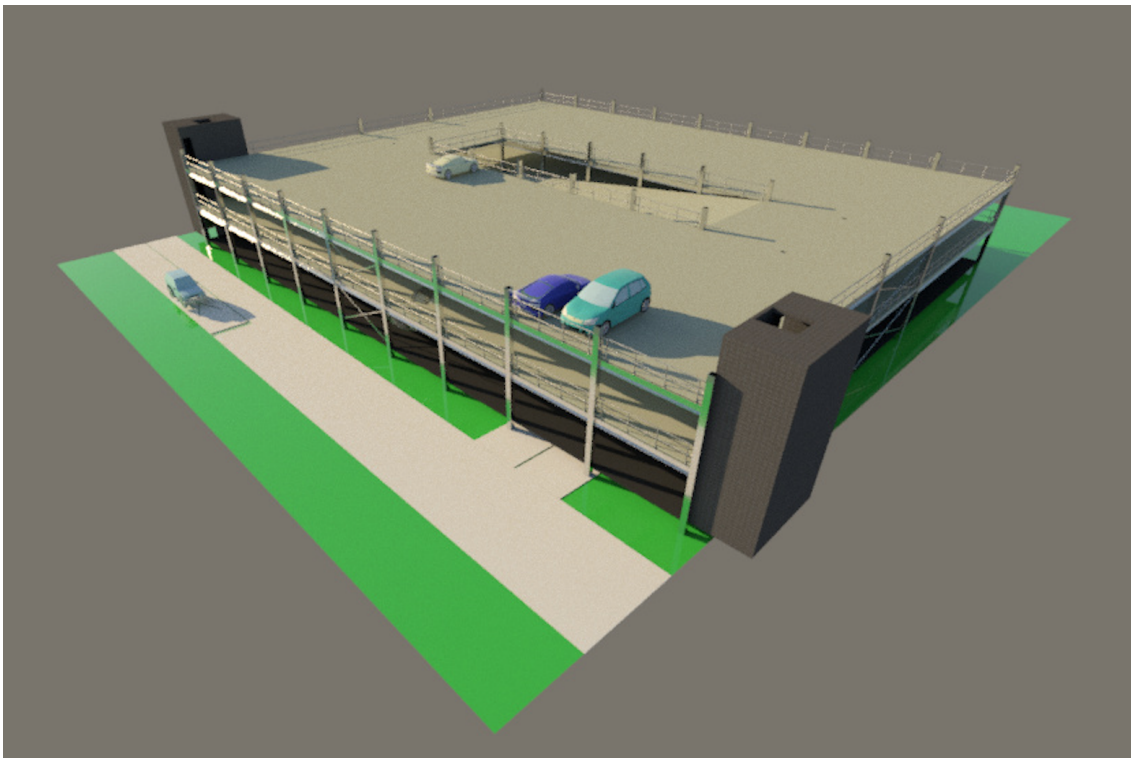
Figure 3.1: 3D impression of a car park
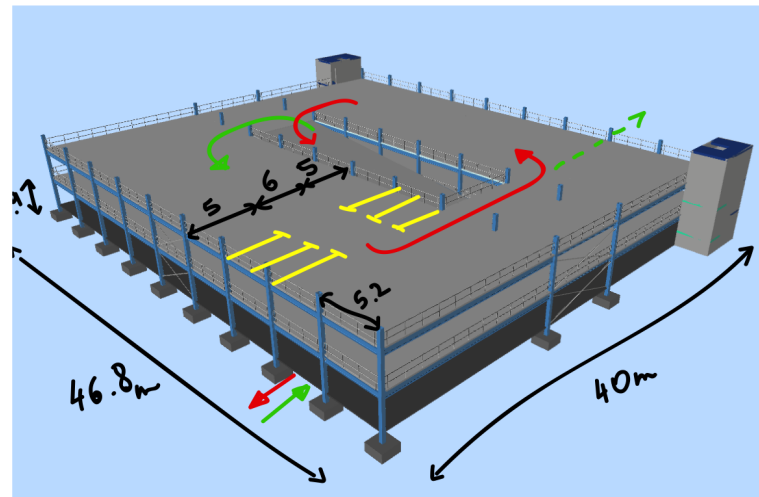
Figure 3.2: Car park concept
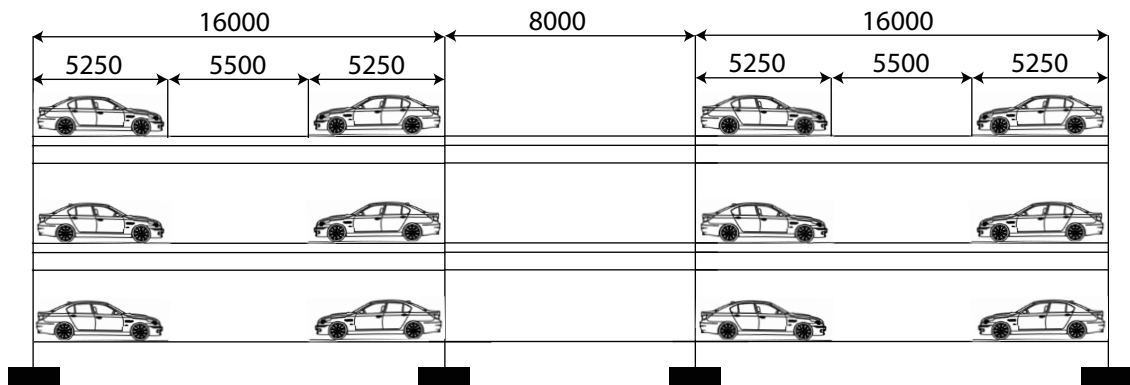
Figure 3.3: Layout of the car park

3.1.1. Goal and scope of the case study

The objective of this case study is to investigate the capacity and functionality of BIM in a context of demountable structures on an example of a car park project. In particular, the main focus is concentrated on an extension of 3D model to 4D, by adding the construction sequence. This includes a concept design, verification of structural members, 3D modeling and animating the construction sequence. Finally, a comparison is made between the prefabricated car park and the in-situ casted car park construction sequence.

3.2. Design description

3.2.1. Geometry

The car park building contains 3 storeys, it is 40 meters wide, 46.8 meters long and each storey is 2.9 meters. The traffic circulation and location of parking spots is shown in a fig. 3.2. It is chosen to make one way circulation with ramp placed in the middle of the structure. The spacing between columns is 5.2 meters, which is the optimal length needed to place the safety rails, which can be attached to the columns. The car parking spots are 2.6m wide and 5m long, which created 6m wide lane for cars circulation. The car park consists out of 3 segments: 2 side segments, where the parking spots are located and a middle one, where the ramp is placed, as illustrated in the figure 3.3.

Most of the structural elements used in the car park are designed as simply supported beams with pinned connections. This is a rather simple and cost effective solution, which is favorable for rapid execution and demountability.

3.2.2. Loads

Variable load according to EC 1991 1991-1-1 [4] category F (traffic areas with vehicle weights ≤ 30kN) is taken as 2.5kN/m^2. In addition an extra variable load of 0.5kN/m^2 is taken into account. Therefore the total characteristic live load is

$$Q_{live} = 3.0kN/m^2.$$

Characteristic snow load on the ground for Netherlands (any location) according to Dutch national annex 1991-1-3 [5] is $s_k = 0.7kN/m^2$. The design snow load on the structure is $s_d = s_k \cdot \mu = 0.7 \cdot 0.8 = 0.56kN/m^2$.

Characteristic wind speed on a structure for the wind zone II in the Netherlands is $v_{b,0} = 27m/s$

3.2.3. Load combinations

Following load combinations were investigated according to Dutch national annex of EN 1990 [3]:

$$1.2G + 1.5Q_{Live}$$

$$1.2G + 1.5Q_{Snow} + 1.5 \cdot 0.7Q_{Live}$$

$$1.2G + 1.5Q_{Wind} + 1.5 \cdot 0.7Q_{Live}$$

3.3. Individual member verifications

In order to obtain internal forces and moments for all elements of the car park and for all load combinations an FEM analysis was conducted with help of Autodesk Robot structural analysis program. The designed model is illustrated in a fig. 3.4

The structure was analyzed according to first order analysis with individual member check, using the equivalent buckling length. This method gives a conservative prediction for the column resistance.

Detailed verification of structural elements as well as design and verification of connections is provided in the annex B.

3.4. Construction simulation

In order to create a 3D model and a construction simulation process of a multi-storey car park, at first, a right choice for software packages has to be made. In the framework of this thesis a number of BIM programs were investigated and tested and an appropriate choice was made based on requirements and specifics of the project.

3.4.1. Structural analysis software

A concept design of a structure had is developed at first by choosing the layout of a car-park, its capacity, number of floors, the global dimensions and sizes of structural elements. When this phase is over, the structural analysis has to be conducted.

For the multi-storey car park simply supported beams and pinned connections are mainly used. In order to conduct structural analysis Robot Structural Analysis by Autodesk was used. The advantage of this program is that it is quiet intuitive and user friendly. It allows to determine internal forces in the structure, verify the members, optimize their size and verify certain types of connections. The example of the car park model in Robot Structural Analysis is depicted in a fig. 3.4.

The disadvantage of this program is that the created model can not be linked or integrated with BIM software. And therefore, the entire model has to be re-drawn again in an appropriate modeling software. An alternative solution to Robot Structural Analysis could be program called SCIA developed by Nementschek group, as it has an option of IFC export.
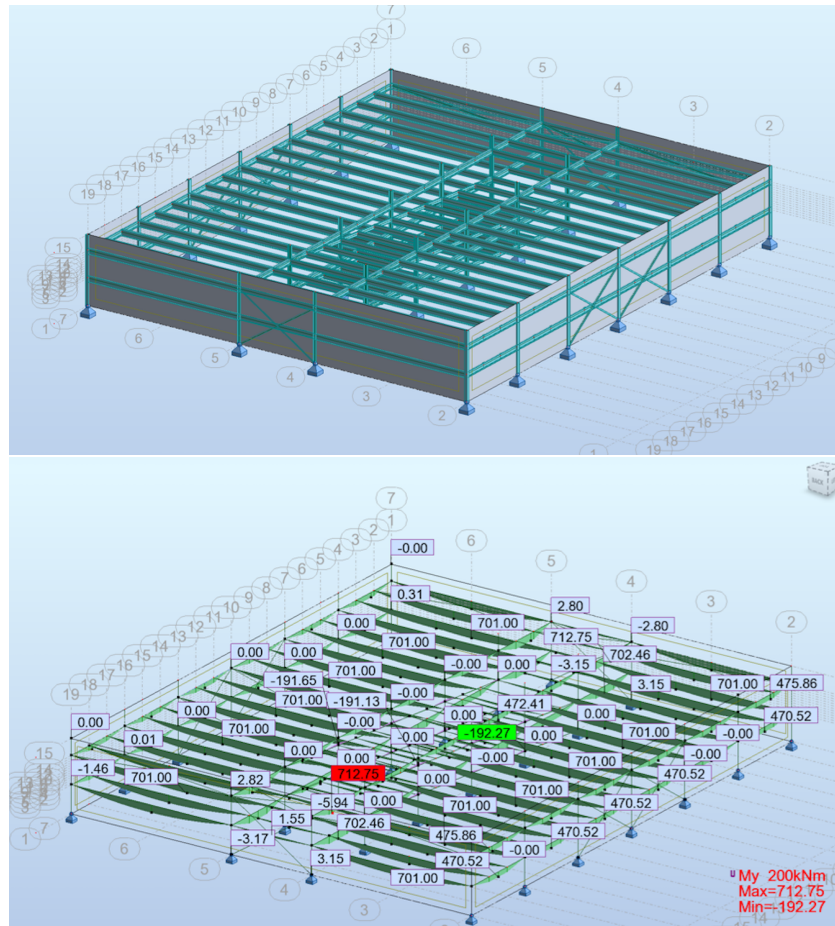
Figure 3.4: Autodesk Robot Structural Analysis

3.4.2. Modeling software

Since the case study structure is predominately steel, a choice for Tekla Structures by Trimble is more appropriate. This software has a wide range of integrated structural details, it is easy to apply and modify them to a structure. However, for 'customized' details, which are not part of Tekla in-build library, it may get challenging to model.

Two other programs, namely, Autodesk Revit and Autodesk Inventor, were investigated. Inventor has a great advantage that it provides absolute freedom to model any shape, size and material. However the generated IFC file does not meet required expectations, as it does not differentiate different members and considers whole structure as one single entity. Revit, on the other hand, fits very well into BIM concept and meets the requirements. It is rather good software for both structural and modeling purposes. However, for the particular application, such as composite car park, Tekla has the most capacity to model the complexity of the structure, including shear studs. Figure 3.5 depicts the car park 3D model created in Tekla structures.

3.4.3. Animation software

In order to create construction sequence simulation an additional software has to be used, which allows further manipulations of 3D model. Navisworks manage developed by Autodesk provides a quiet good platform to review the 3D model and extend it to 5D, by animating the construction and adding pricing analysis. This software does not include any modeling possibilities, user can only import existing models from other programs and perform clash detection analysis.

In the fig. 3.6 the path for the construction visualization is displayed. However, it does not mean that it is the only way to reach the given objective. The choice for the modeling program highly depends on a type of
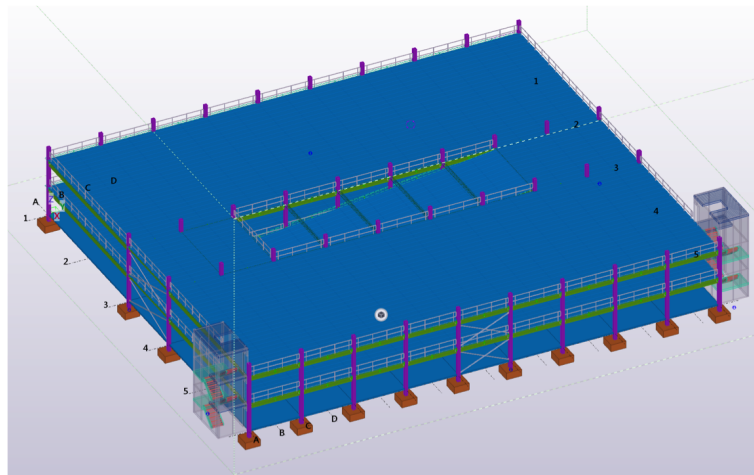
Figure 3.5: Tekla structures

structure and the level of complexity to show during animation. What can be concluded is that Navisworks Manage is a very good tool for performing the animation and recommended for use.
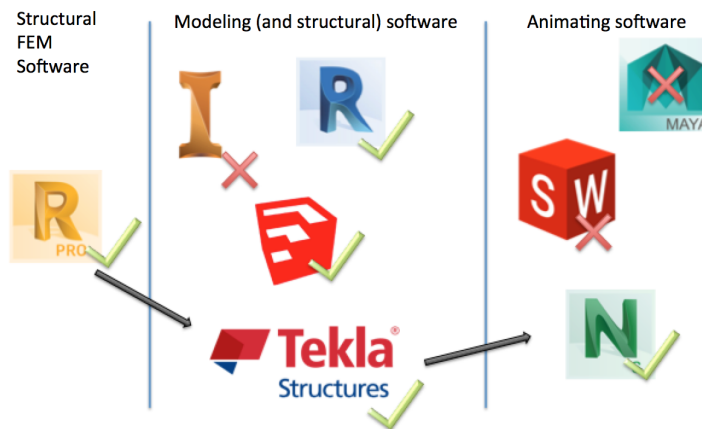
Figure 3.6: Construction visualization work-flow

3.5. Conclusions

A full structural analysis was conducted for a multi-storey building. Verification of structural elements and connections was performed. Following programs were selected for the creation of the construction simulation after conduction of the research and testing of different software packages: Robot Structural Analysis byAutodesk, Tekla structures by Trimble and Navisworks by Autodesk.

As a result of this case study, two visualizations were created. First animation of the car park can be found via link: `https://youtu.be/qcwy7q-Z1i4`. It demonstrates a detailed procedure of car park assembly, including the connections between steel members as well as the shear studs in composite beams. This visualization provides a clear image and understanding of the construction procedure.

One of the objectives was to draw a visual comparison between an cast in-situ multi-storey car park and a prefabricated car park. For that reason second visualization was created, which can be found via link `https://youtu.be/T65MyB48gOY`. This animation demonstrates the differences in construction method and time between casted in-situ and prefabricated structures.

According to the knowledge gaps identified during the literature research on BIM application for the design for deconstruction and reuse, a number of suggestions and future research directions were identified:

- In order to ensure the life cycle data collection of the building, an appropriate data structure system has to be introduced in the BIM software interface.
- In addition, the responsibility and roles of various actors have to be clearly identified for ensuring the maintenance of the developed model and accumulation of information regarding the maintenance and modifications.
- To support the identification of recoverable materials quantities, the elements of BIM model can be enriched with additional information on material types or other specifications.
- The visualization capacity of BIM can be used to demonstrate the deconstruction process, enabling the detection of issues regarding the transportation logistics and waste management.
- The deconstruction/demounting plan could be embedded withing the BIM model from the early stage.
- In case of application of additional software packages or tools to conduct various analysis, the interoperability between these tools and BIM has to be ensured. Therefore there is a need for exploration of IFC on how to extend and support the data exchange.
- When the information from IFC file can be successfully extracted, a separate data base can be created. This database can be considered as a catalog of available or soon-to-become available structural elements that can be reused in upcoming projects. In this way, reuse of either structural parts or complete buildings can be promoted instead of conventional recycling or down cycling strategy.

<div align="right">4</div>

Experimental works

In the framework of the REDUCE (Reuse and demountability using steel structures and the circular economy) project, a number of experimental works were carried out at TU Delft as well as at other partner universities (University of Luxembourg and University of Bradford) as indicated th a figure 4.1. This master thesis project mainly focuses on a four point bending test of a composite beam with demountable shear connectors. The push-out tests were previously conducted by partner universities and the obtained results are used to create FE model as well as to predict the failure load of the composite beam.
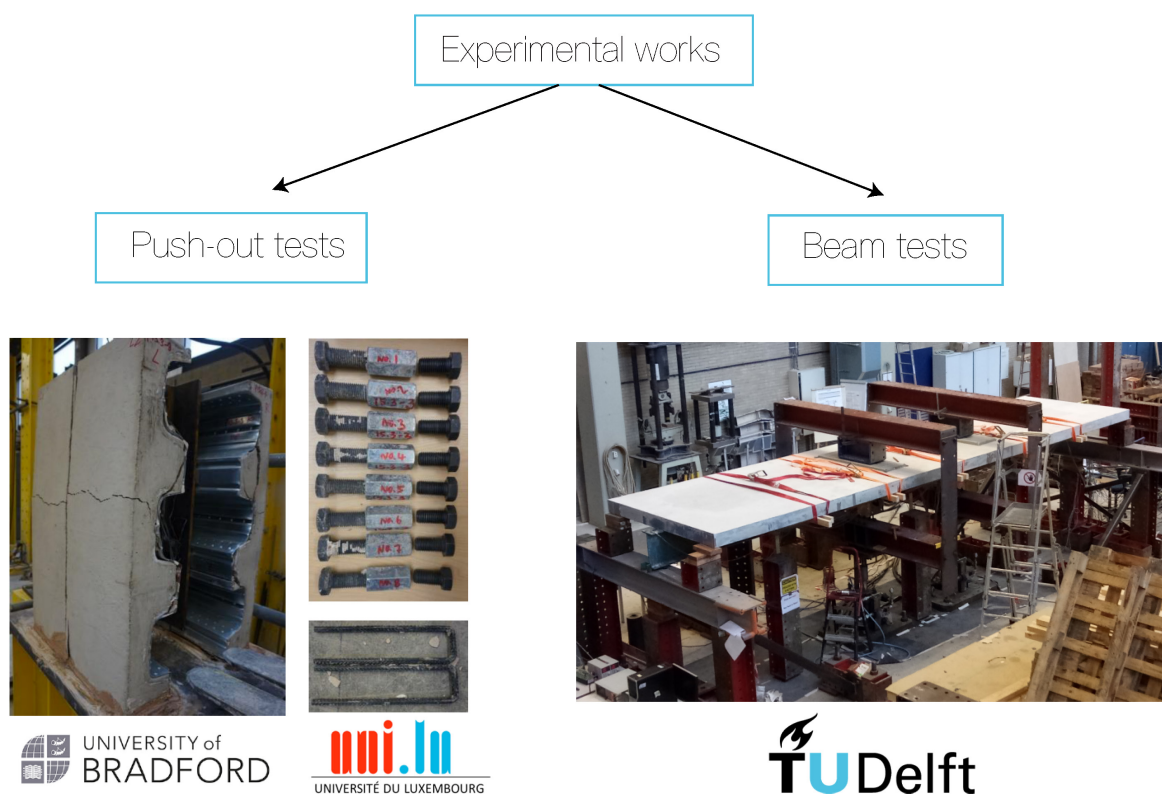
Figure 4.1: Overview of experimental works on demountable shear connectors

A total of 4 beam specimens were manufactured with slightly different characteristics and two types of de-mountable connectors, however, due to the time constraints this master thesis deals in detail with only one specimen testing.

4.1. Experimental program

This section provides a general overview of experimental works that are part of the REDUCE project, which are conducted at TU Delft.

A series of experiments were conducted on a composite slab with metal sheeting at TU Delft and more tests are yet to be performed in order to asses the load-deflection behavior and specimen stiffness in the elastic stage with different type of demountable shear connectors. The experimental results are later used to calibrate numerical models in order to further conduct parametric study.

Specimens were prepared by a contractor and the fabrication process was controlled by TU Delft staff. In this way the quality of manufacturing process is closer to what can be expected in a real situation. After concrete has reached its 28-day strength the specimens were transported to the Stevin II Laboratory at TU Delft and tested.

All specimens consisted of steel beam, concrete slab with ComFlor95 profiled sheeting and demountable shear connectors. The more detailed assembly drawing for one of the specimens is shown in a figure 4.2.

PARTS LIST			
ITEM	QTY	PART NUMBER	DESCRIPTION
1	14	CF95	
2	8000,000 mm	DIN 1025 - IPE 400-8000	Hot rolled I-beam IPE
3	54	CouplerM20	
4	54	ISO 4017 - M20 x 70	Hexagon head screws
5	54	WasherM20	
6	54	ISO 4017 - M20 x 45	Hexagon head screws
8	1	Timber-separator	
9	300,000 mm	DIN 1025 - IPE 400-150	Hot rolled I-beam IPE
11	14	Rebar7mm	
12	53	Rebar7mm2000	
13	54	U-Bar	
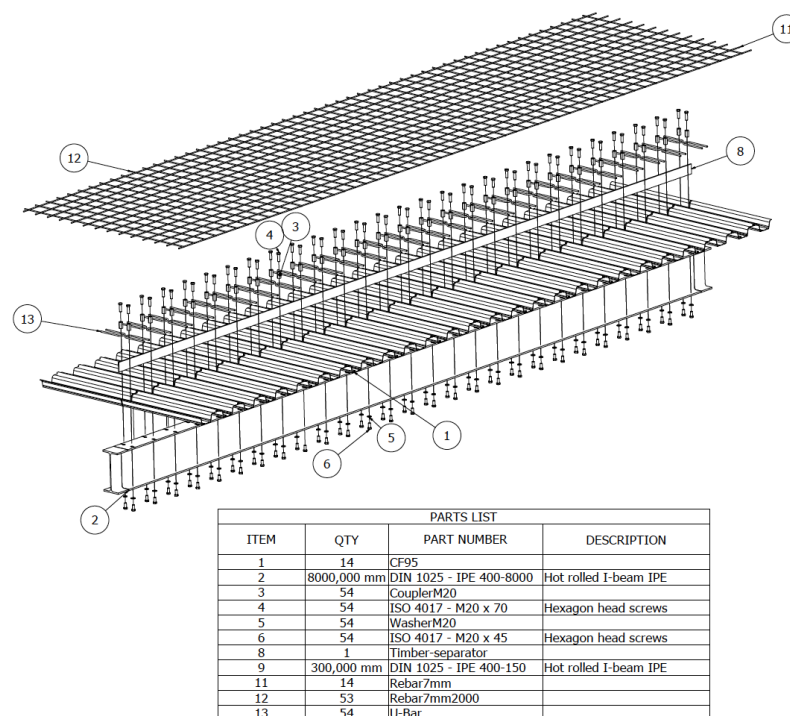
Figure 4.2: Experimental setup overview, specimen B4

A total of 4 specimens were produced, detailed information is given in the table 4.1. Two types of shear connectors were tested as depicted in a fig. 4.3: shear connector consisting of an embedded bolted connector M20 x 140mm (grade 8.8) (2 tests, B1 and B2) and shear connector consisting of an embedded bolt M20 (grade 8.8), coupler (grade 10.9) and external bolt, M20(grade 8.8) (2 tests, B3 and B4). For the tests B2 and B4 with the hole size of 26mm resin was used to fill up the space of oversized hole. For the test B4 resin was injected through the bolt head, whereas for the test B2 through the flange.

Each of 4 specimens were planned to be tested in 2 life cycles. At first, the composite beams were loaded in 4 point bending at different load levels not exceeding the linear-elastic limit. Afterwards, the concrete deck was cut longitudinally in the middle over the timber piece, creating a discontinuous reinforcement. The composite beams were disassembled, resin was removed and then the attempt was made to re-assemble the setup. Finally, if the re-assembly was successful, the specimens were tested again both elastically and up to the failure. Timer element of 18mm thick and 95mm in height was introduced in order to facilitate the procedure of longitudinal cutting, this way only 55mm of concrete has to be cut instead of 150mm.
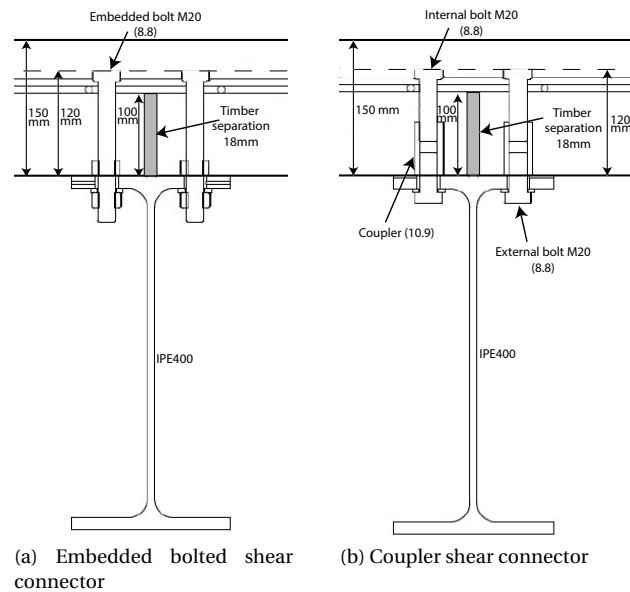
Figure 4.3: Two types of demountable shear connectors

No	Beam	Shear connector type	Slab	Notes
B1	L=8.3m IPE400 S355	Bolted shear connector M20x140mm, hole 21mm	d=150mm b=2m CF95	Un-propped
B2	L=8.3m IPE400 S355	Bolted shear connector M20x140mm, hole 26mm, resin injected	d=150mm b=2m CF95	Propped
B3	L=8.3m IPE400 S355	Bolted shear connector M20 with coupler, hole 21mm	d=150mm b=2m CF95	Un-propped
B4	L=8.3m IPE400 S355	Bolted shear connector M20 with coupler, hole 26mm, resin injected	d=150mm b=2m CF95	Propped

Table 4.1: Test series on composite beams using demountable shear connectors

A visualization of the experimental program for specimen B4 was developed in order to demonstrate in detail the testing procedure. The animated experimental program can be found via link `https://youtu.be/FQMLcSBU6Kk`.

4.1.1. B1 and B2 specimens

As described before specimens B1 and B2 are using embedded bolted shear connectors. The principal difference between these specimens is that the bolt hole in steel flange for B1 is 21 mm and for B2 26mm for M20 bolt. As a consequence, for B2 test specimen the bolt hole is injected with the resin through the hole in the beam flange before testing to obtain slip-resistant shear connection. Additionally, the test girder B2 was propped during casting the concrete slab to avoid unwanted deformations of the shear connections during casting.

The embedded bolted shear connectors were placed in pairs in every trough, at 300mm distances. Once placed during casting, the shear connector can not be removed from the concrete slab and therefore the degree of shear connection can not be changed at later stage. Therefore, the testing program for specimens B1 and B2 consists of only one connector arrangement as indicated on the figure 4.5. U-26 stands for uniform arrangement with 26 shear connectors per half span.
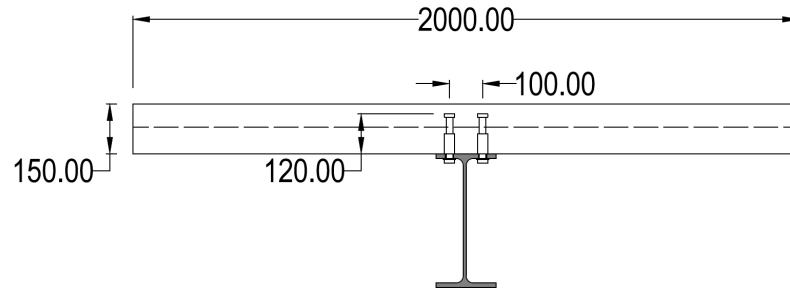
(a) Cross-sectional view of test specimen (dimensions in mm)
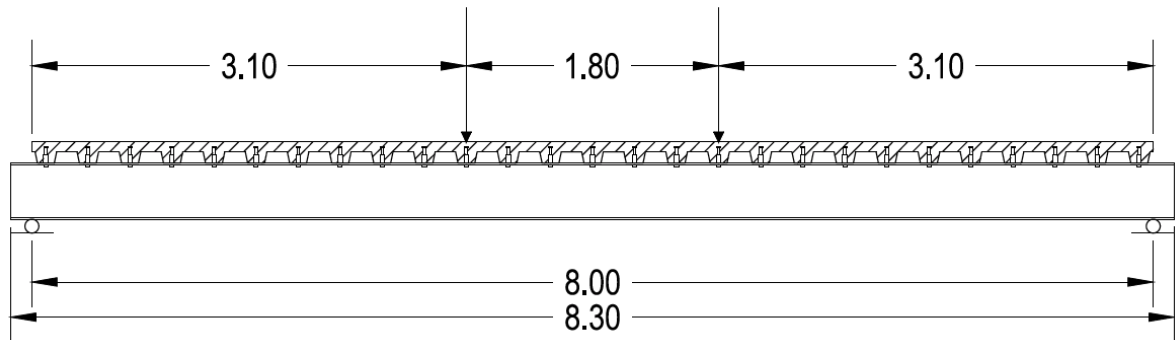
(b) Longitudinal view of test specimen (dimensions in m)

Figure 4.4: Test layout
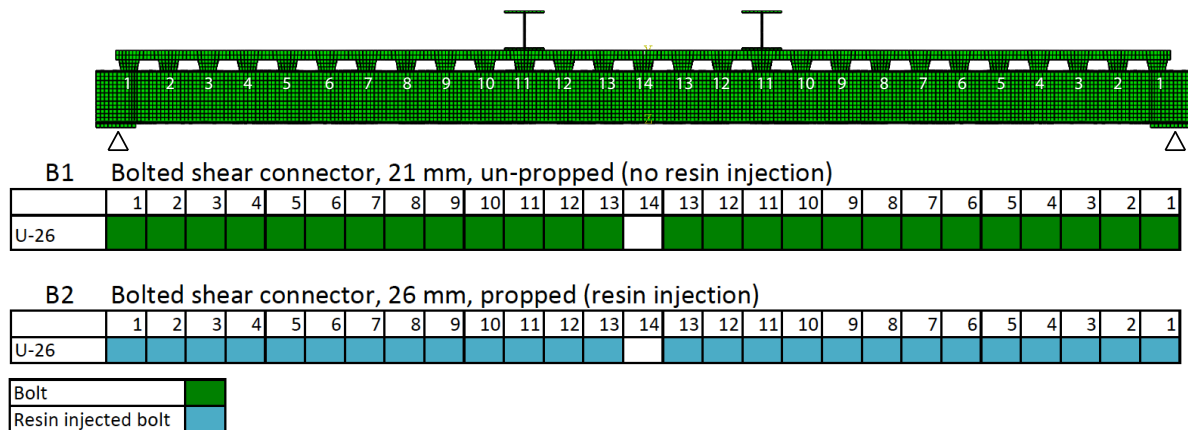
Figure 4.5: Experiment testing program for B1 and B2 specimens

4.1.2. B3 and B4 specimens

B3 and B4 specimens are manufactured with a bolted shear connectors with couplers. Similarly to B1 and B2, the difference between B3 and B4 is that the bolt hole in steel flange for B3 is 21 mm and for B4 is 26mm for M20 bolt. For the B4 specimen the bolt hole is injected with the resin and the specimen was casted in propped condition.

The specimens were casted with shear connectors placed in pairs in every trough at 300mm spacing. However, since B3 and B4 specimens use shear connector consisting of an internal bolt, coupler and external bolt, it provides a possibility to vary the number and location of shear connectors by removing the external bolt. Based on that, multiple testing arrangements were employed as shown in a fig. 4.6. The order of testing arrangements is as indicated in the figure: U-26,NonU-14 and S-08. The testing program is valid for the first life cycle, for the second life cycle only first two arrangements were tested to make sure that the behavior of the

composite beam is not changed and then the beam was loaded up to failure. It was decided to load the beam until failure in the NonU-14 connector arrangement.

B3   Bolted shear connector with coupler, 21 mm, un-propped (no resin injection)

	1	2	3	4	5	6	7	8	9	10	11	12	13	14	13	12	11	10	9	8	7	6	5	4	3	2	1
U-26																											
NonU-14																											
S-08																											

B4   Bolted shear connector with coupler, 26 mm, propped (resin injection)

	1	2	3	4	5	6	7	8	9	10	11	12	13	14	13	12	11	10	9	8	7	6	5	4	3	2	1
U-26																											
NonU-14																											
S-08																											

Bolt	
Resin injected bolt	
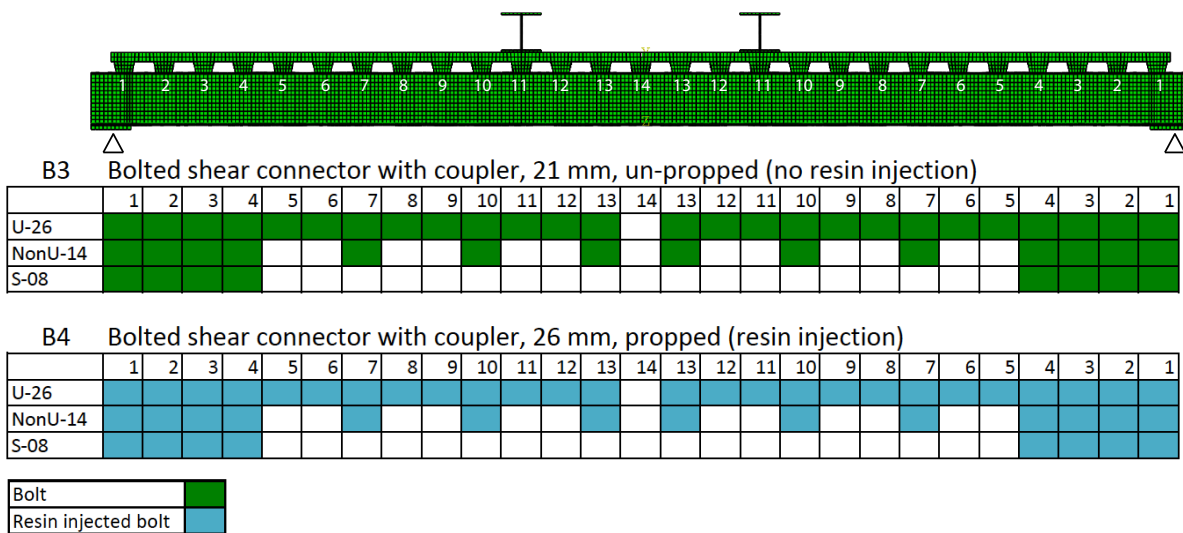
Figure 4.6: Experiment testing program for B3 and B4 specimens

As mentioned before, this master thesis project only deals in detail with one experimental work, namely, B4. It was chosen to focus mainly on that particular test, as it provides more freedom in testing arrangements and therefore more analysis can be conducted.

4.2. Specimen preparation

Prior to the start of preparation works and tests in the lab, a risk safety assessment is conducted, in which all potential risks are listed as well as the measures that should be taken in order to prevent or reduce the consequences of a potential hazard. This risk safety assessment is attached in the annex C.

4.2.1. First life cycle

4.2.1.1   Specimen fabrication

The steel beams were set as a simply supported beams with a span of 8 meters, profiled metal decking was put down on the steel beam on both sides, separated by a timber block in the middle. The demountable shear connectors were installed through pre-drilled holes in the profiled metal decking and steel beam flange to assemble the specimen, as shown in Figure 4.7. The diameter of the pre-drilled holes in the steel beam flange was 21 mm for B1 and B3 specimens and 26 mm for B2 and B4. It provided a clearance of 1 mm and 6 mm, respectively. The connectors were placed in pairs every 300mm along the longitudinal direction of the steel beam. The height of the shear connectors was 120 mm and the diameter was 20 mm.

As mentioned before 2 types of construction method were employed: propped and un-propped. For the un-propped specimens the triangular wooden supporting structure was created as shown on the fig. 4.8. For the stability and safety reasons the additional props were kept during casting procedure, however when the concrete was evenly spread in the form work temporary props were immediately removed. The specimens were cured for at least 28 days before testing.

In order to ensure that during casting the liquid concrete would not escape through the openings between metal sheeting and timber, the foam blocks were placed against the timber separation on both sides of the beam as shown in a figure 4.9. In general, this solution helped preventing big leakages, however, after removing the foam it was discovered that the liquid concrete still escaped and layers of different thickness were created at the steel flange. In most of the cases these layers of concrete could be relatively easily removed with hammering, however, at few locations in was not possible to completely eliminate the created concrete.
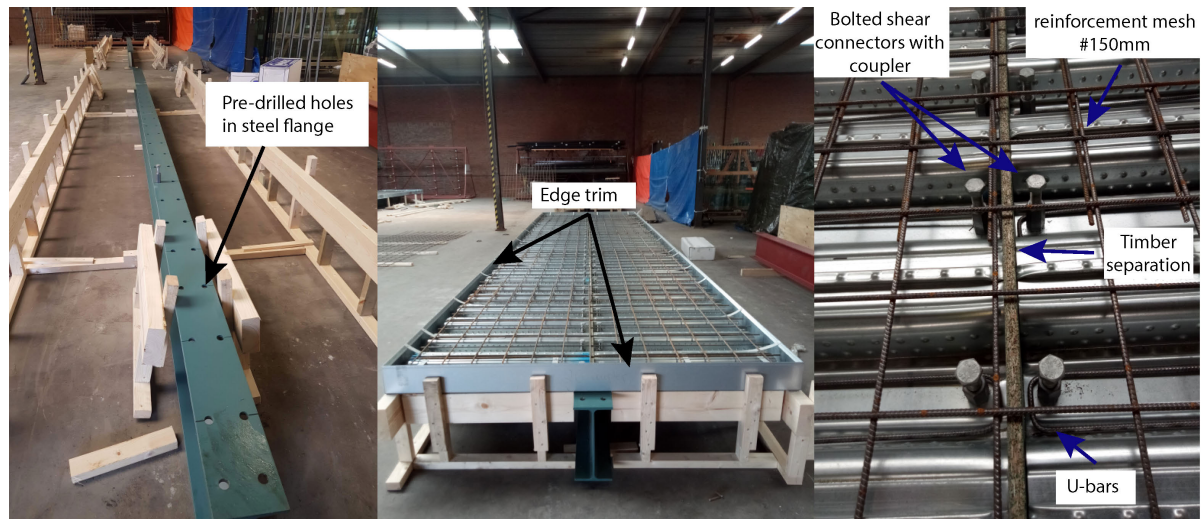
Figure 4.7: Assembled specimen and layout before casting
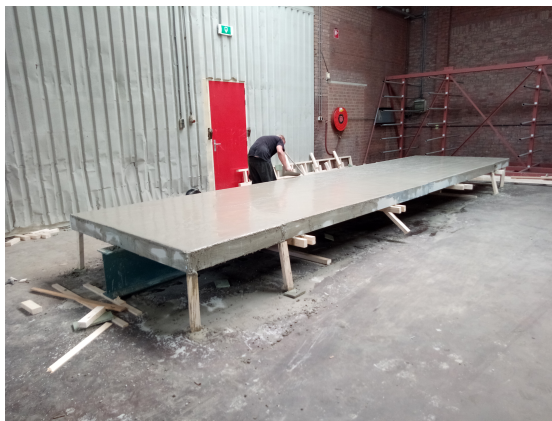
(a) Un-propped specimen after casting

(b) Canteliver support

Figure 4.8: Two types of shear connectors

It turned out that the foam blocks were not placed against the timber separation and because of that few centimeters void space was created, which got filled by liquid concrete. In order to prevent this problem in future, the placement of foam has to be thoroughly controlled or the use of edge trims is suggested instead. The presence of the leaked concrete on the interface between the slab and the steel beam created an additional adhesion, which eventually resulted in a stiffer behavior of the composite beam.

(a) Foam block overview

(b) Foam placed under metal sheeting

(c) Leaked concrete

Figure 4.9: Foam blocks

4.2.1.2   Injection procedure

The injection of the bolts is done after the casting, when the specimens are transported to the lab and placed in the set-up. For the specimen B4, first the external bolt has to be removed and sprayed with the release agent ACMOS 82-2405, as well as the space in the coupler. This is done in order to prevent the adhesion and facilitate the removal of the resin during the demounting. When this step is done, the bolt is placed back and can be injected with the resin. For the injection a two component epoxy resin was used, as indicated on the fig. 4.10. The hardener and resin are mixed together in a proportion 8:100. In total, to inject 56 bolts (B4 specimen) 700 grams of epoxy was sufficient and this procedure took around 40 minutes. Gîrbacea [14] conducted an extensive study on demountable steel-concrete composite flooring systems and, in particular, on costs and time associated with injection of 32mm over-sized holes for M20 bolts and 12mm flange thickness. Injection of 20 holes required 500g of resin and 30 minutes time, 20 seconds per connection. On figure 4.11 the bolt after injection and resin inside of the beam flange hole are shown.

(a) Release agent ACMOS 82-2405   (b) Resin RENGEL SW 404   (c) Hardener REN HY 5159

Figure 4.10: Two component epoxy resin

(a) Resin injected hole in the steel beam flange   (b) Injection bolt

Figure 4.11: Resin injected bolt

For the first life cycle testing the resin was injected in two separate passes, starting from the same end of the beam, as shown in a fig. 4.12.
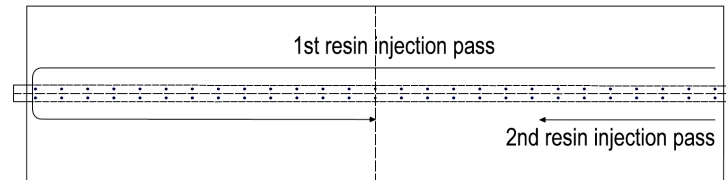
Figure 4.12: Resin injection order for first cycle tests

4.2.2. Second life cycle

4.2.2.1 Longitudinal cutting of the slab

After the first life cycle testing was terminated, in which the beam was loaded in linear elastic stage only, the cutting of the concrete slab had to be performed. The shear connectors were entirely removed and the props were placed on the sides of the slab to support its weight after the cutting.

A center line of the slab was marked, where supposedly the timber separation was placed before fabrication, however, during the cutting process it was discovered that the timber separation did not remain on its original place and was slightly moved during casting procedure. Nevertheless, it did not pose any difficulties to perform the cut. In total it took roughly 40 minutes to install the equipment and perform the cutting. It is worth noticing that the obtained cut was not entirely straight. The use of edge trims on the sides of the slab did bring certain inconvenience, as it was not possible to cut through it entirely with a concrete saw. Instead a different type of saw had to be used to completely separate the two parts of the slab, which required additional time and effort. For that reason, it is highly suggested to avoid application of edge trims at the locations, where the slab cut has to be performed.

4.2.2.2 Lifting of the slab

The slab uplifting was performed by an IPE400 8.3 meters long steel beam. Additionally, hollow section tubes and plates were welded to the ends of lifting beam in order to assure the stability of the concrete slab, since there were no mechanical connections between lifting beam and part of concrete slab. The hoisting of the supporting beam was performed with 4 supporting points, instead of usual 2 points, for extra stability. Figure 4.13 shows modified supporting beam with the half of the slab on top of it.

(a) View on a separated slab

(b) Front view on a lifted half slab

Figure 4.13: Lifting of the slab

It was discovered that the unwanted adhesion took place between the timber piece and concrete slab which had resulted in dragging of one part of the slab, when lifting another, as schematically depicted in a fig. 4.14. During the uplifting the timber separation was damaged and hence it was entirely replaced by similar timber

blocks. It was made in order to ensure the continuity of force transfer between the slabs and to provide a confinement to restrain the deformations of concrete on the edges where the shear connectors are placed.
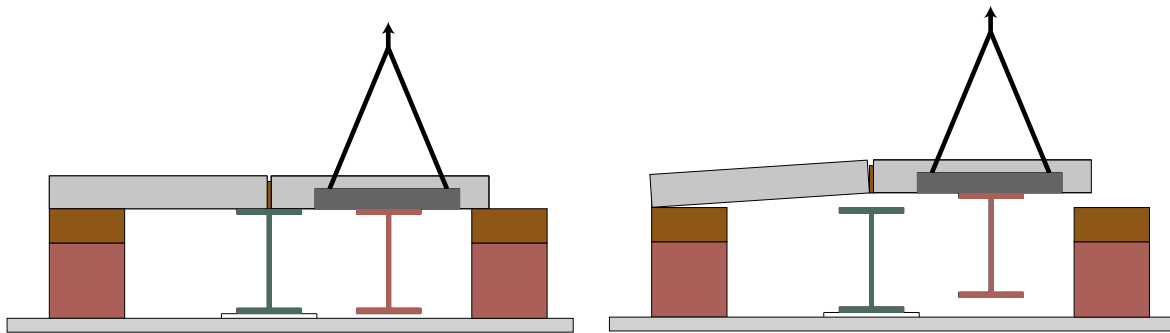
Figure 4.14: Schematic drawing of slab lifting

When the part of the slab was removed from its original position, the half of top steel flange was accessible for inspection and cleaning. It was discovered that the resin injection in most of the cases was quiet successful, however at few locations a rather large volumes of resin escaped the groove space. In addition, quiet large amount of liquid concrete flowed away through the openings between timber separation and profiled sheeting during casting and accumulated at the top steel flange. As a result, it created an additional bond between the steel beam and the metal sheeting. During cleaning procedure the concrete and resin were removed from the steel flange and the grooves, a layer of oil and release agent were applied in order to prevent adhesion and friction during testing in the second life cycle. The view on the beam top flange before and after cleaning is shown in a figure 4.15.
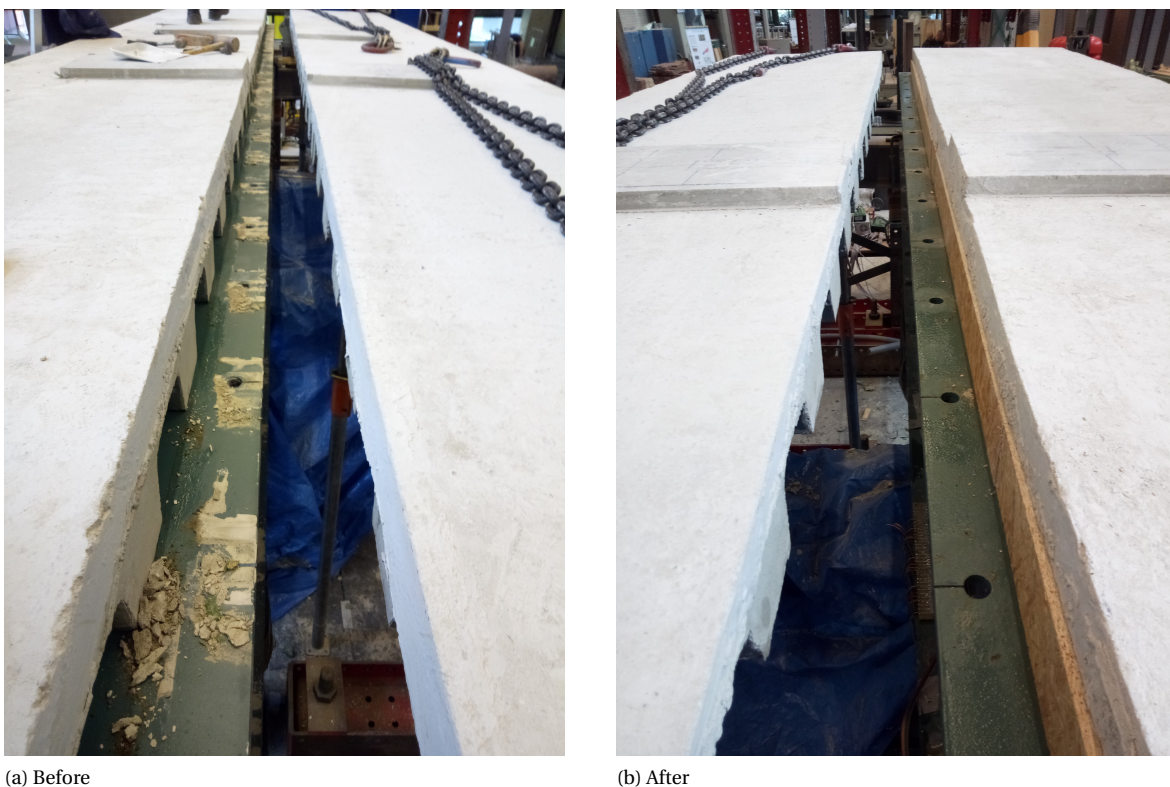
(a) Before

(b) After

Figure 4.15: Steel beam top flange before and after cleaning

Additionally, the condition of the concrete was inspected and several cracks in the ribs were discovered, mainly at the ribs close to the supports. Some damages of the slab are shown in the figure 4.16. Most likely,

these cracks developed as results of the first life cycle testings. However, some damages could also have occurred also due to transportation, uplifting or cutting procedures.

Figure 4.16: View on the cracks in the ribs along the longitudinal cut

Despite the fact that 26mm pre-drilled holes in steel flange were used for M20 bolts, the re-assembly of the components posed additional challenge due to not straight longitudinal cut of the slab in combination with a new timber piece, which, most likely, at some locations had a slightly bigger thickness compared to original timber element.

In total, 5 full working days were required to prepare the specimen for the second life cycle testing.

4.2.2.3   Safety aspects

The second life cycle testing posed additional challenges in terms of safety compared to the first life cycle tests and therefore more effort was required from the lab staff and research team in order to ensure a safe working environment.

During the fist life cycle testing the timber cantilever supporting structures were placed at 5 locations along the beam on both sides as shown in a fig. 4.17. For the second life cycle it was decided to increase this amount from 5 to 8, every 900mm distances.

4.2.2.4   Injection procedure

For the second life cycle, grease and release agent were applied on the interface between steel beam and metal decking to reduce the friction and prevent the adhesion of the resin. In addition, the resin injection was carried out in 4 passes, starting from the mid-span towards the supports as indicated on the fig. 4.18. In this way the consistency of the resin at the moment of injection was identical for the bolts, which are placed symmetrically with respect to the both mid-span and longitudinal axis. After the resin cured, the preloading on the bolts was released prior to the testing.

4.3. Test setup

The specimens were tested under a two-point loading system. In the first life cycle, B4 beam test specimen was equipped with 13 LVDTs (Linear Variable Displacement Transducer) in order to measure its vertical at different locations, the end slip, relative slippage between beam and concrete deck at an intermediate connector

Figure 4.17: Wooden cantilever supporting structure
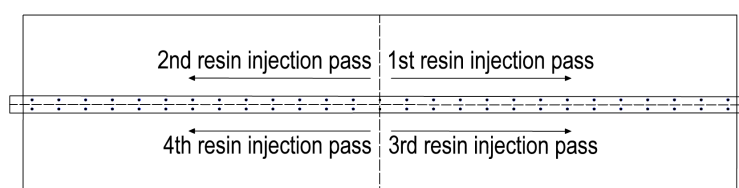
Figure 4.18: Resin injection order for second cycle tests. View on top of the composite beam

as well as the vertical separation between concrete deck and steel beam as shown on the fig. 4.19. LVDTs 1 and 13 are measuring the end slip, LVDTs 2,6 and 9 measure the vertical deflection of the beam, LVDTs 3 and 10 are placed at the location of 7th trough on both ends to measure the relative slippage. LVDTs 4,5,7,8,11 and 12 measure the vertical separation between concrete slab and steel beam on both sides.

For a second life cycle, the specimen was equipped with 4 additional LVDTs. Since after the cutting procedure the concrete deck consisted out of two unconnected slabs it was decided to measure the end slip and relative slippage at the intermediate connectors for both sides of the composite slab. Therefore LVDTs 1L,1R,13L and 13R were placed to measure the end slip for left and right sides on both ends of the slab. Similarly, 3L,3R, 10L and 10R were placed to measure the relative slippage between the steel beam and concrete decks.

Additionally, strain gauges were put at the middle section and at the sections of point load application on the steel beam flange and web. A central computer-controlled logging system was used to record all data.

The hydraulic jacks, LVDTs and strain gauges were calibrated before starting testing procedure. The displacement by hydraulic jacks was applied with a constant rate of 0.2mm/s. A total of 5 cycles were performed for each connector arrangement test as indicated in a figure 4.20. Total testing time for one connector arrangement, in general, does not exceed 30 min time. A maximum allowed displacement was set to 30mm at the mid span. In addition to maximum deflection, a limit for an applied load was set in order to prevent plastic deformation in the steel beam.

A notation of working load (WL) was introduced in order to indicate different load level during testing. It was considered to chose the WL equal to 50kN (force of one point load), the equivalent uniformly distributed load acting on the beam, therefore, is equal to $q = 2 \cdot 50kN/4m/8m = 3.125kN/m^2$.

Even though the surface finishing of the composite slab was relatively good, an extra layer of few centimeters of cement at the locations of the loading beams was applied in order to even out the surface and ensure a good contact between the loading beam and concrete slab.
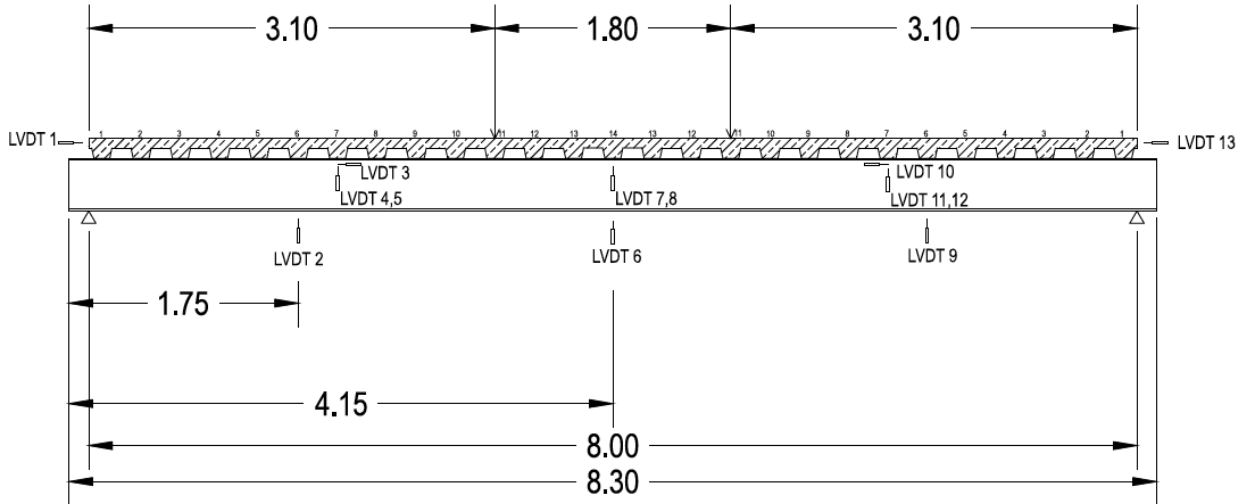
(a) Test layout and positions of LVDTs during first life cycle tests (dimensions in m)
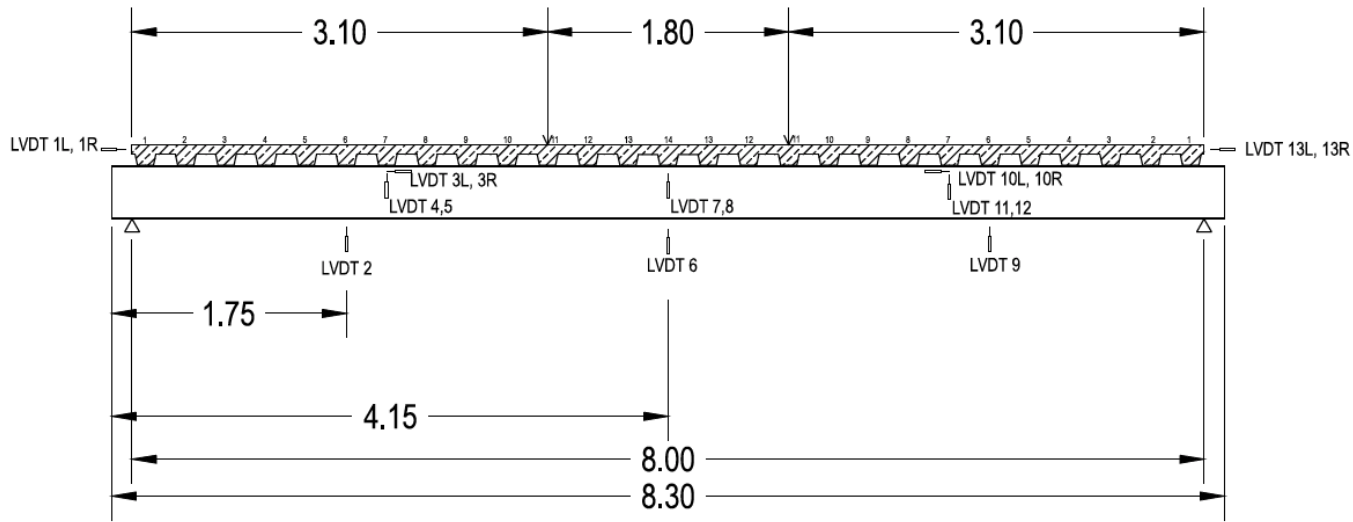
(b) Test layout and positions of LVDTs during second life cycle tests (dimensions in m)
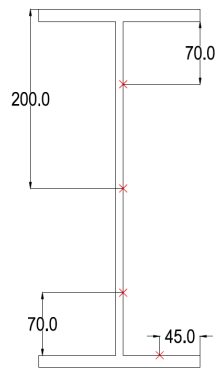
(c) Positions of strain gauges on steel beam (dimensions in mm)

Figure 4.19: Test layout and positions of measuring devices
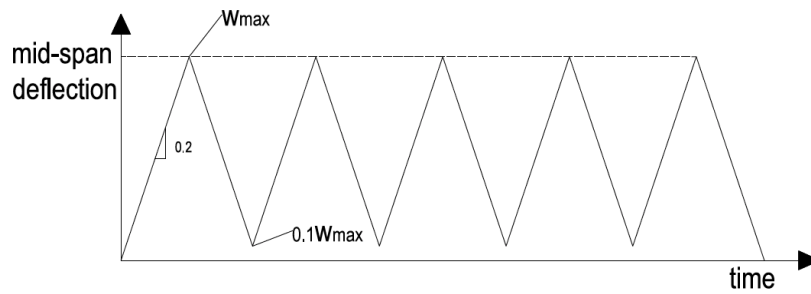
Figure 4.20: Cyclic loading program

4.4. Experimental results

The experimental results for the specimen B4 are presented in this section. Firstly, the results of a first life cycle are presented and discussed, then the results of second life cycle are demonstrated. Afterwards, the comparison of two life cycle testings is conducted. Additionally, the existing analytical solutions are applied in order to analyze the obtained results. Finally, based on a conducted work, a number of practical recommendations and discussion of the obtained results are presented. A total of 5 cycles were conducted for each arrangement in order to make sure that the specimen is settled down. For analysis and post-processing the averaged data obtained over 4 last cycles was used.

It was decided to evaluate the results of experiments in terms of effective bending stiffness and the effective shear stiffness parameters, which were defined as follows:

$$k_{b,eff} = \frac{\Delta F}{\Delta u} \tag{4.1}$$

$$k_{s,eff} = \frac{\Delta F}{\Delta s} \tag{4.2}$$

where:
  $k_{b,eff}$ = Effective bending stiffness
  $k_{s,eff}$ = Effecting shear stiffness
  F   = Point load force applied to the test specimen
  u   = Deflection of the composite beam at the mid span
  s   = Relative slippage between the concrete deck and steel beam

These parameters were defined for two force intervals between 40kN-70kN (force applied by one point load) and 70kN-100kN , which corresponds to an equivalent uniformly distributed load between 2.5kN/m^2–4.4kN/m^2 and 4.4kN/m^2–6.25kN/m^2, respectively.

4.4.1. First life cycle

The first preliminary loading had shown that the specimen behaved much stiffer compared to the expected results based on FE modeling. A number of actions was taken in order to detect and eliminate the reasons that could result in a stiffer behavior of the specimen. Firstly, the preloading on the bolts was released. That did contribute to a less stiff behavior, however not significantly. A second action was an attempt to break the adhesion between the steel beam and the ComFlor decking caused by excessive flow of resin during the injection process. In order to achieve that, a number of bolts close to the supports were removed and the specimen was loaded again. During that loading, observed cracking noises signified that the bondages were being broken, a decrease in bending stiffness was achieved. However, the measuring devices still showed unsymmetrical development of end slips, which could signify that at certain places the bonds were not entirely broken. Nevertheless, after this, the bolts were placed back. However it was not possible to put entirely all bolts back at their locations and at few places the injected resin got damaged and was entirely removed. It was decided to not make an attempt to re-inject the bolts, as it could have led to exactly same problem of additional adhesion. As a consequence of this action, at some places connectors experienced additional slip due the hole clearance.

4.4.1.1 Deflection of the composite beam

The deflections along the beam at different loading levels for different connector arrangements are shown in figure 4.21. Based on the obtained deflection results, it can be concluded that the SLS limit for the deflections which is 32mm is fulfilled by all shear connector arrangements under the working load.
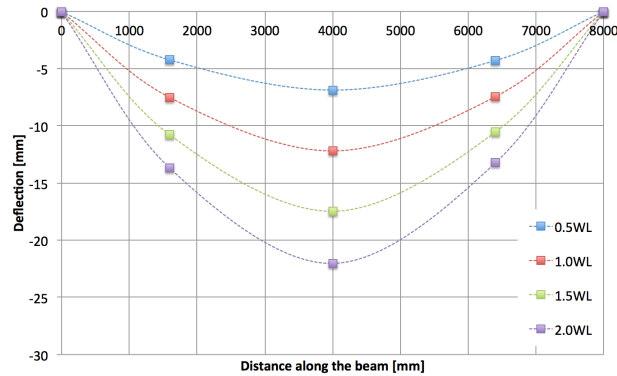
(a) U-26 connector arrangement
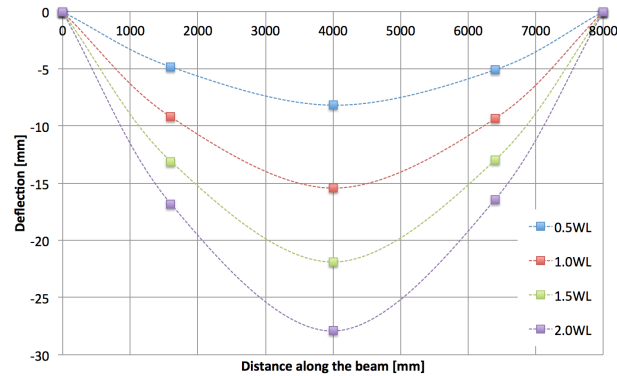
(b) NonU-14 connector arrangement
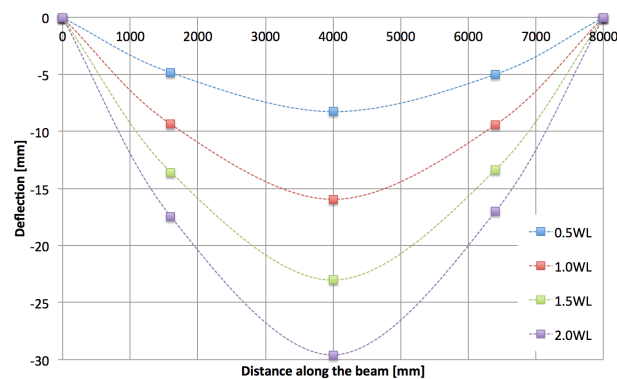
(c) S-08 connector arrangement

Figure 4.21: Deflection along the beam for various connector arrangements at different load levels during first life cycle testing

The deflection of composite beam was worked out using Dutch national annex to 1994-1-1 [7]. Additionally, deflections were calculated based on effective bending stiffness for flexible shear connectors according to Leskela [22]. This comparison is only applicable to the case of uniformly distributed shear connectors arrangement, namely U-26.

The deflection of a composite beam assuming full composite action under two point loads can be calculated

as follows:

$$\delta = \frac{P \cdot a (3L^2 - 4a^2)}{24 EI_{comp}} \tag{4.3}$$

where:
  P   = Point load
  L   = Length of a beam
  a   = Distance from support to application of a point load
  EI_{comp} = Bending stiffness assuming full composite action

The comparison between measured mid span deflection and deflection predicted by hand calculations for different load levels is presented in the table 4.2. Both analytical solution and formula provided by NEN1994-1-1 greatly underestimate the deflection at low working loads(at most by 40.5%). For higher applied loads the deviation between the analytical solution and experimental results decreases to 11.4%.

Test	P, kN	Measured mid-span deflection	Deflection predicted by EN1994	Deflection predicted by analytical solution
B4:U26	25kN (0.5WL)	6.9 mm	4.1 mm (-40.5%)	4.9 mm (-29.0 %)
	50kN (1.0WL)	12.2 mm	8.2 mm (-32.8%)	9.8 mm (-19.7%)
	75kN (1.5WL)	17.5 mm	12.3 mm (-29.7%)	14.6 mm (-16.6%)
	100kN (2.0WL)	22.0 mm	16.4 mm (-25.5%)	19.5 mm (-11.4%)

Table 4.2: Comparison of predicted deflection with experimental results of 1st life cycle

4.4.1.2 Load–deflection behavior of the composite beam

The curves presented in fig. 4.22 show the evolution of the maximum deflection, measured on the bottom of the steel girder at mid-span with the increase of the applied point force. Since the specimen was loaded only in linear elastic stage, the obtained curves clearly exhibit the linear behavior. It can be noted that for test arrangements NonU-14 and S-08 a slight decrease in the slope is observed in the beginning of the loading (up to 40kN applied load), which could occur due to the initial slip of the connectors, where the resin was removed. For the NonU-14 during the first cycle a larger force was applier to the specimen in an attempt to break the remaining adhesion between the steel beam and metal decking.

Table 4.3 summarizes the evaluated effective bending stiffness $k_{b,eff}$ for different connector arrangements and for two intervals of applied forces. As expected, the effective bending stiffness decreases with decreasing number of shear connectors. The bending stiffness shows on average an increase of 8.5% between two evaluated force intervals.

Arrangement	$k_{b,eff}$		Change in stiffness between two intervals
	40kN-70kN	70kN-100kN	
U-26	4.73 kN/mm (-)	5.18 kN/mm (-)	+9.7%
NonU-14	3.77 kN/mm (-20.3%)	4.08 kN/mm (-21.2%)	+8.2%
S-08	3.53 kN/mm (-25.4%)	3.80 kN/mm (-26.6%)	+7.6%

Table 4.3: Effective bending stiffness $k_{b,eff}$ for various shear connector arrangements during first life cycle testing

The effective bending stiffness based on analytical solution was also calculated for U-26 shear connector arrangement, which is equal to 5.12kN/mm. The obtained value matches well with the experimental results for the force interval of 70kN-100kN.

4.4.1.3 Interface slip

The end slip as well as the relative slippage at 7th shear connector on each side of the beam were measured. Figure 4.23 show the development of slips at both ends of the composite beam. It is clearly observed that one side of the beam behaves stiffer compared to the other for all three arrangements, although the applied point loads on both sides of the beam were identical. The differences in shear stiffness between two ends

(a) U-26 connector arrangement

(b) NonU-14 connector arrangement

(c) S-08 connector arrangement
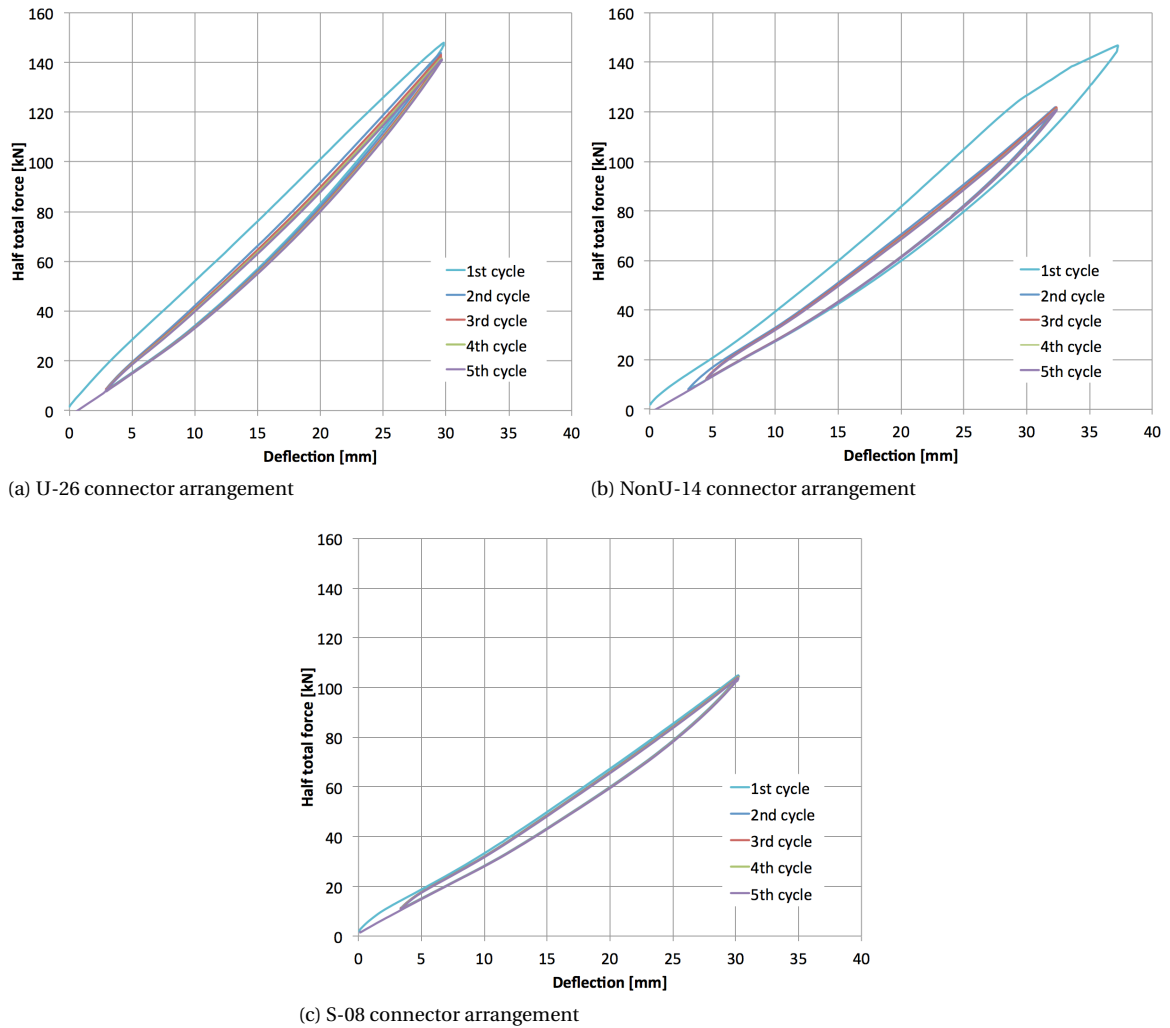
Figure 4.22: Load-mid span deflection for various shear connector arrangements during first life cycle testing

vary between 1.5-2.0 times depending on the connectors configuration. The averaged value of the slips were calculated and further comparison and analysis was conducted based on these values. Figure 4.24 demonstrates the development of averaged end slip and averaged relative slippage at the 7th trough location (1.9m from the support) for 3 different arrangements.

The evaluation of an effecting shear stiffness was conducted and summarized in the tables 4.4 and 4.5 for end slip and relative slippage at intermediate connector, respectively.

| Arrangement | $k_{s,eff}$ | | Change in stiffness |
	40kN-70kN	70kN-100kN	between two intervals
U-26	109.72 kN/mm (-)	123.22 kN/mm (-)	+12.3%
NonU-14	65.60 kN/mm (-40.2%)	76.92 kN/mm (-37.6%)	+15.0%
S-08	55.56 kN/mm (-49.4%)	68.18 kN/mm (-44.7%)	+22.7%

Table 4.4: Effective end slip shear stiffness $k_{s,eff}$ for various shear connector arrangements during first life cycle testing

For the development of the end slip, when looking at the averaged values, one can observe that at initial stage the specimen behaves relatively stiff, then there is a decrease in stiffness and after that, the slip behaves almost linear, gradually increasing the stiffness. Similarly to the effective bending stiffness, the effective shear stiffness of the specimen increases with the increasing applied load. On average, 16.7 % increase in end slip shear stiffness was observed between two measured force intervals.
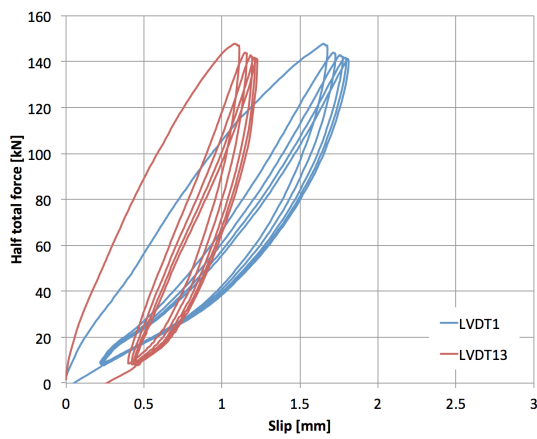
(a) U-26: End slip on both sides of the slab
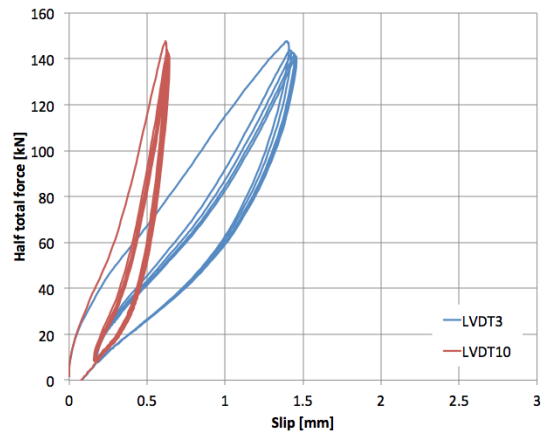
(b) U-26: Slip at intermediate connector on both sides of the slab
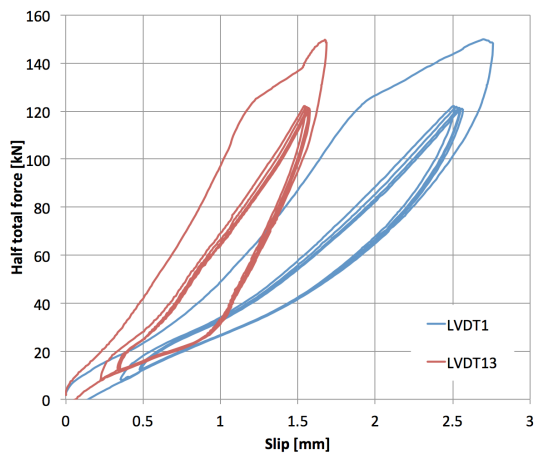
(c) NonU-14: End slip on both sides of the slab
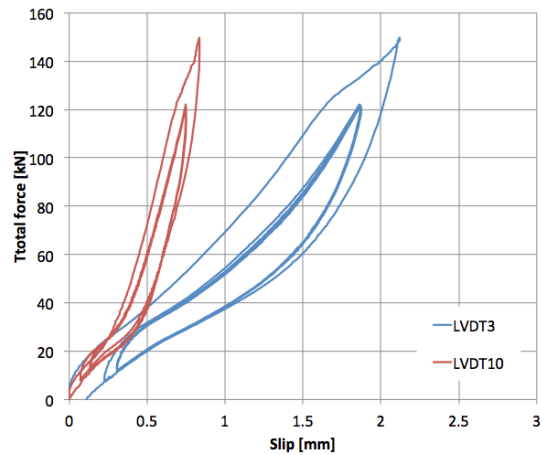
(d) NonU-14: Slip at intermediate connector on both sides of the slab
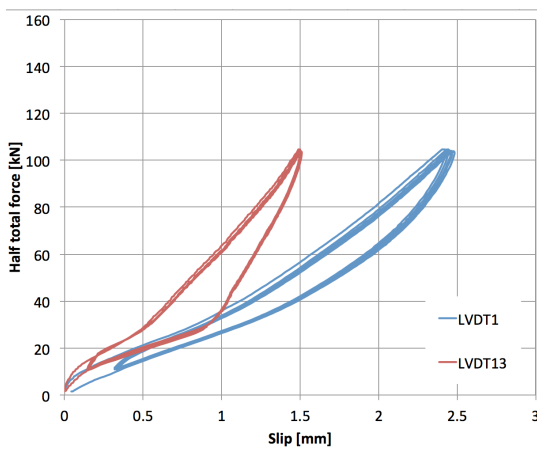
(e) S-08: End slip on both sides of the slab
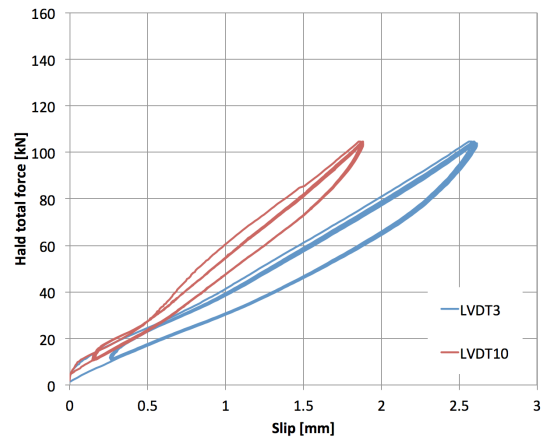
(f) S-08: Slip at intermediate connector on both sides of the slab

Figure 4.23: Interface slip on both sides of the slab for various connector arrangements during first cycle tests

The effective shear stiffness according to analytical solution for U-26 is equal to 71.43kN/mm, which underestimates considerably (by 34.9 % and 42.0%) the results obtained by experiments for both force intervals.

The evolution of the slip at the intermediate connector is quiet similar to the end slip for U-26 and NonU-14, however, the slippage for S-08 behaves almost linear and develops even higher slip than the one at the end of

(a) U-26: Averaged end slip

(b) U-26: Averaged slip at intermediate connector

(c) NonU-14: Averaged end slip

(d) NonU-14: Averaged slip at intermediate connector

(e) S-08: Averaged end slip

(f) S-08: Averaged slip at intermediate connector
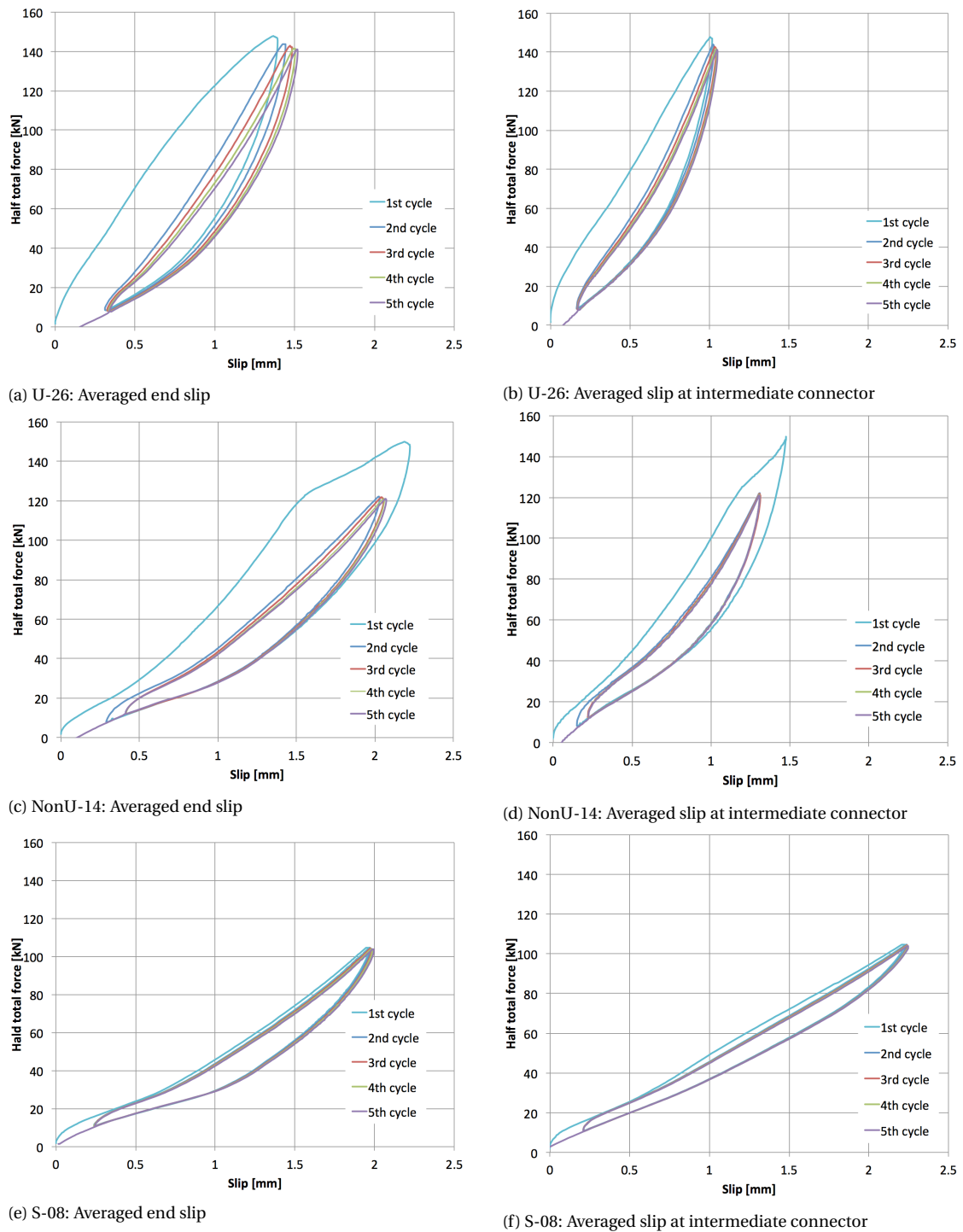
Figure 4.24: Averaged interface slip for various connector arrangements during first cycle tests

the beam for the same arrangement. This happens due to the particular arrangement, where as all connectors are located solely at the supports and, therefore, the slip can freely develop at intermediate connectors. This observation is also reflected in the table 4.5, where for U-26 and NonU-14 an averaged increase of 38.4% can be seen, whereas for the arrangement S-08 there is only a slight increase of 6.4%.

| Arrangement | $k_{s,eff}$ | | Change in stiffness |
	40kN-70kN	70kN-100kN	between two intervals
U-26	123.78 kN/mm (-)	164.42 kN/mm (-)	+32.8%
NonU-14	83.33 kN/mm (-32.7%)	120.0 kN/mm (-27.0%)	+44.0%
S-08	45.46 kN/mm (-63.3%)	48.39 kN/mm (-70.6%)	+6.4%

Table 4.5: Effective shear stiffness $k_{s,eff}$ at intermediate connector for various shear connector arrangements during first life cycle testing

| | Position of the neutral axis in steel beam (from bottom of the steel section) | | |
Load level	U-26	NonU-14	S-08
0.5WL	268.0 mm (-)	236.1 mm (-)	223.3 mm (-)
1.0WL	280.9 mm (+4.8%)	237.9 mm (+0.8%)	226.0 mm (+1.2%)
1.5WL	287.3 mm (+7.2%)	242.6 mm (+2.8%)	228.8 mm (+2.5%)
2.0WL	295.7 mm (+10.3%)	247.2 mm (+4.7%)	232.5 mm (+4.1%)

Table 4.6: Position of the neutral axis in the steel beam section for various shear connector arrangement during first life cycle

4.4.1.4 Normal stresses at the mid span section

Figure 4.25 presents longitudinal stress distributions at the mid-span section for U-26, NonU-14 and S-08 shear connector arrangements at different load levels. It can be seen that the neutral axis in the section shifts slightly upwards as the load increases, although it always remains in the steel web. In the table 4.6 position of the neutral axis is summarized for various load levels. For the connector arrangement U-26, the neutral axis shifted the most, by 10.3% (27.7mm) between 0.5WL and 2.0WL, for NonU-14 and S-08 the change in the neutral axis location is less and, on average, is 4.4% between 0.5WL and 2.0WL.

(g) U-26 (h) NonU-14 (i) S-08
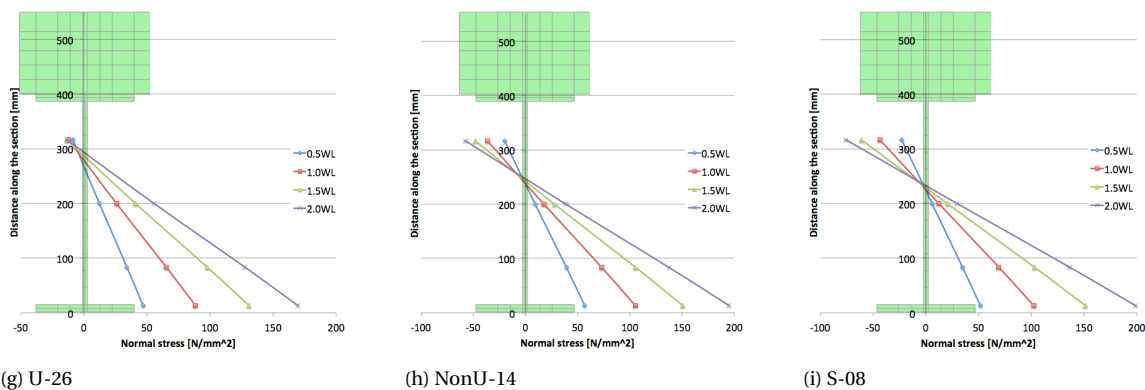
Figure 4.25: Normal stresses in the steel section at different load levels for various connector arrangements during first life cycle testing

The longitudinal stress distribution at the mid-span obtained for the connector arrangement U-26 from first life cycle can be compared with an analytical solution according to Girhammar [15] calculations described previously. The results of comparison are presented in a figure 4.26. The stress distribution calculated according to analytical solution is in a good agreement with the experimental results. For the lower load levels the location of neutral axis obtain from experiments is lower, however it increases with the increasing load and it matches better the hand calculations.

4.4.1.5 Vertical separation

It was of interest to investigate the influence of various shear connectors arrangements on a vertical separation between the slab and the steel beam. 1994-1-1 [6] defines limits on longitudinal shear connector spacing, which should not be greater than 6 times of the total slab thickness or 800mm in order to maintain the vertical restraints. In research conducted by Naraine [26], it was found out that in case of uniformly distributed load
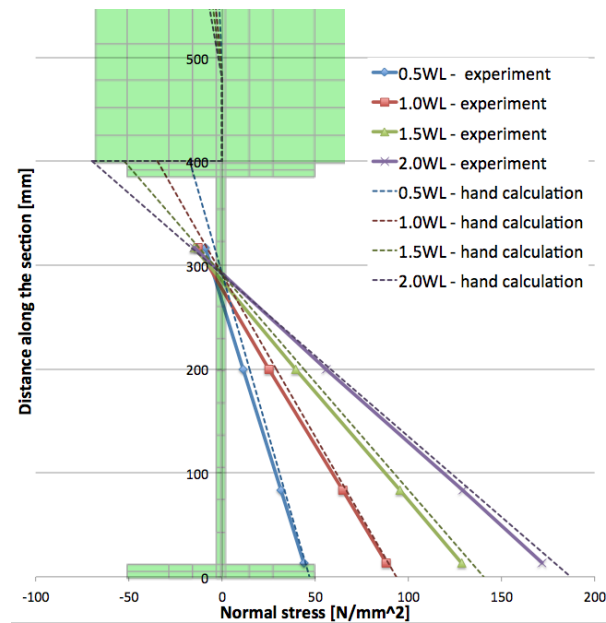
Figure 4.26: Comparison of experimental and hand calculation results of longitudinal stress distributions at mid-span section

the uplift of a slab is not significant when considering the elastic stage. Whereas for the case of point loads, a high negative uplift force was observed beneath the point load, when the elastic range is exceeded.

Therefore, a number of LVDT's was placed at three locations along the beam. At each location a pair of measuring devices was placed and an averaged value is presented in the figure 4.27. For all arrangements the absolute value of the separation did not exceed 1mm and the largest recorded value was 0.7mm (S-08 arrangement). LVDT's 4,5 and 11,12 were placed symmetrically and therefore it was expected to observe similar measured data. For U-26 and S-08 the separation on "Left" and "Right" locations showed relatively similar behavior, however, for NonU-14 a quiet significant difference is observed between the "Left" and "Right" results. The vertical separation at the mid span was smallest for S-08 arrangement and largest for NonU-14 configuration.

4.4.2. Second life cycle

During the second life cycle tests two connector arrangements namely, U-26 and NonU-14, were investigated in the elastic range and then, in a separate test run, the composite beam was loaded up to the failure in NonU-14 shear connector arrangement.

4.4.2.1   Deflection of the composite beam

The deflections along the beam at different loading levels for various connector arrangements are shown in figure 4.28. Similarly to the first life cycle testings, the SLS limit for the deflections which is 32mm is fulfilled by all shear connector arrangements under the working load.

4.4.2.2   Load–deflection behavior of the composite beam

The load-mid span deflection relationship for two connector arrangements is presented in the fig. 4.29. A decrease of around 15 % is observed for NonU-14 compared to U-26. Similarly to the first life cycle tests, the effective bending stiffness demonstrates an increase with the increased load, on average, 9.4%, as demonstrated in the table 4.7.
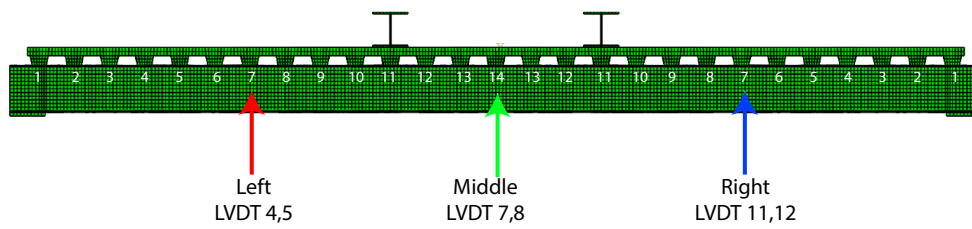
(a) Indication of LVDT's
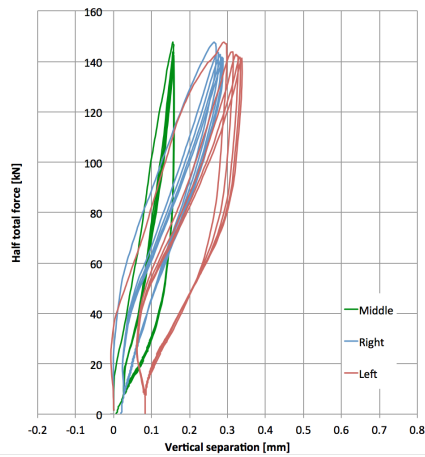
(b) U-26 connector arrangement
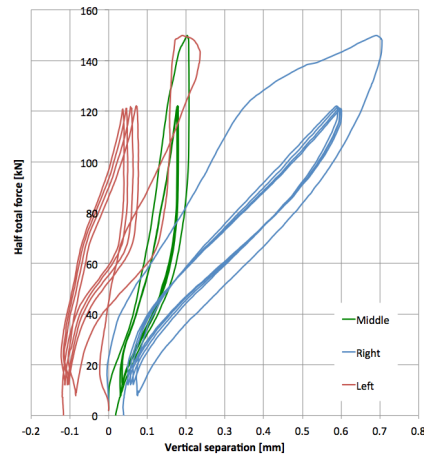
(c) NonU-14 connector arrangement
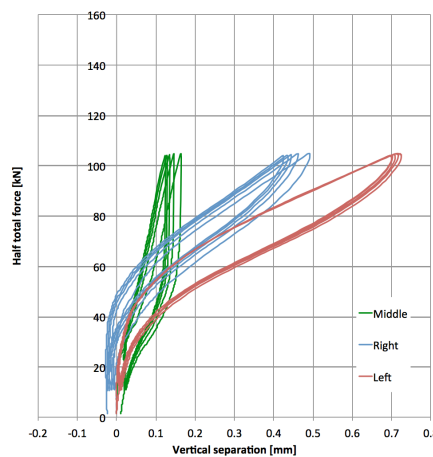
(d) S-08 connector arrangement

Figure 4.27: Vertical separation between steel bean and concrete slab at different locations for various connector arrangements

| Arrangement | $k_{b,eff}$ | | Change in stiffness |
	40kN-70kN	70kN-100kN	between two intervals
U-26	4.10 kN/mm (-)	4.48 kN/mm (-)	+9.3%
NonU-14	3.46 kN/mm (-15.6%)	3.79 kN/mm (-15.4%)	+9.5%

Table 4.7: Effective bending stiffness $k_{b,eff}$ for various shear connector arrangements during second life cycle

4.4.2.3 Interface slip

Despite the fact that the steel beam flange was cleaned from concrete and the bolts were injected in a symmetric way, one side of the composite beam behaved much stiffer compared to the other. However, in the second life cycle tests the difference in shear stiffness between two beam ends has increased to nearly 5 times. An

(a) U-26 connector arrangement   (b) NonU-14 connector arrangement
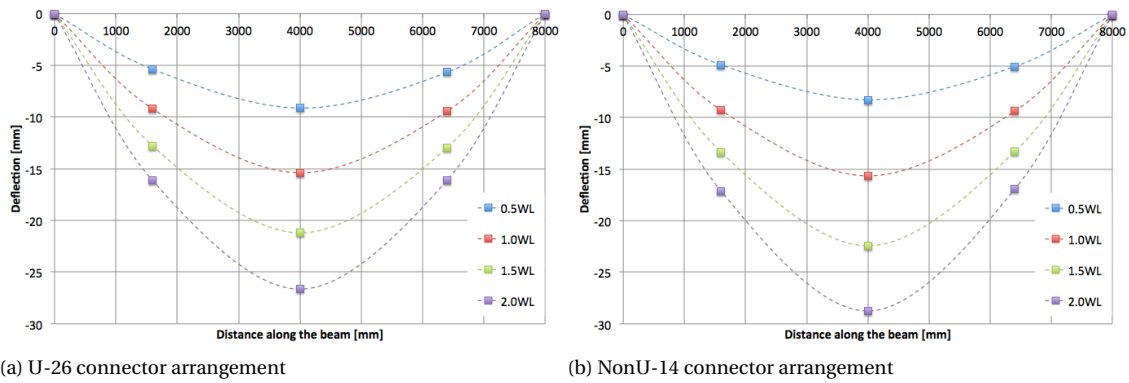
Figure 4.28: Deflection along the beam for different connector arrangements at various load levels during second life cycle testing

(a) U-26 connector arrangement   (b) NonU-14 connector arrangement
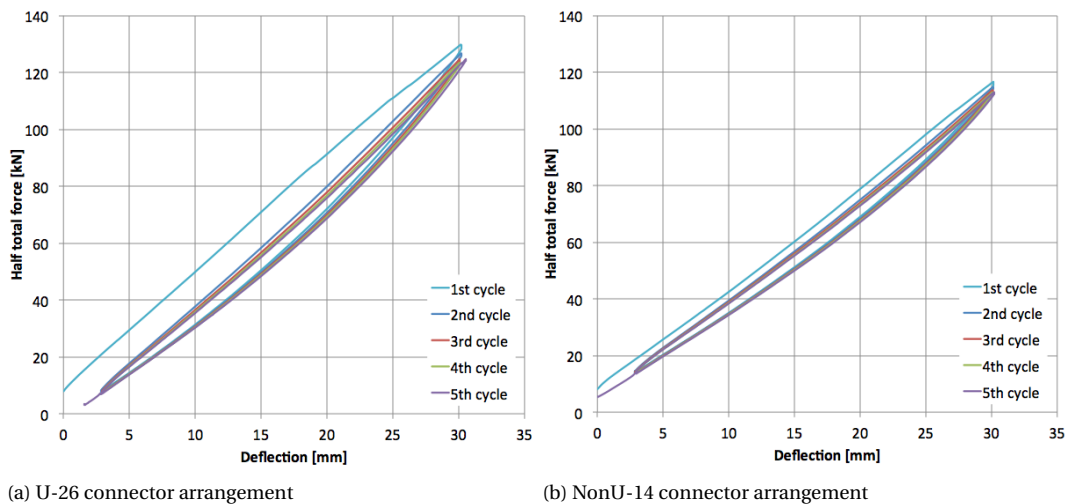
Figure 4.29: Load-mid span deflection for various shear connector arrangements during second life cycle testing

abnormally hight effective shear stiffness of around 324kN/mm for U-26 and 261kN/mm for NonU-14 was observed. The likely explanation for this behavior is the presence of the wooden supporting structure, which could have acted beneficially in transferring the longitudinal forces from the slab to the steel beam. The development of the end slip on each side of the beam is presented in the figure 4.30. It can be seen that the difference is observed not only for two ends, but also for left and right sides of the same beam end.

The averaged values of end slip are presented in the figure 4.31. The evaluation of effective shear stiffness is conducted based on averaged values and is summarized in the table 4.8. The end slip demonstrates, in general, a linear development and based on evaluated effective shear stiffness an increase of 8% between two force intervals is observed.

The relative slippage at intermediate connector location demonstrated a bigger scatter between left and right sides of the slab compared to the end slip as can be seen from the fig. 4.32. At certain locations slip develops linearly (10R,3L), whereas at others a non-linear behavior is observed (10L,3R). The averaged values of relative slippage were calculated and plotted on the fig. 4.33. The effective shear stiffness was calculated and presented in the table 4.9. Between two force intervals and increase of 26% is observed.

4.4.2.4 Normal stresses at the mid span section

The normal stresses for different load levels and two shear connector arrangements are shown on the fig. 4.34. The neutral axis (n.a.) for both arrangements remains in the web, however, its position increases with the increasing load. The location of the n.a. is summarized in the table 4.10. For U-26 a shift of 37.5mm

(a) U-26 connector arrangement   (b) NonU-14 connector arrangement
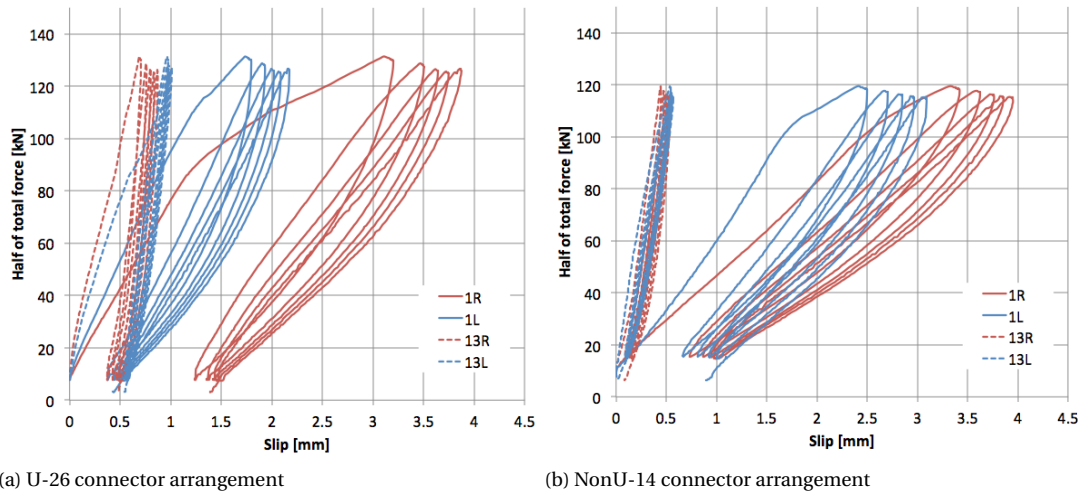
Figure 4.30: End slip on both ends and sides of the composite beam for various shear connector arrangements during second cycle loading

(a) U-26 connector arrangement   (b) NonU-14 connector arrangement
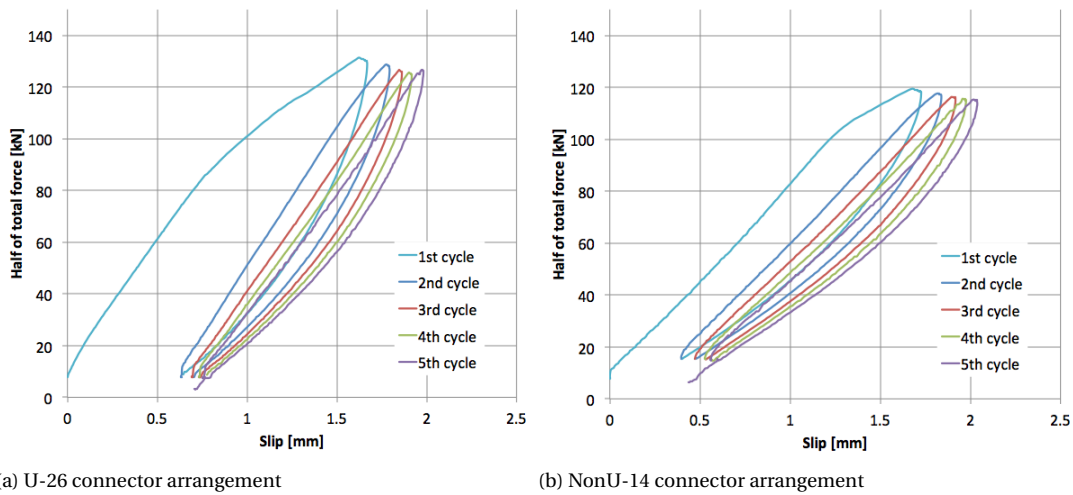
Figure 4.31: Averaged end slip for various shear connector arrangement during second cycle loading

(17%) in neutral axis location between 0.5WL and 2.0WL is observed. For NonU-14 the shift of n.a. position is 14.2mm (6.3%)

4.4.2.5   Vertical separation

Similarly to the first life cycle tests, the obtained data on slab uplift during second life cycle tests did not show consistent results. Figure 4.35 demonstrates the development of vertical separation at different locations for two shear connector arrangements. The uplift on left and right sides of the beam do not show symmetrical results.

4.4.2.6   Analytical analysis of 2nd cycle tests

Similarly to the first life cycle test U-26 the analytical solution can be applied to the U-26 configuration in the second life cycle. However, the assumption of the initial shear connector stiffness $k_{sc} = 20kN/mm$ does not seem correct as the specimen demonstrated a decrease in bending, averaged shear stiffness and drop in the

Arrangement	$k_{s,eff}$		Change in stiffness
	40kN-70kN	70kN-100kN	between two intervals
U-26 (Averaged)	94.96 kN/mm (-)	100.77 kN/mm (-)	+14.7%
NonU-14 (Averaged)	65.85 kN/mm (-31%)	72.30 kN/mm (-28%)	+9.8%
U-26 (LVDT 1L,1R)	54.07 kN/mm (-)	58.88 kN/mm (-)	+8.9%
NonU-14 (LVDT 1L,1R)	42.25 kN/mm (-22%)	35.20 kN/mm (-40%)	-6.7%
U-26 (LVDT 13L,13R)	333.33 kN/mm (-)	314.05 kN/mm (-)	-5.8%
NonU-14 (LVDT 13L,13R)	260.87 kN/mm (-22%)	260.87 kN/mm (-17%)	0%

Table 4.8: Effective end slip shear stiffness $k_{s,eff}$ for various shear connector arrangements in second life tests

(a) U-26 connector arrangement   (b) NonU-14 connector arrangement
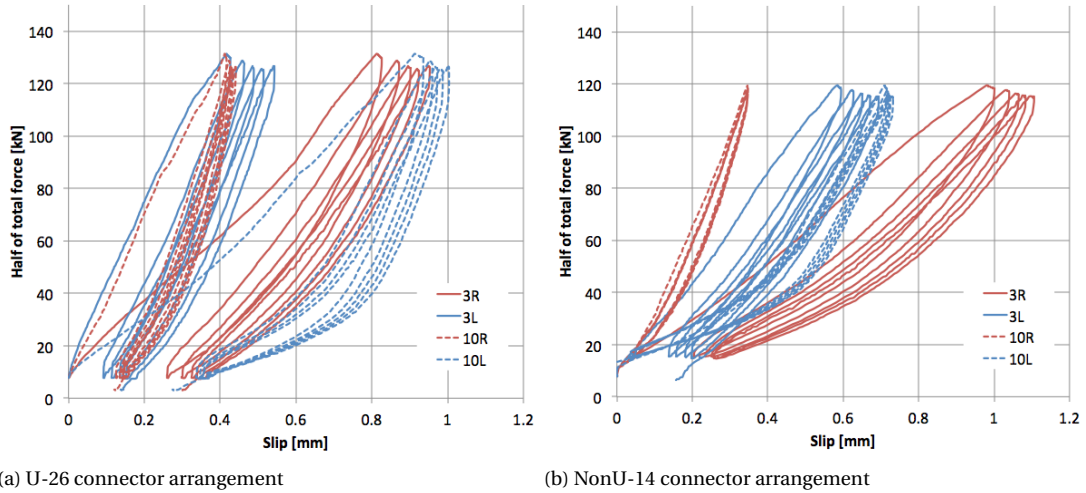
Figure 4.32: Relative slippage on both ends and sides of the composite beam at intermediate connector for various shear connector arrangement during second cycle loading

(a) U-26 connector arrangement   (b) NonU-14 connector arrangement
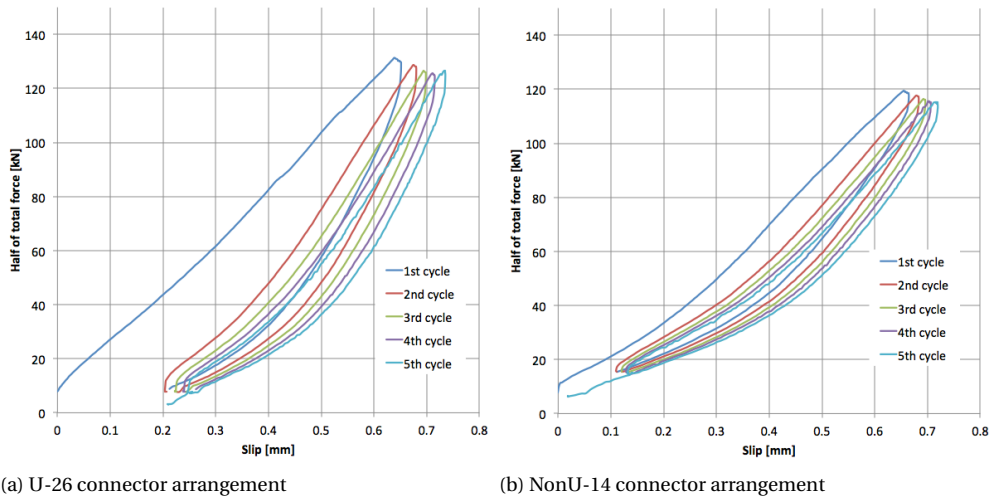
Figure 4.33: Averaged relative slippage at intermediate connector for various shear connector arrangement during second cycle loading

neutral axis position. Therefore the analytical solution was applied in an inverse order. Various initial stiffnesses of shear connectors were studied in order to obtain an agreement for effective bending stiffness and location of the neural axis in the steel section. The shear connector stiffnesses between k_{sc} = 10kN/mm and k_{sc} = 30kN/mm are analyzed and corresponding effective bending, shear stiffness and neutral axis location are presented in the table 4.11.

| Arrangement | $k_{s,eff}$ | | Change in stiffness |
	40kN-70kN	70kN-100kN	between two intervals
U-26	243.93 kN/mm (-)	300.82 kN/mm (-)	+24.6%
NonU-14	174.70 kN/mm (-28.4%)	223.90 kN/mm (-25.6%)	+28.2%

Table 4.9: Effective shear stiffness $k_{s,eff}$ at intermediate connector for various shear connector arrangements

(a) U-26 connector arrangement   (b) NonU-14 connector arrangement
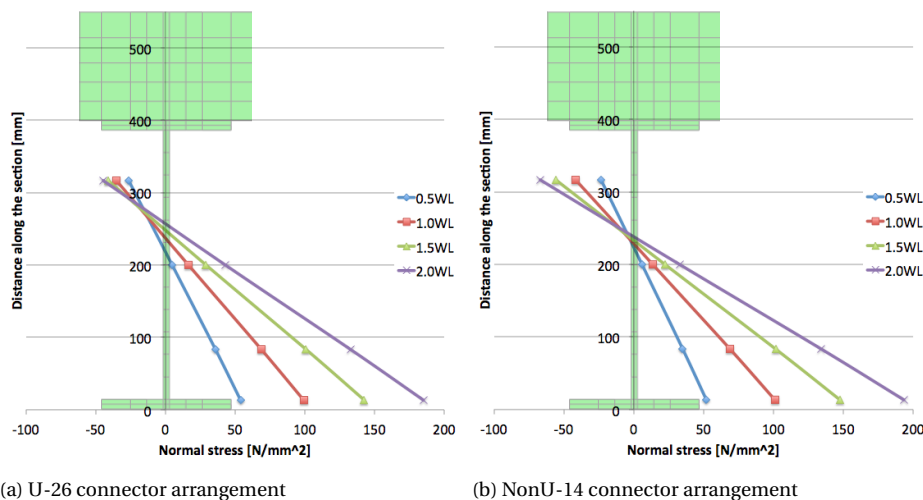
Figure 4.34: Normal stresses at the mid span section for various shear connector arrangement during second cycle loading

From the table 4.11 it can be concluded that the realistic value for the shear connector stiffness lies between 10kN/mm and 15kN/mm. For the value $k_{sc} = 12$kN/mm the analytically obtained and experimental effective bending stiffness have a difference of around 2%, for the location of neutral axis the difference is 3%, however the effective shear stiffness is underestimated by nearly 50% with analytical solution.

4.4.3. Comparison of two life cycles results

First and foremost, the bending stiffness of the specimen demonstrated a decrease in the second life cycle after the longitudinal cut and re-assembly of the slab. For U-26 a drop of 13.4% is observed, whereas for NonU-14 a decrease is, on average, 7.65 %. The comparison between the effective bending stiffness parameter for two life cycle tests and two shear connector arrangements is summarized in the table 4.12.

The bending stiffness of a composite section in elastic stage is based on bending stiffness of a steel section, of a concrete slab and initial stiffness of a shear connector. Therefore, a decrease in bending stiffness of the composite beam during second life cycle tests happened due to decrease in stiffness of the individual components. It can be ruled out that the steel beam bending stiffness was affected during the cutting and re-assembly procedure. The bending stiffness of the slab, on contrary, might have been affected due to a change in longitudinal stress distribution across the slab width after cutting. Alternatively, the initial stiffness of the shear connectors might have got affected, potentially, by the damages which could have had occurred during re-assembly.

| | Position of the neutral axis in steel beam (from bottom of steel section) | |
Load level	U-26	NonU-14
0.5WL	220.5 mm (-)	224.8 mm (-)
1.0WL	238.3 mm (+8.1%)	229.5 mm (+2.1%)
1.5WL	248.6 mm (+12.7%)	233.3 mm (+3.8%)
2.0WL	258.0 mm (+17.0%)	239.0 mm (+6.3%)

Table 4.10: Position of the neutral axis in the steel beam section for various shear connector arrangement during second cycle loading
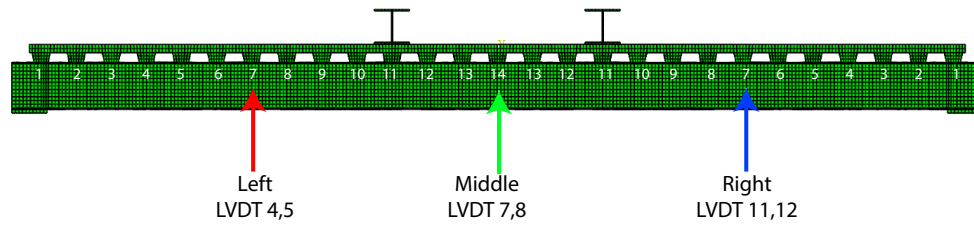
(a) Indication of LVDT's
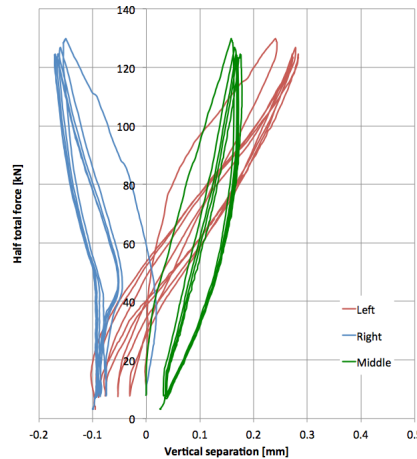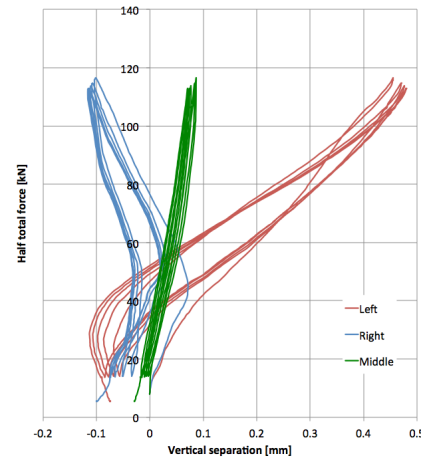
(b) U-26 connector arrangement (c) NonU-14 connector arrangement

Figure 4.35: Vertical separation between steel beam and concrete slab at different locations for various shear connector arrangement during second cycle loading

Initial stiffness of the shear connector k_sc [kN/mm]	Effective bending stiffness $k_{b.eff}$ [kN/mm]	Effective shear stiffness $k_{s.eff}$ [kN/mm]	Position of the neutral axis (from bottom of steel section) [mm]
10	4.16	45.81	257.39
12	4.39	50.75	265.56
15	4.70	58.16	276.45
20	5.12	70.52	291.66
30	5.77	95.24	314.45

Table 4.11: Effective bending, shear stiffness and neutral axis position for various shear connector initial stiffness according to analytical solution

Therefore, a potential explanation for the decrease in effective bending stiffness of the composite beam during second life cycle can lie in the decrease of the components of the composite beam. It can be ruled out that the steel section h

The position of the neutral axis for same connector arrangements dropped in the second life cycle testings. Table 4.13 illustrates the comparison of neutral axis location. For U-26, on average, a decrease of 14.8% is observed, for NonU-14 the neutral axis shifted downwards by 3.9%.

The averaged effective shear stiffness $k_{s,eff}$ based on the end slip development demonstrates, in general, a decrease of 15.6 % for U-26 and 2.8% for NonU-14 as shown in the table 4.14. However, when comparing the end slips on both ends of the beam individually, the stiffer end (LVDT 13) has become even more stiffer, whereas the weaker side of the beam (LVDT 1) has shown a decrease in the shear stiffness.

For the relative slip at the intermediate connector a large increase of 94.1% in shear stiffness in the second life cycle was observed compared to the first one, as can be seen from the tab. 4.15. A potential reason for this behavior might be in the injection procedure, which was followed in the second life cycle. The resin was fist

Arrangement	Force interval	Effective bending stiffness $k_{b,eff}$	
		1st life cycle	2nd life cycle
U-26	40kN-70kN	4.73 kN/mm	4.10 kN/mm (-13.3%)
	70kN-100kN	5.18 kN/mm	4.48 kN/mm (-13.5%)
NonU-14	40kN-70kN	3.77 kN/mm	3.46 kN/mm (-8.2%)
	70kN-100kN	4.08 kN/mm	3.79 kN/mm (-7.1%)

Table 4.12: Comparison of effective bending stiffness $k_{b,eff}$ for two life cycles for various shear connector arrangements

Arrangement	Load level	Location of n.a. (from bottom of steel section)	
		1st life cycle	2nd life cycle
U-26	0.5WL	268.0 mm	220.5 mm (-17.7%)
	1.0WL	280.9 mm	238.3 mm (-15.2%)
	1.5WL	287.3 mm	248.6 mm (-13.5%)
	2.0WL	295.7 mm	258.0 mm (-12.7%)
NonU-14	0.5WL	236.1 mm	224.8 mm (-4.8%)
	1.0WL	237.9 mm	229.5 mm (-3.5%)
	1.5WL	242.6 mm	233.3 mm (-3.8%)
	2.0WL	247.2 mm	239.0 mm (-3.3%)

Table 4.13: Comparison of n.a. location during first and second life cycles (distance from bottom of steel section)

Arrangement	Force interval	Effective shear stiffness $k_{s,eff}$	
		1st life cycle	2nd life cycle
U-26	40kN-70kN	109.72 kN/mm	94.96 kN/mm (-13.5%)
	70kN-100kN	123.22 kN/mm	100.77 kN/mm (-18.2%)
NonU-14	40kN-70kN	65.60 kN/mm	65.85 kN/mm (+0.4%)
	70kN-100kN	76.92 kN/mm	72.31 kN/mm (-6.0%)

Table 4.14: Comparison of effective shear stiffness $k_{s,eff}$ for two life cycles for various shear connector arrangements

Arrangement	Force interval	Effective shear stiffness $k_{s,eff}$	
		1st life cycle	2nd life cycle
U-26	40kN-70kN	123.78 kN/mm	243.93 kN/mm (+97.1%)
	70kN-100kN	164.42 kN/mm	300.82 kN/mm (+83.0%)
NonU-14	40kN-70kN	83.33 kN/mm	174.7 kN/mm (+109.6%)
	70kN-100kN	120.0 kN/mm	223.9 kN/mm (+86.6%)

Table 4.15: Comparison of effective shear stiffness $k_{s,eff}$ at intermediate connector for two life cycles for various shear connector arrangements

injected at the middle connectors towards the end. It is well possible that the unwanted adhesion took place at the connectors close to mid span and, therefore, contributed to a stiffer behavior of the specimen at the intermediate connectors.

Another observation that could potentially explain the abnormally high shear stiffness is the positioning of the wooden cantilever supports, which ensured the stability and safety of the setup. The wooden triangular structures were connected on both sides over the top of slab by means of highly tensioned band. In comparison to the first life cycle tests three additional supports were install in second life cycle tests, located every 900mm. The location of wooden supports is indicated in the figure 4.36. It can be well possible that the presence of additional triangular wooden supports had provided extra resistance for the slip development at both intermediate connectors and end of the beam.

Figure 4.36: Indication of the cantilever support placed next to LVDT 3L,3R,10L,10R

4.4.4. Failure

The test for determining the maximum bending capacity of the composite beam had to be performed in three loading-unloading passes. The reasons for that was the limited capacity of the jack stroke and the reached maximum range of several LVDT's, which were adjusted each time after unloading.

During the last loading the stroke capacity of the jack was exceeded and, therefore, the test was terminated. From the obtained load-mid span deflection curve it can be seen that the curve was reaching a plateau, which can be interpreted that the ultimated bending capacity of the beam was reached at the averaged load of 225kN as depicted on the fig. 4.37 a. In the table 4.16 the failure load and corresponding ultimate bending moment capacity are summarized.

The linear-elastic limit is reach at 60% of the maximum load. Since a displacement controlled loading was used, the applied point loads did not develop equally and the difference between two loads at the end of the test was 25%, which is demonstrated on the fig. 4.37 b.

Test	P, kN	Ultimate bending moment capacity excluding self-weight kNm	Ultimate bending moment capacity including self-weight kNm
B4	225	697.5	748.5

Table 4.16: Ultimate moment capacity

(a) Averaged force - mid span deflection

(b) Force per jack - deflection at 6th trough location
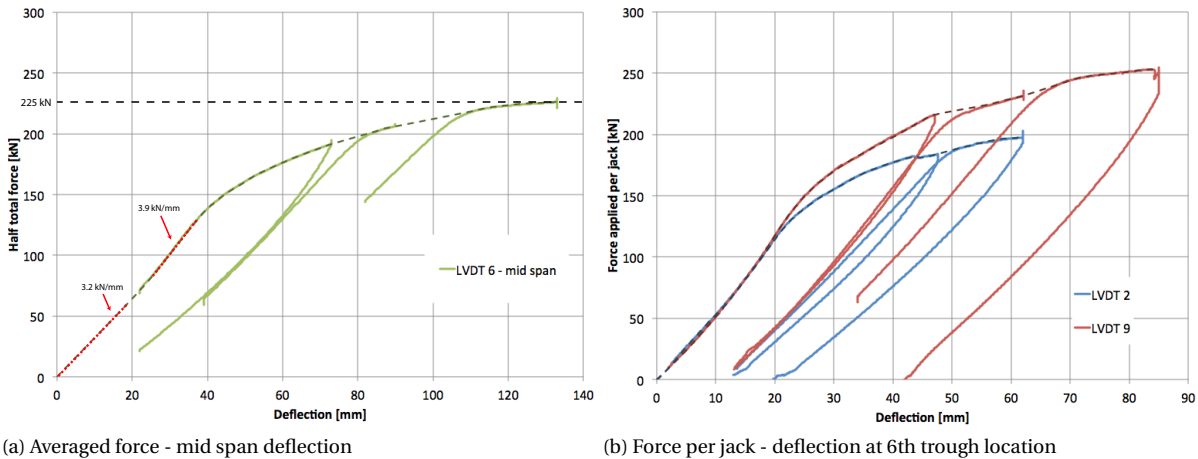
Figure 4.37: Load-deflection behavior of the specimen during failure loading

Although the beam was manufactured symmetrically the slip on one side developed considerably more, compared to the other, what was already pointed out during series of elastic tests. The averaged end slip and relative slippage at the intermediate connectors are presented in the figure 4.38. While the end slip recorded by LVDTs 13L,R develops linearly, the end slip on the other end of the beam (LVDTs 1L,R) demonstrates an increase of stiffness at higher loads. The slips on both ends developed linearly until 60% of the maximum load.

During the test it was observed that on one side (LVDT 1L, 1R) the two half-slabs were distancing from each other, opening a larger gap at the location of timber joist. This contributed to the loss of confinement provided by timber piece and therefore the maximum shear resistance of a connector on that end of the beam has also decreased.

(a) End slip

(b) Relative slip at 7th connector
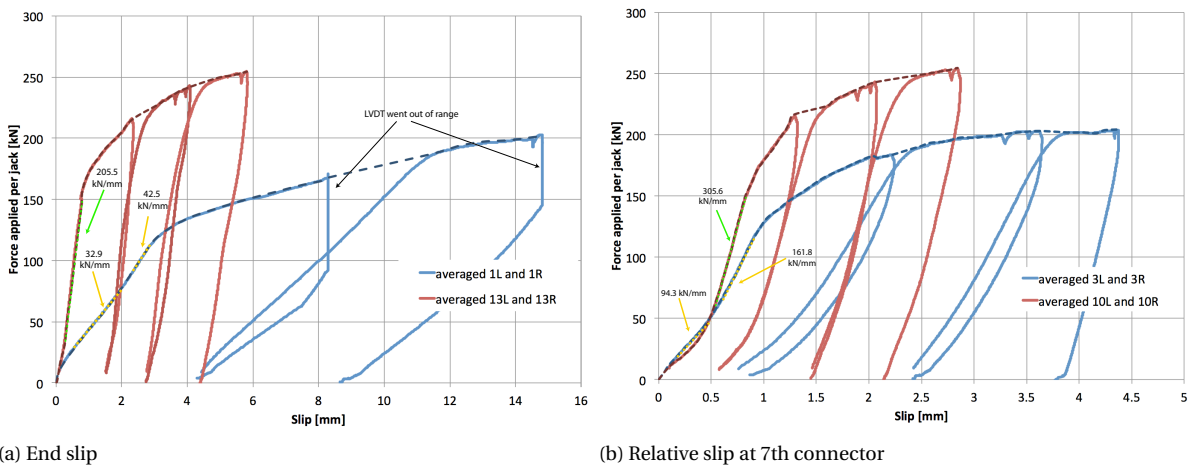
Figure 4.38: Development of end slip and slippage at the intermediate connector during failure loading

4.4.4.1 Analysis of bending moment capacity

The bending moment resistance at critical cross section was also calculated by means of rigid plastic theory. The positive contribution to the bending moment resistance of the metal sheeting and reinforcement bars is not taken into account. The strength of steel and concrete were assumed as: $f_{yd} = 355 N/mm^2$ and $f_{cd} = \frac{30 N/mm^2}{1.5} = 20 N/mm^2$

Number of shear connectors to mid span is $n_{sc} = 14$. The shear connector resistance is $P_{Rk} = 59 kN$.

$N_{sc.Ed} = P_{Rk} \cdot n_{sc} = 826 kN$ Compression force in the slab

$N_{a.Rd} = A_a \cdot f_{yd} = 2999.75 kN > 826 kN$ Tension resistance of the beam

$N_{w.Rd} = t_w \cdot h_w \cdot f_{yd} = 1138.8 kN > 826 kN$ Tension resistance of the web

$N_{f.Rd} = \dfrac{N_{a.Rd} - N_{w.Rd}}{2} = 930.5 kN$ Tension resistance in the fange

$N_{sc.Ed} = 826 kN < N_{w.Rd} = 1138.8 kN \rightarrow$ PNA lies in the web

$N_{c.Rd} = 0.85 \cdot f_{cd} \cdot h_c \cdot b_{eff} = 2380 kN$ Compression resistance of concrete

$x_c = h_c \cdot \dfrac{N_{sc.Ed}}{N_{c.Rd}} = 24.3 mm$ Depth of concrete in compression

$\eta = \dfrac{N_{sc.Ed}}{\min(N_{c.Rd}, N_{a.Rd})} = 0.35$ Degree of shear connection

Plastic bending moment resistance of composite beam (PNA in web):

$$M_{pl,comp} = N_{sc.Ed} \cdot (h_a/2 + h_p + h_c - x_c/2) + W_{a.pl} \cdot f_{yd} - \frac{N_{sc.Ed}^2}{4 t_w f_{yd}} = 687.2 kNm$$

The beam test is conducted with 2 point loads P located at 3.1m from the supports to create a constant shear zone. Therefore the bending moment, including the self-weight, is given by:

$$M_{Ed} = 3.1 P + \frac{3.2 kN/m \cdot 2m \cdot (8m)^2}{8} = 3.1m \cdot P + 51 kNm$$

Therefore, the point load at failure $P = (687.2 - 51)/3.1 = 212 kN$

The comparison of a predicted and measured bending moment resistance of the composite beam is summarized in the table 4.17. It can be seen that the rigid plastic theory gives a conservative estimation of the maximum bending resistance. For the case when the shear connector resistance is taken as $P_k = 59 kN$, the calculated bending moment resistance is 10% smaller than the value obtained from the experiment.

No	Shear connector resistance P_R		Degree of shear connection		EC4 rigid plastic theory M_{exp}/M_{calc}	
			$P_k = P_R$	$P_k = 0.9 P_R$	$P_k = P_R$	$P_k = 0.9 P_R$
B4	59 kN		0.35	0.31	1.10	1.12

Table 4.17: Comparison of ultimate moment capacities

4.5. Summary

4.5.1. Summary of 1st life cycle tests

For the first life cycle a total of 3 arrangements of shear connectors were tested. The serviceability limit criterion of 32mm was fulfilled by all shear connector arrangements for working load (WL) regime. The formula provided by 1994-1-1+C1/NB [7] greatly underestimates the deflection of composite beam (by 32.8% for 1.0WL). The deflection predicted by analytical solution demonstrated under-prediction of 19.7%. Therefore the applied formulas cannot be safely used to predict the maximum deflection of the demountable composite slab floor system in first life cycle.

The effective bending stiffness for various shear connector arrangements did not remain constant within the evaluated force intervals and showed an increase of 8%, on average. For U-26 configuration the effective bending stiffness was worked out using the analytical solution. It was demonstrated that for the force interval of 70kN-100kN the difference between experimental and analytical results was 1.2%.

Although the beam was manufactured symmetrically, one side of the beam always showed a higher stiffness compared to another, despite the fact that equal point load forces were applied to both sides of the beam. In general, a difference of 1.5-2 times in the effective shear stiffness on both ends was observed depending on the shear connector configuration. The origin of that behavior can be explained by the presence of adhesion between the metal decking and the steel beam at certain locations, caused by excessive flow of resin during injection and concrete during casting procedures.

In general, the development of end slip was comparable for all connector arrangements tests. At initial stage, when the force of around 30kN per jack was applied, the initial shear stiffness of the specimen was higher. Afterwards, a small decrease in the shear stiffness was observed, which was followed by a gradual increase. On average, the effective shear stiffness demonstrated an increase of 20% for the tested connector arrangements between two evaluated force intervals. The prediction of the effective shear stiffness by analytical solutions had demonstrated a poor agreement. The actual effective shear stiffness of the specimen was, on average, 36% larger than expected. The stiffer behavior of the specimen most likely was caused by the concrete and resin presence at the interface of metal decking - beam flange.

The location of the neutral axis for all connector arrangements remained in the steel web. The position of the neural axis was shifting gradually upwards with the increasing load. This observation is in accordance with the facts that the effective bending and effective shear stiffnesses of the specimen also demonstrate growth as the applied load increases. The hand calculations to determine the position of the neutral axis and magnitude of the normal stress were carried out and demonstrated a good agreement with the experimental results.

Given the discrepancy in the experimental results of vertical uplift, especially for the connector arrangement NonU-14, the question of the reliability of the obtained data can be raised and, therefore, more investigations have to be carried out. Nevertheless, the absolute value for the measured vertical separation between the slab and steel beam did not exceed 0.7mm, which could indicate that in the elastic stage the uplift of the slab is not significant.

4.5.2. Summary of 2nd life cycle tests

For the second life cycle 2 arrangements of shear connectors were tested. The serviceability limit criterion of 32mm was fulfilled by both shear connector arrangements for working load regime.

The effecting bending stiffness for various shear connector arrangements did not remain constant within the evaluated force intervals and showed an increase of 9.4%, on average.

In the second life cycle tests the difference in the shear stiffness of both ends of the slab had increased to nearly 5 times. The shear stiffness of the specimen on the stiffer end was 323.7kN/mm for U-26, which is unusually high for the bolted shear connector initial stiffness of $k_{sc} = 20$kN/mm. The likely explanation for this behavior is the presence of the wooden supporting structure, which could have acted beneficially in transferring the longitudinal shear from the slab to the steel beam.

The development of the end slip demonstrated a rather linear behavior, however the development of the

relative slippage at the intermediate connector showed a tendency of increasing shear stiffness of, on average, 26.4% between two force intervals. The behavior might originated either from the injection procedure or from the presence of the wooden cantilever supporting structure.

Moreover, the development of the slip at intermediate connector at different locations of the composite beam demonstrated a rather big scatter, compared to the similar measurements at the ends of the slab. This behavior could originate from the relative slip generated at the interface between metal decking and concrete slab.

Similarly to the first life cycle tests the location of the neutral axis shifted upwards with the increasing load. For the U-26 arrangement this behavior is more pronounced and demonstrates an increase of 17% (37.5mm) between 0.5WL and 2.0WL, whereas for NonU-14 the neutral axis went up by 6.3% (14.2mm) between same load levels.

Previously used analytical model for the prediction of bending, shear stiffness and neutral axis location were based on the assumption of the initial connector stiffness of $k_{sc} = 20kN/mm$. For the second life cycle tests this assumption was no longer valid at the specimen had demonstrated an overall decrease in bending and shear stiffnesses. Therefore the analytical model was used in an inverse order to propose a realistic assumption for the connector initial stiffness. It was found that $k_{sc} = 12kN/mm$ provides a good agreement with experimental results in terms of effective bending stiffness and new location of the neutral axis. Nevertheless the prediction of effective shear stiffness remained highly (by almost 50%) underestimated.

4.5.3. Comparison of two life cycle tests

The bending stiffness of the composite beam did not remain the same in two life cycles. The effective bending stiffness parameter was evaluated for two load intervals for all tests. Based on that parameter it can be concluded that after the cutting and re-assembly of the slab the specimen demonstrated a decrease of 13.2 % in bending stiffness for U-26 and 7.7% for NonU-14 arrangements. It was observed that the effective bending stiffness has a tendency to increase with the increased applied load. For the 1st life cycle tests the bending stiffness increased by 8.5%, whereas during 2nd life cycle tests it demonstrated an increase of 9.4%.

In the second life cycle tests a decrease of the averaged shear stiffness for the end slip and more linear behavior was observed. However, the absolute difference between the end slips on both ends of the beam had increased from 2-2.5 to more than 5 times.

The relative slippage at the intermediate connector during second life cycle has also shown a significant increase of 94.1% compared to first life cycle.

A drop in the position of the neutral axis in second life cycle tests was observed. For the U-26 shear connector arrangement a shift downwards of neutral axis was, on average, by 14.8%, whereas for NonU-14 a decrease of 3.9% was noted.

4.5.4. Failure

During the failure loading the specimen demonstrated highly unsymmetrical behavior. A displacement controlled loading was used and at the loads close to the failure the difference in the applied forces was 25%.

During the test it was observed that at the end of the beam with a smaller shear stiffness an opening at the timber joist location was becoming larger. This had contributed to a loss of a positive effect of the confinement, which was ensured by timber piece and therefore the shear resistance of the connector was reduced on that end. The application of the edge trims at the location of the timer joist can potentially increase the ductility and shear resistance of the connector. The stiffer end of the composite beam demonstrated abnormally high initial stiffness and maximum resistance.

When averaging the applied point loads a failure load of 225kN was obtained. The ultimate moment capacity of the demountable composite beam predicted by plastic theory was 10% smaller compared to the experimental results.

4.6. Practical recommendations for the use of demountable flooring systems

Based on a conducted experimental work it was proven that the in-situ casted composite beam with demountable shear connectors and resin injected bolts can be relatively easy demounted after first life cycle and placed back to its original location for a second life cycle in laboratory conditions. However, a number of challenges regarding the preparation of the specimen for second life cycle was encountered and, therefore, recommendations for practical use of demountable composite floor system are summarized below.

4.6.1. Longitudinal cut

Experiments have shown that it was not entirely possible to create a perfectly straight longitudinal cut in the middle of the slab. This fact affects significantly the re-assembly procedure. It was proven that halves of the separated slab do fit each other, nevertheless, it can not be guaranteed that two arbitrary half-slabs would fit to each other in the second life cycle.

This potential problem can be tackled in several ways. Firstly, more advanced and precise tool can be used for the cutting procedure, which would guarantee the straightness of the longitudinal cut. Alternatively larger tolerances have to be adopted. In the conducted experiment a cut of 3mm wide was performed, which in practice does not provide sufficient freedom for the re-assembly. A potential solution is to preform wider or multiple cuts. Or alternatively the slab can be cast with a discontinuous reinforcement and taller timber separation as shown in the fig. 4.39 a. In this case the thickness of the timber separation can be reduced. This design is more favorable in terms of dismantling and re-assembly. However, because of discontinuous reinforcement, the cracking of the concrete over the timber joist is likely to appear due to concrete shrinkage. Further investigation on the design of longitudinal joint have to be carried out.

(a) Discontinous slab   (b) Semi-continious slab
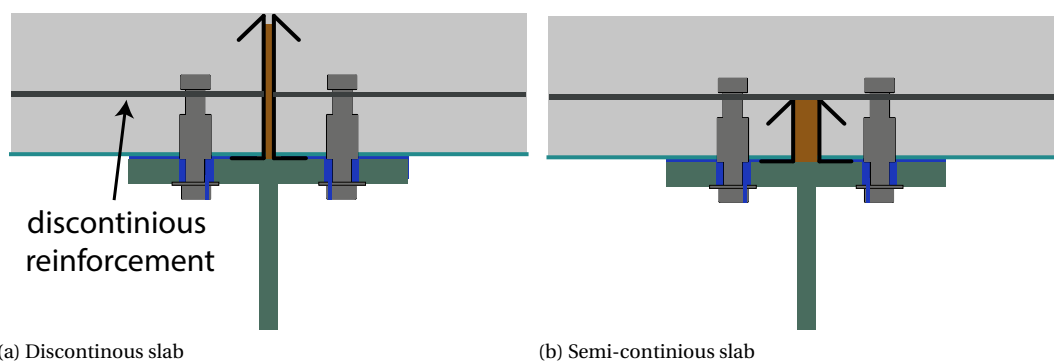
Figure 4.39: Types of slab with timber separation

Additionally, it was not possible to make a complete cut at the slab end through concrete and edge trim together. Instead, an additional tool had to be used to accomplish the full separation of the slab halves. Therefore, the use of the edge trims as a formwork at the perimeter of the specimen should be avoided or, alternatively, the edge trim has to be discontinuous, with a separation at the location, where the timber piece is located.

It was found that when longitudinal cut was made, the half slabs were still well connected to each other due to the adhesion to the wooden piece. Therefore, the use of edge trims between the slab and timber separation is recommended. The edge trim can be placed in two ways as shown on figure 4.40. If the bottom side of the edge trim is shorter than the distance to the bolt, then the installation is rather easy, nevertheless for the resin injection procedure it might become problematic. Due to additional thickness of the edge trim the metal decking might not be in a perfect contact with the top flange steel beam and therefore additional space will be created for the resin to flow during injection. It would result in a higher resin consumption and additional adhesion. Alternatively the edge trim bottom side can be enlarged, which would require pre-drilling of the holes. It is more labor extensive installation, however it could potentially improve the resin injection procedure by preventing resin over-flow and adhesion.

(a) Longer edge trim   (b) Shorter edge trim
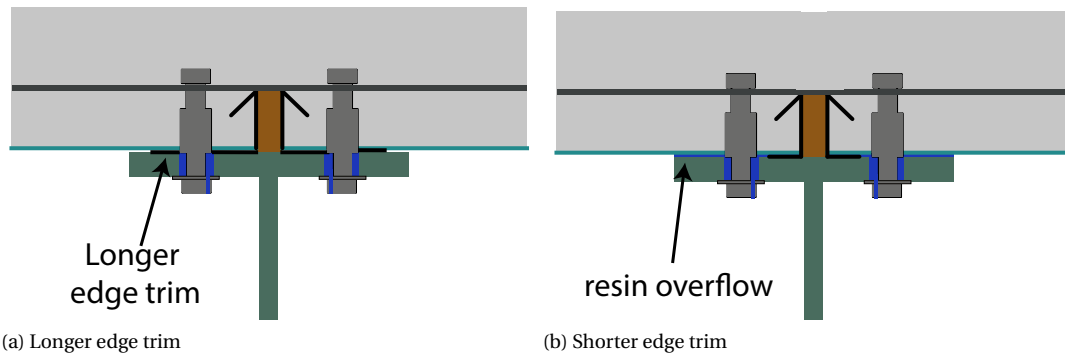
Figure 4.40: Edge trim between the slab and timber separation

4.6.2. A possible uplift procedure

The uplifting of the half of the slab posed an additional challenge and for lab staff and researchers. However, for this concept to be able to be used in the real-life conditions at the construction site, a safer and quicker procedure has to be developed.

In the laboratory conditions only part of the composite floor was tested, in which sides of the slabs were hanging unsupported as a cantilever, which makes the uplifting of the flooring system in the laboratory more complicated and the use of temporary props is required for the stability. Moreover, since there is no mechanical connection between the lifting beam and half slab there is a risk that the slab might tilt and slide off the lifting beam. In practice, however, the composite slab spans between the supporting steel beams and the stability of the system does not pose an issue after cutting procedure. Nevertheless, the application of the lifting beam as a tool to remove the slabs is not practical for industrial use and, therefore, an alternative concept has to be used.

In contrary to the prefabricated concrete slabs, the in-situ casted slab with metal decking is more flexible and cannot be lifted by supporting it on both ends as shown on the fig. 4.42. The possible solution is the application of a lifting vehicle, which would uplift the slab from below on a platform. A schematic concept of such a device is demonstrated on the fig.4.41. The attention has to be paid to the self weight of the vehicle and additional load of the lifted slab(s), when needed the additional supports have to be installed under the lower floor level. Alternatively, an application of the vacuum lifter can be adopted, which is shown on the fig. 4.43.
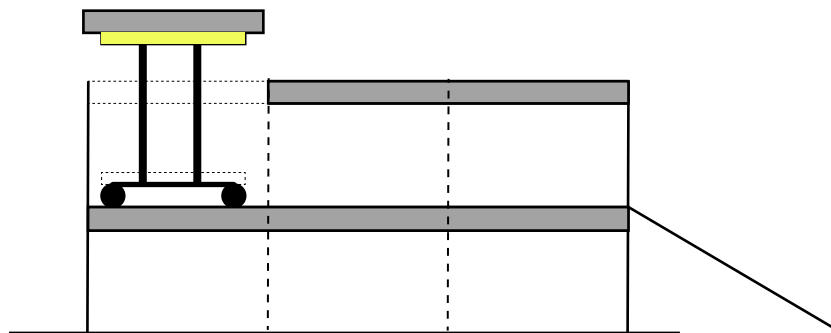
Figure 4.41: Schematic representation of a slab lifting vehicle

The proposed solutions serve as an indication of future research lines and more detailed study of possible execution processes has to be conducted in a collaboration with the professionals who have experience and knowledge in the field of construction management.

(a)   (b)
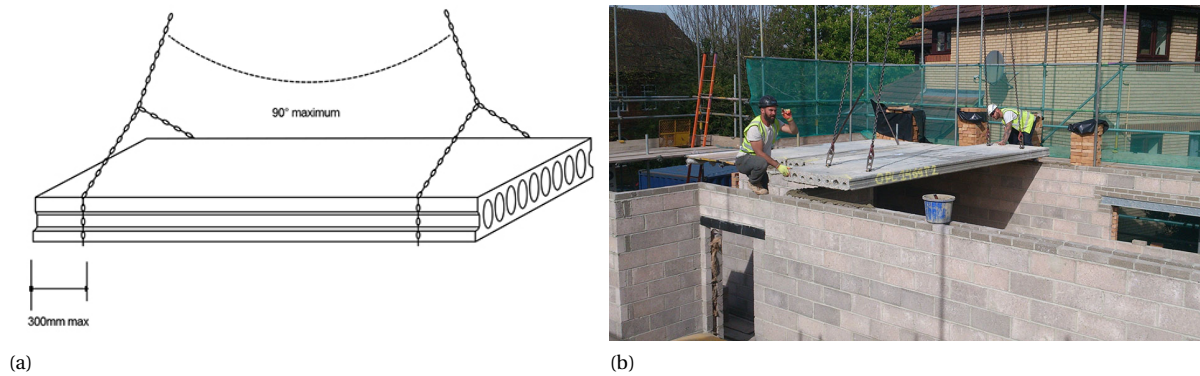
Figure 4.42: Lifting of the hollow core slab

Figure 4.43: Vacuum lifter - up to 20000kg

4.6.3. Steel beam tolerances

With help of additional tools it was possible to remove and place back the bolts after the cutting and uplifting of the half slabs. However, it is highly unlikely that the re-assembly would be successful if the half-slab would be placed to the opposite side of the steel beam or to another identical beam, because a large amount of bolts were already in contact with the beam top flange when specimen arrived to the lab. Therefore, it can be concluded that 26 mm hole clearance it sufficient for successful demounting of the composite slab, however, for a successful reuse of the slab a larger clearance of the hole on the steel beam flange is required. Similar conclusion was drawn in the work conducted by Gîrbacea [14] when performing the feasibility study on the composite beam with prefabricated solid slabs with bolted shear connectors.

4.6.4. Resin injection procedure

In order to re-use the whole composite floor system, the steel beam has to be cleaned from injected resin prior to the second life cycle. The procedure of removing the parts of remained resin from the groove was not very fast and efficient, because the resin was well connected to the beam. In order to facilitate this process, a release agent has to be applied prior to the casting.

In this experimental study grooves have been used as an indication of successful injection. However, in fu-

ture the grooves have to be eliminated and the injection should be based on a fixed volume of the resin. Depending on the type of epoxy resin hardener, steel top flange thickness and diameter of pre-drilled hole the consumption of resin can vary from structure to structure. Therefore more experimental work has to be conducted to quantify sufficient amount of resin needed for successful bolt injection depending on the parameters of the connector.

4.7. Conclusions

- It was demonstrated that dismantling and re-assembly is possible in laboratory conditions. However, for this concept to be successfully applied in the practice a number of recommendations and future research guidelines were proposed in section 4.6.

- The serviceability limit criterion of 32mm was fulfilled by all shear connector arrangements in both life cycles for working load (WL) regime.

- The analytical solution provides a good prediction of the effective bending stiffness and location of the neutral axis for the first life cycle results. However, the development of end slip is not captured well by the analytical model.

- The analytical solution and formula provided by 1994-1-1+C1/NB [7] under-predict the mid-span deflection by 32.8% and 19.7%, respectively, for 1.0WL.

- The composite beam had demonstrated a decrease in bending stiffness of 13.2% for U-26 and 7.7% for NonU-14 in the second life cycle.

- A decrease in bending and shear stiffness of the composite beam hypothetically occurred due to the change in longitudinal stress distribution across the slab width, which decreased the effective width or, alternatively, the initial stiffness of shear connectors got decreased by potential damages in the slab during re-assembly. More numerical and experimental investigations have to be carried out to identify the origin of this behavior.

- Based on analytical solution, a new shear connector initial stiffness of $k_{sc} = 12kN/mm$ for second life cycle results was proposed. It provided a good agreement in terms of effective bending stiffness (2%) and location of neutral axis (3%). However, the prediction of effective shear stiffness remained under-estimated (by almost 50%).

- The development of the interface slip for elastic and plastic tests in the second life cycle had demonstrated highly unsymmetrical results for both ends of the beam. An unusually high shear stiffness of 260.9kN/mm was observed for one end, whereas the other end demonstrated stiffness of 38.7kN/mm for NonU-14 configuration. The high shear stiffness of the specimen potentially originated from the application of the wooden cantilever supporting structure, which might have been engaged in the unwanted transfer of longitudinal forces.

- The experimental results have demonstrated that the measured uplift of the slab at several locations is inconsistent between various shear connector arrangement tests. A different method for recording the vertical separation has to be adopted to obtain more reliable data.

- It was demonstrated that the prediction of bending moment resistance by means of plastic-rigid theory is 10% smaller than the experimental result.

<div align="right">5</div>

Numerical analysis

5.1. Introduction

A number of finite element analyses was conducted as a part of this master thesis research project. Several FE models were built, validated with analytical solutions, described in the section 2.2.2 and then calibrated according to the results obtained from experimental works described in the chapter 4. Afterwards, the obtained calibrated models were used to conduct a parametric study to optimize the design of composite slabs. Finite element analyses were performed using Abaqus/CAE version 6.14-1 [41].

FE model description of the 4 point bending test of the composite beams is given in this section. The geometry, connector modeling, loading steps, mesh and material models are presented in following sections.

5.2. Geometry and boundary conditions

Since two types of construction method, propped and un-propped, were tested, two FE models were created in order to reflect the difference in the behavior of composite slabs. Both models consist out of 4 elements: steel beam, metal decking, concrete slab and beam through which the point load is applied, as shown in a figure 5.1.
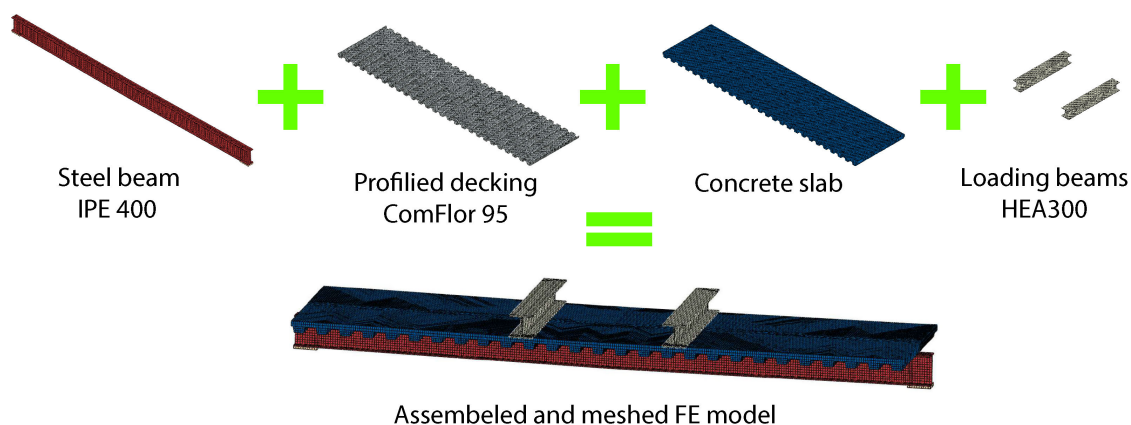
Figure 5.1: Assembled and meshed FE model

Steel beam is 8.3 meters long IPE400 section, with a distance of 8m between supports. The concrete slab is 2 meters wide and 8 long made out of C30/37. The slab is 150mm thick with ComFlor 95 metal sheeting of 0.9mm thickness.

To simplify the problem only half of the span is modeled with a symmetry boundary condition, as indicated in the figure 5.2.
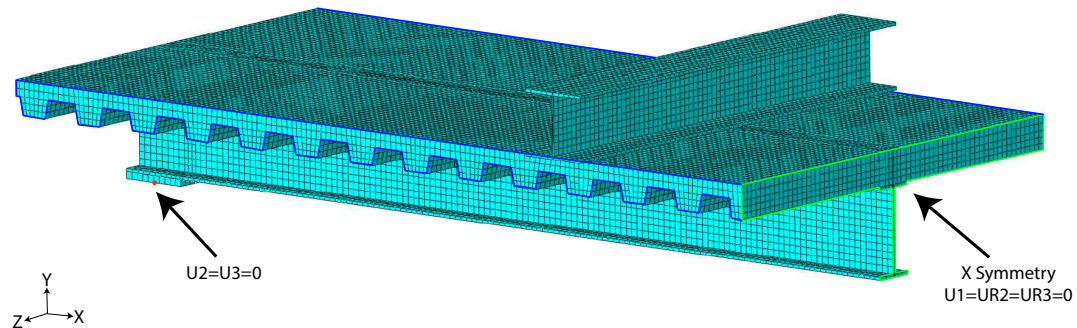
Figure 5.2: FE model of 4 point bending test. Boundary conditions

5.3. Interaction contact and constraint

Once all elements of the FE model were assembled, as shown previously in the figure 5.2, the appropriate contact model, interaction and constrains were defined. For all surfaces in the model the general contact (standard) interaction was chosen. The normal behavior is described by "Hard" Contact, whereas for tangential behavior the Penalty friction formulation is chosen with a friction coefficient of 0.14. For the contact between profiled sheeting and concrete slab a tie constrain was assumed.

Shear connectors between concrete slab and the beam were modeled as non-linear springs in x(along the beam) and z and in y direction the spring is assumed to behave rigidly. The springs were defined between the surface of profiled sheeting and the top flange of the steel beam. The load-slip behavior of the shear connectors was obtained previously from the experiments conducted by Bradford university as a part of EU project REDUCE [42]. The load-slip behavior of bolted shear connector with embedded nut and bolted shear connector with coupler are shown in a figure 5.3.

It is important to mention that in the push-out tests conducted at Bradford university 150mm edge trims were used at the joint between two discontinuous slabs without timber separation. The edge trims provide a strong confinement and therefore increase the shear resistance and ductility of the shear connector.

5.4. Element type and finite element mesh

The three dimensional eight-node solid brick element C3D8R with reduced integration was used to mesh the concrete slab and steel beams. In this type of element, each node has 3 translational degrees of freedom (DOF) and prevents shear locking. In addition, the brick elements might give a solution of comparable accuracy at a better rate of convergence and less computational time needed than using some other elements. The profiled metal decking is very thin material, therefore shell element with reduced integration (S4R) was used. Generally, this type of element is very useful for thin walled structures which might experience large deformation under load. The element size for all elements was chosen as 30mm.

5.5. Loading steps

5.5.1. Propped model

During propped construction method the weight of the wet concrete is carried by temporary supports, until the concrete is hardened. Later, when supports are removed the composite action is achieved and the weight
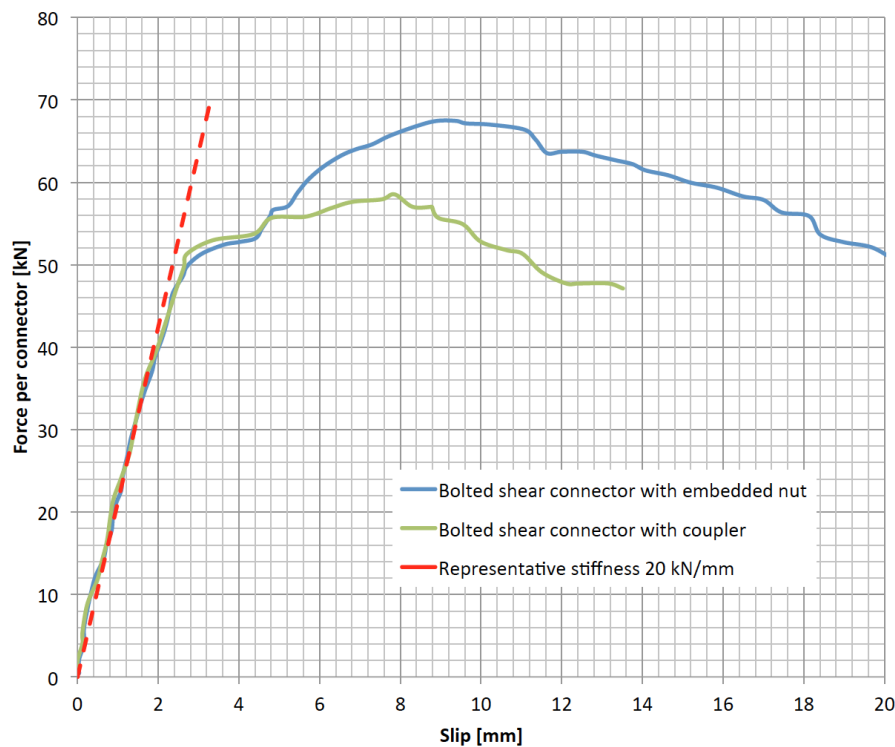
Figure 5.3: Load-slip behavior of two types of bolted shear connectors

of concrete is carried by a composite section.

When FE model is assembled a single step denoting uniformly distributed or point load has to be created. In this way the imposed load will be immediately carried by a composite section.

5.5.2. Un-propped model

During un-propped construction method the composite slabs are executed without temporary supports. Therefore at the initial stage the weight of wet concrete is carried entirely by steel section. However, when concrete is hardened the imposed load will be carried by a composite section.

In order to simulate this construction method with FE model several steps have to be taken. At first, to simulate the properties of wet and hardened concrete the temperature dependent E modulus has to be created. For wet concrete it is assumed to be a very low value of $10N/mm^2$.The shift between wet and hardened concrete properties is done by means of temperature dependent fields.

The casting step is created first, during this stage the concrete E modulus is set low value and the selfweight load is applied to concrete slab. As the result of this step the whole weight of the beam will be carried only by the steel beam.

Next step would be to return the value of E modulus back to its standard value and apply the imposed load. However, a small trick is required at first. The connectors have to be re-set and for that two additional steps are needed in order to disable and enable the connectors. Once this is done, the imposed load can be applied

5.6. Material properties

Since the main focus of this study is the behavior of composite beam under service loads, where there is no plastic deformation, the linear-elastic material models are considered to be sufficiently accurate.

For the S355 steel beam and profiled decking E modulus is set to $210000N/mm^2$ with poisson's ratio of 0.3, the

(a) Shear connectors every 300mm   (b) Shear connectors every 600mm
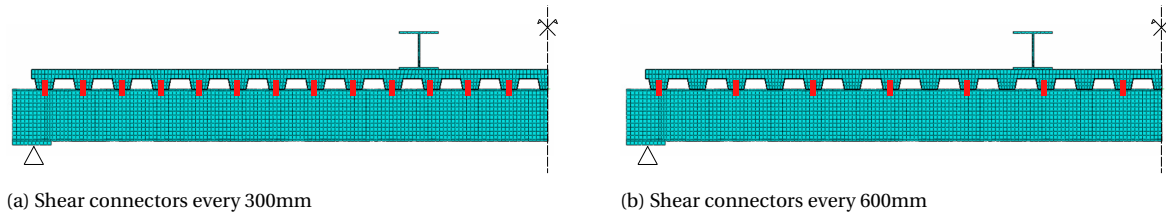
Figure 5.4: Location of uniformly distributed shear connectors

yield stress is set to 355N/mm^2. For the concrete slab E modulus for wet concrete is considered as 10N/mm^2 and for hardened concrete 33000N/mm^2, the poisson's ratio is 0.2.

5.7. Validation using analytical solutions

In this section results of finite element model are compared to the analytical solutions described in the chapter 2.2.2. Those analytical models are applicable for the case of uniformly distributed load and therefore FE models loading was adjusted in order to fit the limitations of the analytical solution. Two models, simulating propped and unpropped construction method, were validated. In addition, a constant connector stiffness of 20kN/mm for the shear connectors was used instead of the test data.

The validation was conducted for 2 types of shear connector distributions: placed in every trough at 300mm distances in pairs and placed in every second trough at 600mm distances in pairs. The arrangements of shear connectors are illustrated on the figure 5.4.

Calculations according to Girhammar and Leskelä approaches were conducted. The effective bending stiffness, midspan deflection and end slip for different load levels were calculated. The detailed calculation are provided in the annex A.

5.7.1. Midspan deflection

Most importantly, the behavior of midspan deflection as a function of applied load was investigated. Figure 5.5 (a) depicts the numerical results for 2 types of connector arrangements and analytical solutions for un-propped beam. Similarly, figure 5.5 (b) represents the propped method. As it can be seen, two analytical solutions (acc. to Girhammar and Leskelä) provide almost identical results which are in a rather good agreement with numerical prediction, slightly under-predicting the deflection. The serviceability limit for the deflection L/250 = 32mm is marked with the red line. Additionally, the midspan deflections for fully rigid beam and beam with no composite action are plotted, indicating the upper and lower limits for the deflection. A black dashed line represents the casting stage, in which only the self weight is applied to the beam. A principal difference between two models is the behavior during the casting stage, it is clear from the plots that for the case of un-propped beam there is no composite action during casting, whereas for the propped beam the composite action is achieved from the beginning.

5.7.2. End slip

Similarly to the midspan deflection, the end slip as a function of reaction force (half of total force) was investigated. Figure 5.6 depicts the numerical prediction and analytical solutions for two type of connector arrangements. Here, two analytical solutions provide slightly different results and both over-predict the end slip compared to the numerical prediction. Analytical solution according to Leskelä is closer to the results of FE modeling. Nevertheless, it can be concluded that the numerical model predicts the linear-elastic behavior of the beam with partial shear interaction with rather good accuracy.

(a) Un-propped

(b) Propped
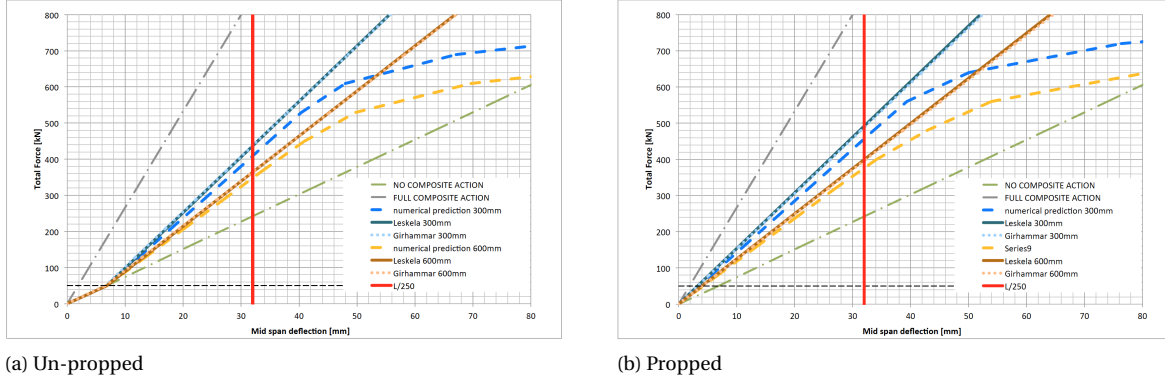
Figure 5.5: Midspan deflection vs total load

(a) Un-propped

(b) Propped
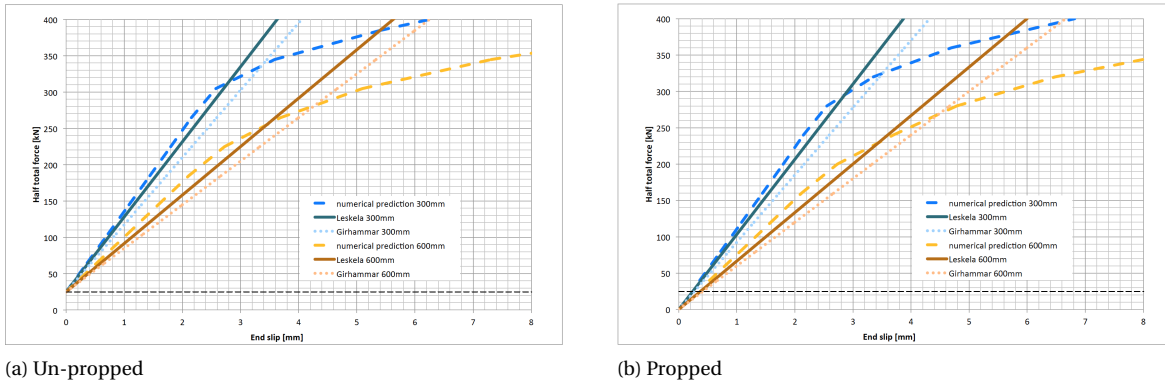
Figure 5.6: End slip vs half of total load

5.7.3. Stresses in the section

In order to verify the FE model, a hand calculation of sectional stresses was conducted and compared to the results obtained from numerical analysis. The effective normal stresses were calculated at the middle section of the composite beam, according to [16]. The effects of creep, shrinkage and duration load were not considered.

At first, the distance from the neutral axis $h_{na.i.eff}$ of each sub component to the extreme fiber has to be determined. For the calculation of the internal stresses a configuration of uniformly distributed shear connections placed every 300mm in pairs was considered. Based on a previously calculated effective bending stiffness it can be found that:

$$h_{na.c.eff} = h_c/2 + (1 - \frac{EI_0}{EI_{eff}}) \frac{EI_{eff}}{E_c A_c r} = 69.94 \text{mm}$$

$$h_{na.a.eff} = r_a + (1 - \frac{EI_0}{EI_{eff}}) \frac{EI_{eff}}{E_a A_a r} = 291.95 \text{mm}$$

The location of these values is shown in a figure 5.7. It can be observed that $h_{na.c.eff} \approx h_c$ which means that the neutral axis related to the concrete slab is located just at the edge of the concrete slab and it is fully under compression.

Knowing the position of the neutral axis in each sub-element, the normal stresses in the section can be evaluated for M = 160kNm (which is generated by a UDL of q = 5.0kN/m^2) as follows:

$$\sigma_{c,eff,top} = -\frac{E_c \cdot h_{na.c.eff} \cdot M}{EI_{eff} \cdot L} = -3.64 \text{N/mm}^2$$
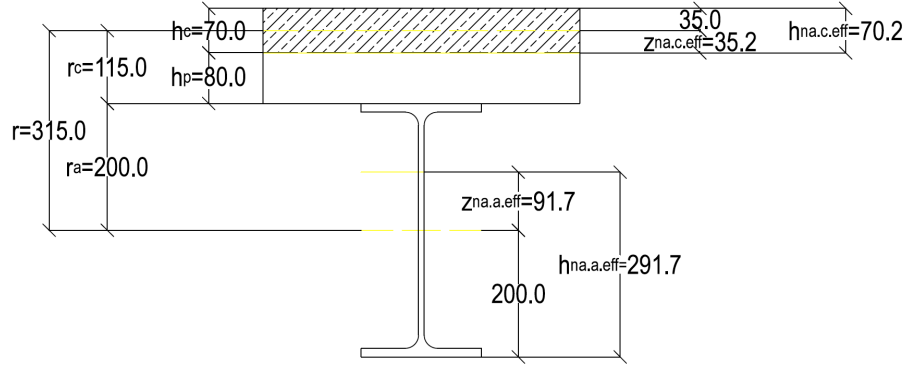
Figure 5.7: Position of n.a. in the composite section with partial interaction

$$\sigma_{c,eff,bot} = -\frac{E_c \cdot (h_{na.c.eff} - h_c) \cdot M}{EI_{eff} \cdot L} = 3.4 \cdot 10^{-3} \, N/mm^2$$

$$\sigma_{a,eff,top} = \frac{E_c \cdot (h_{na.a.eff} - h_a) \cdot M}{EI_{eff} \cdot L} = -36.17 \, N/mm^2$$

$$\sigma_{a,eff,bot} = \frac{E_c \cdot h_{na.a.eff} \cdot M}{EI_{eff} \cdot L} = 96.5 \, N/mm^2$$

Figure 5.8 shows the comparison of the normal stresses stresses in the section obtained form FE model and from hand calculations for two different load levels ($2.5 kN/m^2$ and $5.0 kN/m^2$). It can be observed that numerical and hand calculations are in a good agreement with each other.
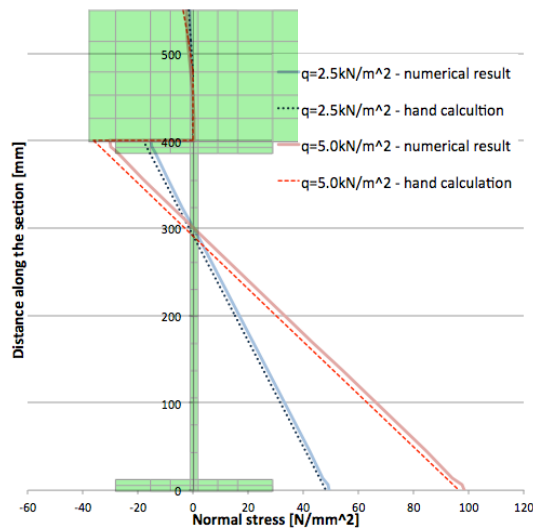
Figure 5.8: Comparison of normal stress distribution in the steel section at different load levels

5.7.4. Conclusion

Based on a conducted numerical and analytical analysis it can be concluded that the FE model provides results, which are in a good agreement with the analytical solutions. It gives a good indication that the FE model is relatively accurate and the step towards the realistic testing conditions can be made.

5.8. Validation using experimental results

In this section the FE model results are compared with the results obtained from the experimental works. First, the results of the 1st life cycle elastic tests are compared with numerical results, afterwards the second life cycle elastic tests are compared. Finally the numerical predictions of the bending moment resistance is compared to experimental result.

5.8.1. First life cycle

5.8.1.1   Load-mid span deflection behavior

(a) U-26 connector arrangement   (b) NonU-14 connector arrangement

(c) S-08 connector arrangement
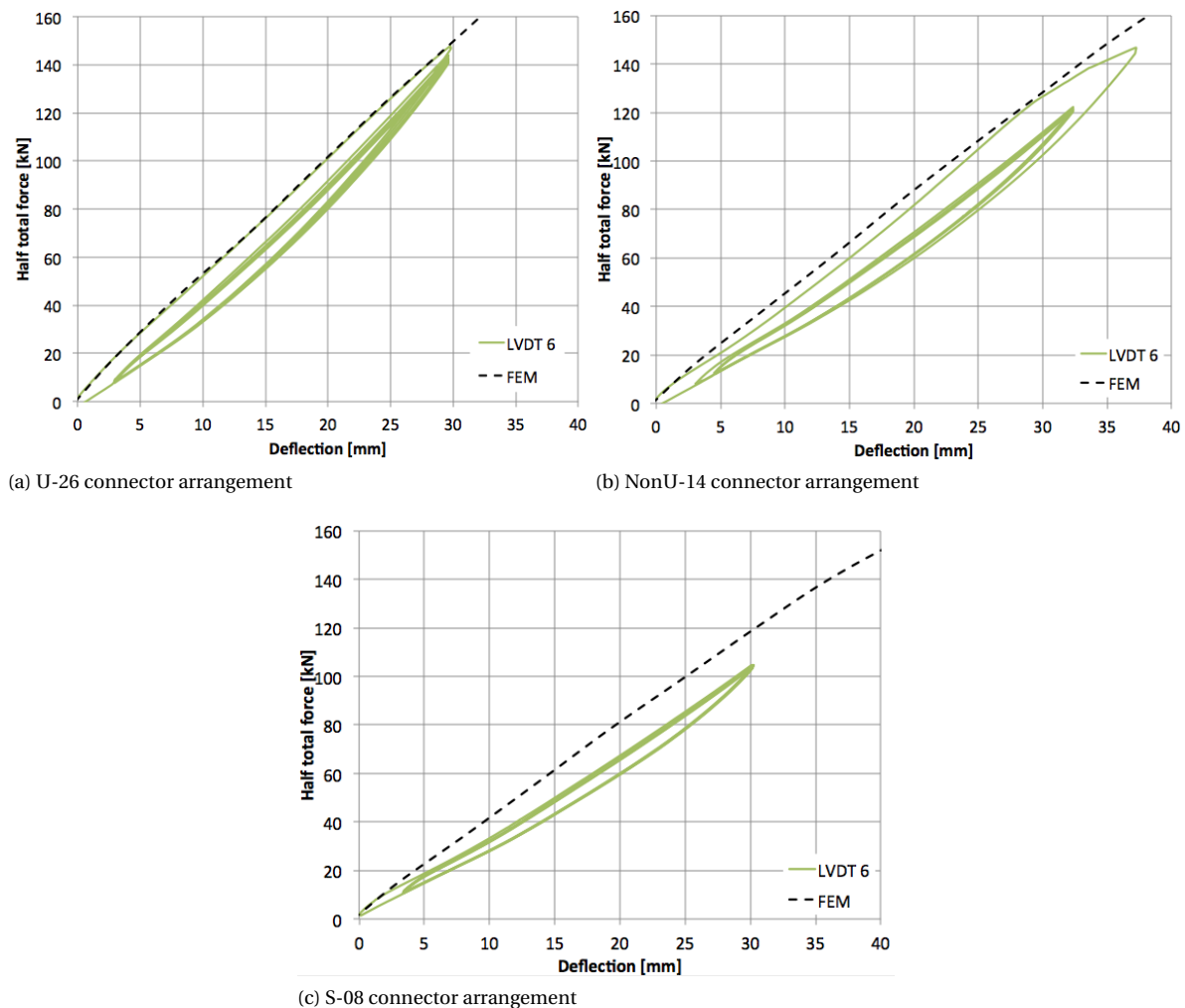
Figure 5.9: Comparison of FE analysis with the experimental results of load-mid span deflection behavior for various shear connector arrangements during first life cycle tests

The comparison of FE and experimental results is presented in the fig. 5.9. Table 5.1 summarizes the experimental results and numerical prediction for the effecting bending stiffness parameter for two intervals.

It can be observed that for NonU-14 and S-08 at force interval between 40kN and 70kN the FE model greatly (by 12.9% on average) over-predicts the effective bending stiffness. This can be explained by the slip, which occurred during testing due to the hole clearance at the locations where resin had to be removed. For the rest of the analyzed data, a quiet good agreement between test results and numerical model is achieved.

Arrangement	40kN-70kN		70kN-100kN	
	Exper.	FEM	Exper.	FEM
U-26	4.69 kN/mm	4.69 kN/mm (0%)	5.08kN/mm	5.0 kN/mm (-1.57%)
NonU-14	3.75 kN/mm	4.22 kN/mm (+12.5%)	4.11kN/mm	4.23 kN/mm (+2.9%)
S-08	3.53 kN/mm	4.0 kN/mm (+13.3%)	3.80 kN/mm	3.8kN/mm (0%)

Table 5.1: Comparison of the effective bending stiffness for various shear connector arrangements during first life cycle tests

5.8.1.2 Load-slip behavior

Figure 5.10 demonstrates the results of FE analysis describing the development of an end slip vs the experimental data for three connector arrangements. It can be observed that the FE model was able to capture the general pattern of the end slip development, where at the initial load levels a stiffer behavior is noted, then there is a slight decrease in stiffness, which is then followed by almost linear behavior. In reality, however, the shear stiffness gradually increases with the applied load.

In terms of accuracy, the FE model, in general, predicts lower values of slip compared to experimental data. A summary of the effective shear stiffness parameters for end slip and for the slippage at the 7th connector are presented in the tables 5.2 and 5.3, respectively.

(a) U-26 connector arrangement

(b) NonU-14 connector arrangement

(c) S-08 connector arrangement
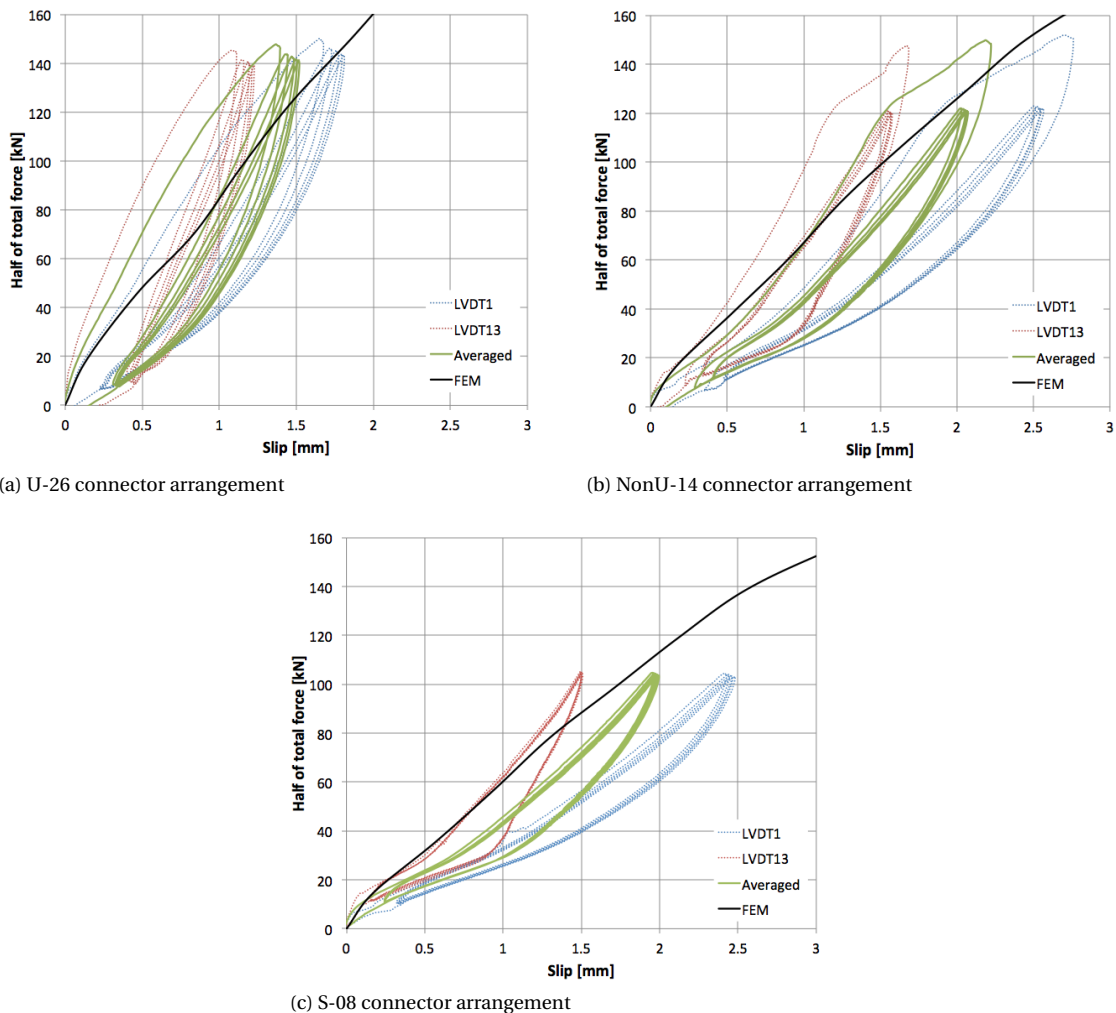
Figure 5.10: Comparison of FE analysis with the experimental results of end slip development for different connector arrangements

The difference between the numerical and experimental results could potentially originate from the friction

(a) U-26 connector arrangement

(b) NonU-14 connector arrangement

(c) S-08 connector arrangement
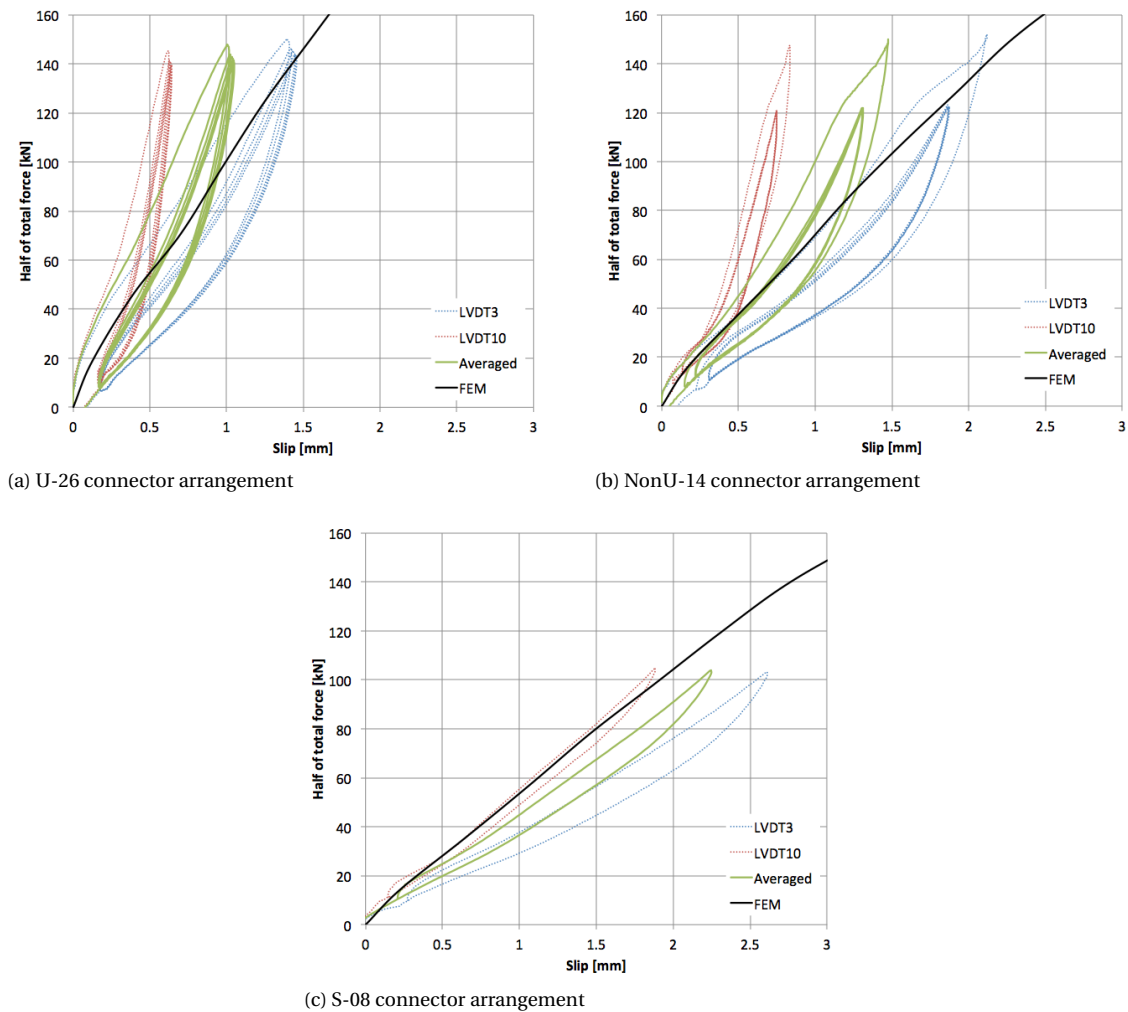
Figure 5.11: Comparison of FE analysis with the experimental results of relative slippage for different connector arrangements

Arrangement	40kN-70kN		70kN-100kN	
	Exper.	FEM	Exper.	FEM
U-26	103.45 kN/mm	68.18 kN/mm (-34.1%)	125.0 kN/mm	88.24 kN/mm (-29.4%)
NonU-14	63.83 kN/mm	61.86 kN/mm (-3.1%)	76.92 kN/mm	63.16 kN/mm (-17.9%)
S-08	55.56 kN/mm	58.0 kN/mm (+4.4%)	68.18 kN/mm	51.7 kN/mm (-24.2%)

Table 5.2: Comparison of the effective end slip shear stiffness for various shear connector arrangements

Arrangement	40kN-70kN		70kN-100kN	
	Exper.	FEM	Exper.	FEM
U-26	120 kN/mm	82.19 kN/mm (-31.5%)	166.67 kN/mm	96.77 kN/mm (-41.9%)
NonU-14	84.75 kN/mm	65.22 kN/mm (-23%)	121.46 kN/mm	68.18 kN/mm (-43.9%)
S-08	45.46 kN/mm	51.72 kN/mm (+13.8%)	48.39 kN/mm	50.0 kN/mm (+3.3%)

Table 5.3: Comparison of the effective shear stiffness at the intermediate connector for various shear connector arrangements

and adhesion, which was caused by excessive flow of resin and concrete during casting.

5.8.1.3   Normal stresses in the mid-span section

Figure 5.12 demonstrates the results of experimental and numerical analysis for various connector arrangements and different load levels. The magnitude of normal stresses at the bottom flange predicted by FE model is in a good agreement with the experimental results, however, the position of the neutral axis is over-predicted by numerical analysis. At the higher load levels the experimental location of n.a. shifts upwards and matches better the numerical results. For load levels of around 1WL the difference between FE and experiments is, on average, 12.4%. For loads of around 2.0WL the difference drops to 5.4 %.

(a) U-26 connector arrangement

(b) NonU-14 connector arrangement

(c) S-08 connector arrangement
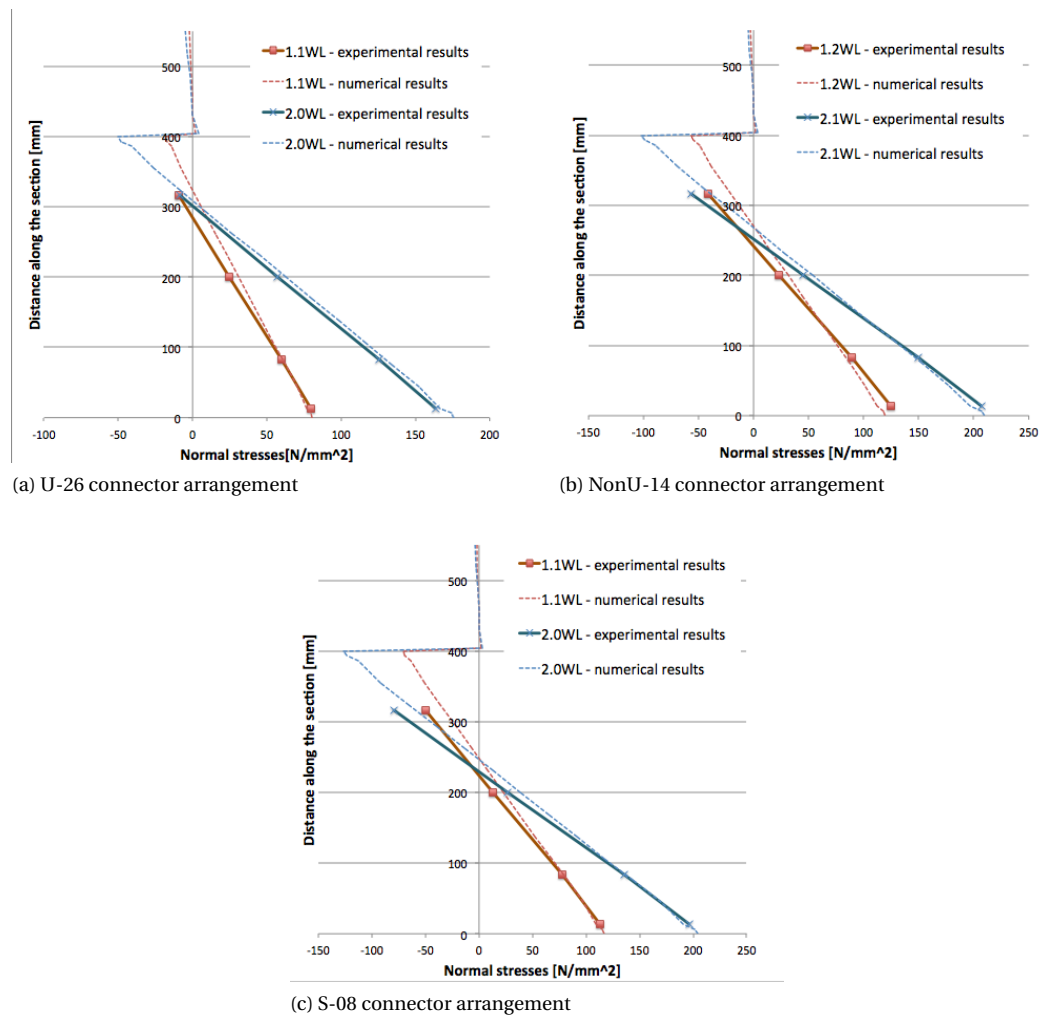
Figure 5.12: Comparison of FE analysis with the experimental results of normal stresses at different load levels for various connector arrangements

5.8.1.4   Vertical separation

A comparison was conducted between numerical and experimental results for the vertical separation. It was found that FE model greatly under-predicts the slab uplift (between 4 and 10 times). In the numerical model an assumption of rigid spring behavior in vertical direction was made. A numerical investigation on the influence of the spring vertical stiffness on the slab uplift was carried out and the results demonstrated no significant difference between rigid and flexible connector definitions.

5.8.2. Second life cycle

Since the experiments demonstrated a difference between the first and second life cycle test results the FE model used for validation of the first life cycle can not be used for second life cycle tests unless modified. According to the analysis of the second life cycle tests conducted in section 4.4.2.6, the new value for the initial connector stiffness of k_{sc} = 12kN/mm was proposed, which is 40% less than the initially estimated initial connector stiffness from the push-out tests. Therefore the originally used data in the numerical model for load-slip behavior of the connector was reduced by 40%.

5.8.2.1 Load-mid span deflection behavior

The finite element prediction based on a reduced stiffness of the shear connector demonstrates a better agreement with the experimental results than the originally estimated stiffness as can be seen form the fig. 5.13. The table 5.4 summarizes the comparison of FE and experimental effective bending stiffness for two force intervals. The maximum deviation between numerical and test results is 9%.

| (a) U-26 connector arrangement | (b) NonU-14 connector arrangement |
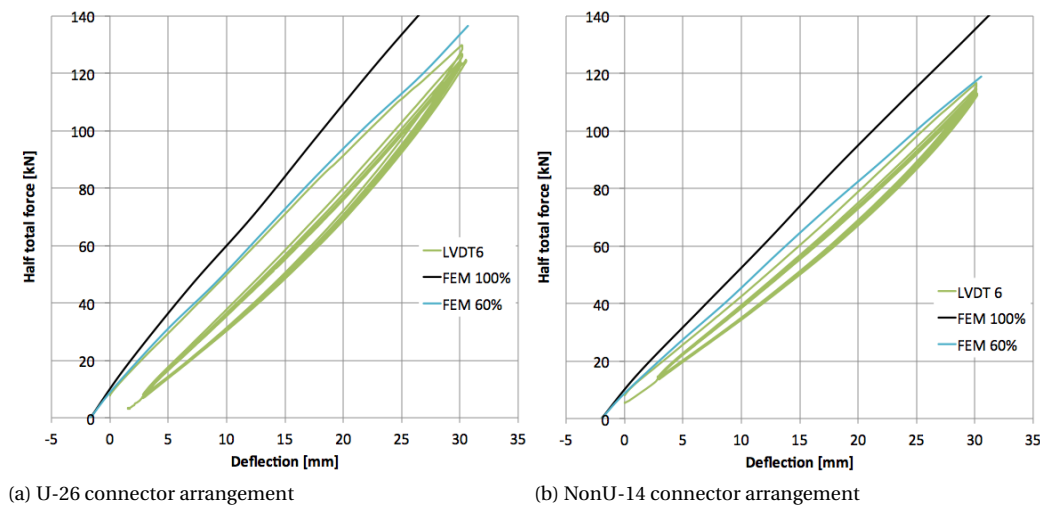
Figure 5.13: Comparison of FE analysis with the experimental results of load-mid span deflection behavior for various shear connector arrangements during second life cycle tests

Arrangement	40kN-70kN		70kN-100kN	
	Exper.	FEM 60%	Exper.	FEM 60%
U-26	4.10 kN/mm	4.29 kN/mm (4.6%)	4.48 kN/mm	4.17 kN/mm (-6.9%)
NonU-14	3.46 kN/mm	3.77 kN/mm (9.0%)	3.79 kN/mm	3.57 kN/mm (-5.8%)

Table 5.4: Comparison of the effective bending stiffness for various shear connector arrangements during second life cycle tests

5.8.2.2 Load-slip behavior

Figure 5.14 demonstrates the comparison of experimental and numerical results for slip development at the end of the beam. It can be observed that the original numerical model (FEM 100%) shows relatively good agreement with the averaged values of end slips, whereas the model with the reduced shear connector stiffness (FEM 60%) captures well the development of the slip at the beam end with LVDT1R and LDVT1L. Table 5.5 summarized the comparison of effective shear stiffnesses.

The development of the relative slip at the intermediate connector was not captured well by either of the models. The specimen in the experiment showed considerably stiffer behavior compared to numerical predications.

(a) U-26 connector arrangement

(b) NonU-14 connector arrangement
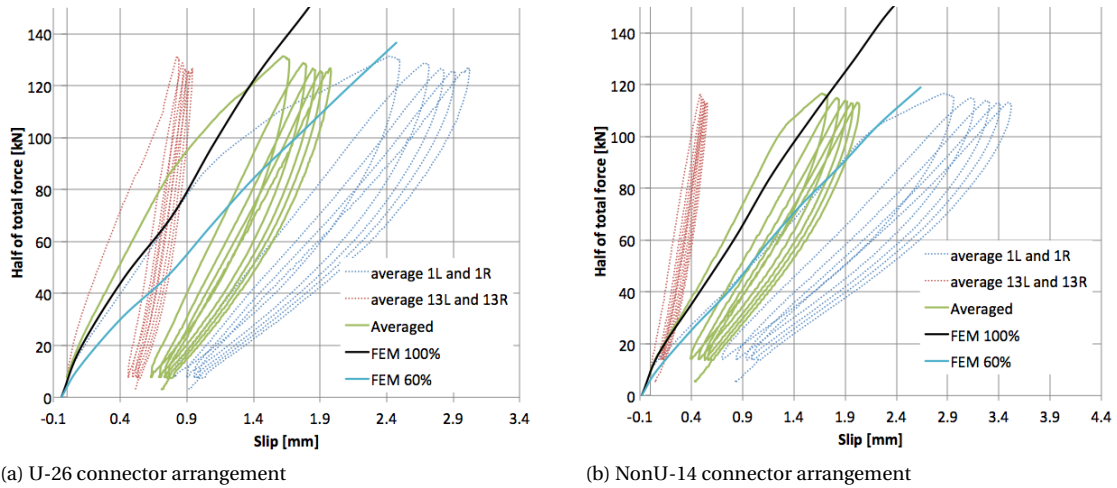
Figure 5.14: Comparison of FE analysis with the experimental results of end slip development for different connector arrangements during second life cycle tests

(a) U-26 connector arrangement

(b) NonU-14 connector arrangement
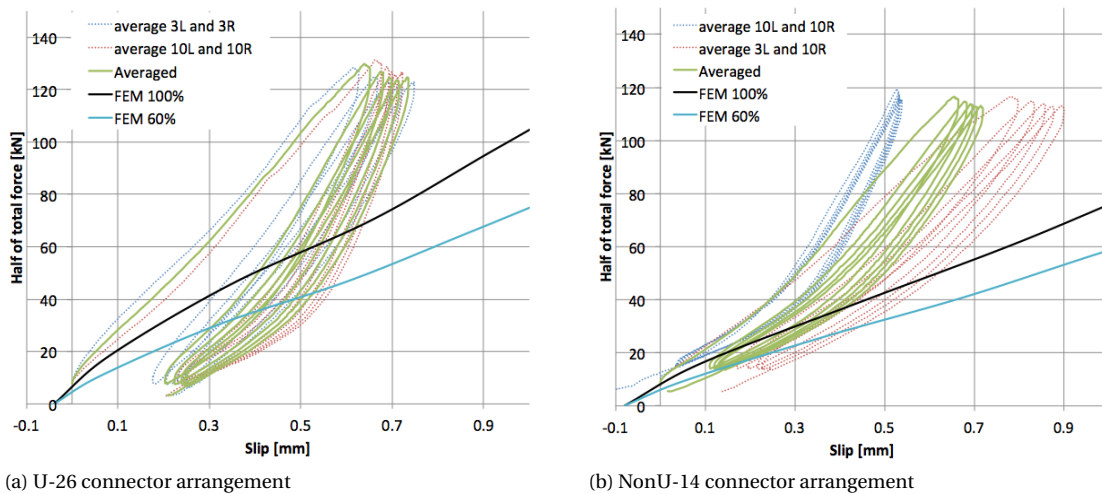
Figure 5.15: Comparison of FE analysis with the experimental results of relative slippage for different connector arrangements during second life cycle tests

Arrangement	40kN-70kN		70kN-100kN	
	Exper.	FEM 60%	Exper.	FEM 60%
U-26 (Averaged)	94.96 kN/mm	56.60 kN/mm (-40.4%)	100.77 kN/mm	52.60 kN/mm (-47.8%)
NonU-14 (Averaged)	65.85 kN/mm	47.62 kN/mm (-27.7%)	72.30 kN/mm	42.25 kN/mm (-41.6%)
U-26 (LVDT 1L, 1R)	54.07 kN/mm	56.60 kN/mm (+4.7%)	58.88 kN/mm	52.60 kN/mm (-10.7%)
NonU-14 (LVDT 1L, 1R)	42.25 kN/mm	47.62 kN/mm (+12.7%)	35.20 kN/mm	42.25 kN/mm (+20.0%)

Table 5.5: Comparison of the effective end slip shear stiffness for various shear connector arrangements during second life cycle tests

5.8.2.3   Normal stresses in the mid-span section

Figure 5.16 demonstrates the experimental results and numerical analysis based on a model with reduced shear connector stiffness of the normal stresses in the steel section for various shear connector configurations. Similar observations can be drawn as in the first life cycle tests. The magnitude of the normal stresses is relatively accurately predicted by FE analysis, however the location of the neutral axis is overestimated by FEM.

(a) U-26 connector arrangement (b) NonU-14 connector arrangement
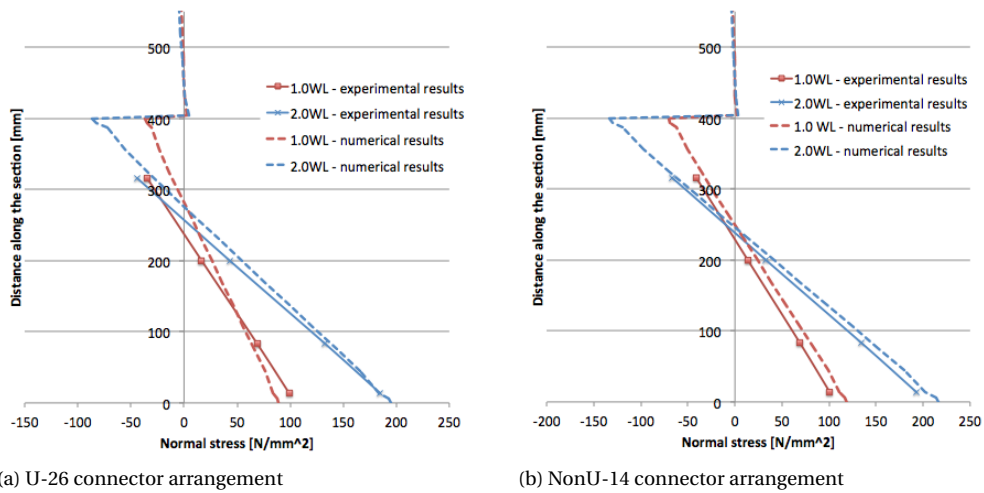
Figure 5.16: Comparison of FE analysis with the experimental results of normal stresses at different load levels for various connector arrangements during second life cycle tests

5.8.3. Failure

An attempt was made to predict numerically bending moment resistance of the composite beam. A series of FE analysis was conducted with various shear connector stiffnesses reduction in order to asses the sensitivity of the model to shear connector stiffness input. The shear connector stiffness was reduced by 25%, 40% and 55 %. The results of the sensitivity analysis are plotted versus the experimental results in the figures 5.17 and 5.18.

From the load-mid span deflection graph 5.17 it can be seen that the failure load is relatively well predicted by model FEM 75%. However, the initial bending stiffness is better captured by the model FEM 45%.

The prediction of the end slip by FEM is shown on the figure 5.18. The development of the stiffer end of the beam could not been predicted by any of the considered models. The initial stiffness of the weaker end of the specimen is predicted well by model FEM 45%, however the further development of the slip is underpredicted. This can be explained by the reduced shear connect resistance during the test due to the opening at the timber joist and loss of positive effect of confinement provided by timber piece.
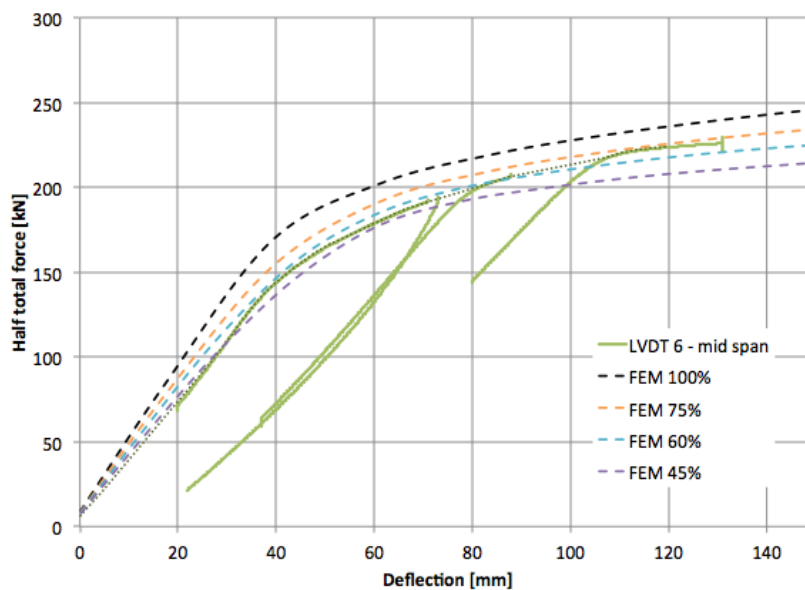
Figure 5.17: Load-mid span defection behavior
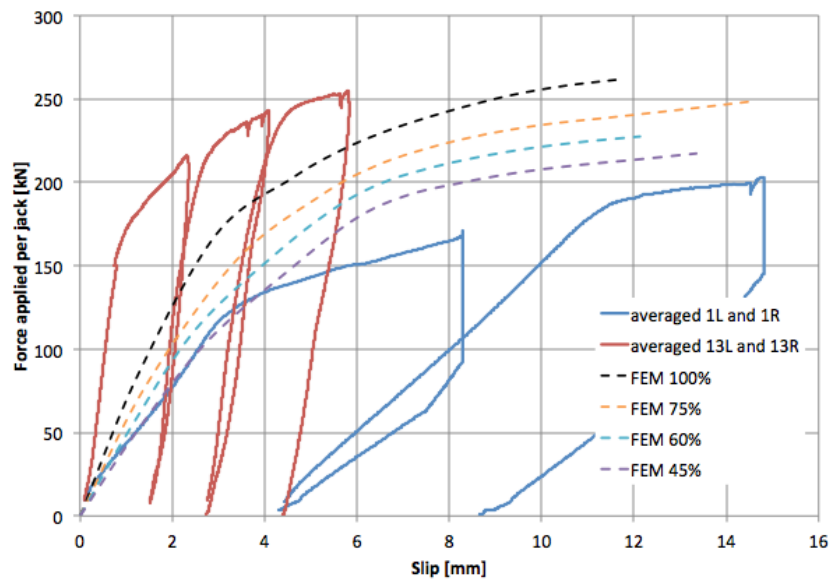
Figure 5.18: Load-end slip behavior

5.9. Conclusions

- The comparison of FEM results with the analytical solution had demonstrated a good agreement in terms of bending and shear stiffness and the location of neutral axis in the steel section.

- The validation of the model with set of experimental results was partially successful. On average, a rather good agreement was achieved for the effective bending stiffness of the specimen in both life cycles (maximum deviation of 13.3%).

- Numerically predicted location of the neutral axis was always higher than the actual position of the neutral axis. However, for the higher load levels, the difference between test results and model decreases.

- Since the specimen behavior has changed in the second life cycle, the original model over-predicted the effective bending stiffness. Therefore, in order to validate the experimental results, a reduced shear connector stiffness was adopted. Based on hand calculations, an initial connector stiffness of $k_{sc} = 12kN/mm$ was proposed, which is 40% smaller than the original value. The modified FE model has demonstrated a good agreement with the experiments in terms of effective bending stiffness, with maximum deviation of 9.0%.

- The prediction of load-slip behavior for end and intermediate connectors showed quiet poor agreement with the experimental results for both life cycle tests. In most of the cases, the numerical model predicts a lower effective shear stiffness than the one observed from tests. The comparison of the end slip development in the second life cycle tests with the numerical model was carried out based on the averaged value of slips on both ends and sides. However, it was observed that the numerical results agrees better with the slip at side of LVDT 1L, 1R.

- It was not possible to achieve an agreement between numerical model and experimental results for the vertical uplift of the slab. Further experimental and numerical investigations have to be carried out to describe the development of the vertical separation between the components.

- The FE analysis demonstrates that the load-mid span deflection development in second life cycle is relatively accurately predicted when the shear connector load-slip relationship is reduced by 40%.

6

Parametric study

6.1. Composite slab floor system optimization

In this parametric study various shear connector configurations are investigated for the demountable composite slab floor system for application in an office building with 4x8m grid. The thickness of the slab and steel section were kept the same: 150mm with ComFlor 95 metal decking of 0.9mm and IPE400. The un-propped construction method is of interest with beam spacing of 4m. The live load of 3 $\frac{kN}{m^2}$ was taken as it is a typical loading for office buildings specified in 1991-1-1 [4]. In addition a variable load of 0.5 $\frac{kN}{m^2}$ was considered. Safety factors were applied to the loadings. The effective modulus of elasticity for concrete was taken as $E_{cm}/2$ to account for the effects of creep, according to NEN-EN 1994-1-1 clause 5.4.2.2. Two uniform and two optimized shear connector arrangements were investigated as indicated in the fig. 6.1.
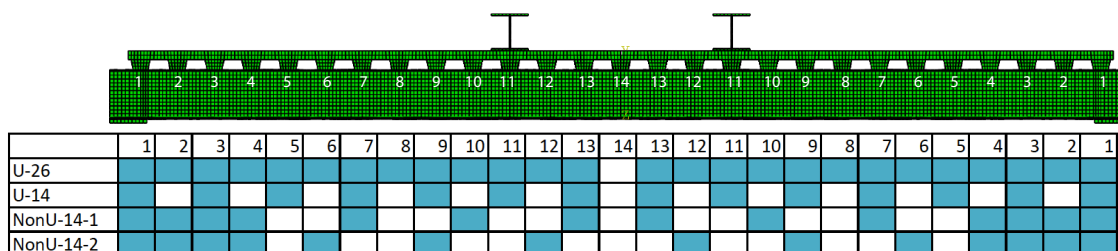
Figure 6.1: Investigated connector arrangements in parametric study

For the uniform arrangement every 300mm (U-26) a total of 52 connectors were placed. For the uniform arrangement every 600mm (U-14) and two optimized arrangements (NonU-14-1 and NonU-14-2) a total of 28 connectors were used in each configuration.

Hand calculations using analytical formulas for flexible shear connectors as well as FE analysis were performed for two uniform arrangements. For two other optimized arrangements only numerical analysis was conducted. The maximum mid-span deflection was calculated for all studied configurations and compared with SLS requirement of L/250 = 32mm. Since un-propped construction method is considered, at first stage the self-weight is carried by the steel beam alone, whereas after casting, the applied live load is carried by the composite section. An overview of obtained results is summarized in the table 6.1.

	U-26		U-14		NonU-14-1	NonU-14-2
	Analytical result	FE result	Analytical result	FE result	FE result	FE result
IPE400	26.4mm	25.2mm	28.8mm	27.7mm	27.2mm	26.9mm

Table 6.1: Mid-span deflections for different steel beams and various shear connector arrangements

The non-uniform connector arrangements NonU-14-1 and NonU-14-2 demonstrate an improved service-ability performance compared to U-16 and U-14 configurations, as the shear connectors act more beneficial if placed towards the supports. NonU-14-2 arrangement showed an improvement of 3% in terms of mid-span deflection compared to an equivalent uniformly distributed shear connector arrangement U-14.

In the work conducted by Gîrbacea [14] an extensive study was performed to determine the economic viabil-ity of two demountable steel-concrete composite flooring systems. Based on the assumption of composite slab thickness of 120mm and initial connector stiffness of 30kN/mm it was discovered that the demountable profiled sheeting slabs demonstrated a minor increase in costs of 5% compared to traditional profiled sheet-ing slab with headed studs. However, due to significantly lower initial stiffness of a connector the application of such flooring system does not pose a large advantage. For only 26% of investigated cases the demountable profiled sheeting slabs were more economical solution compared to a non-composite alternative. A sensitiv-ity analysis of the algorithm on the connector costs was conducted. It was obtained that in case of reduction of the costs related to the connector by 50% the demountable composite solution with profiled sheeting was more economic in 42% of the cases. Nevertheless, the traditional in-situ casted system remains always more economic than the composite beam with the prefabricated solid deck.

6.2. Conclusions

- The optimized shear connector arrangement has an advantage of 3% in terms mid span deflection compared to an equivalent uniform shear connector arrangement for the considered composite beam dimensions and 8x4m grid for the office building application.

- Due to a lower demountable shear connector stiffness compared to headed welded stud, the applica-tion of such flooring system does not pose a major economic advantaged compared to a non-composite alternative. However, by reducing the costs associated with the connectors by 50%, a demountable composite slab floor system becomes more economic for 42% of the cases.

- A further cost analysis can be conducted for the demountable composite floor systems considering various initial shear connector stiffness.

<div align="right">

7

</div>

Conclusions and future work

7.1. Conclusions

Based on literature research regarding BIM functionality and conducted case study of cast in-situ multi-storey car park building, following conclusions have been formulated:

- The literature review and use of BIM software had demonstrated a need for the improvement of BIM interface and functionalities for the successful application in the context of demountable structures. The improvement is required in identification of recoverable materials and interoperability with existing BIM softwares.

- In the case study, a research and testing of different software packages was conducted and following programs were selected for creation of the construction simulation: Robot Structural Analysis by Autodesk, Tekla structures by Trimble and Navisworks by Autodesk.

A full scale demountable composite beam was tested in two life cycle tests. The following is concluded regarding the structural behavior of a demountable composite beam with a composite slab, using M20 grade 8.8 injection bolts with a coupler as demountable shear connectors:

- It was demonstrated that dismantling and re-assembly is possible in laboratory conditions. However, for this concept to be successfully applied in the practice a number of recommendations and future research guidelines were proposed in section 4.6.

- The elastic beam behavior in the first life cycle is relatively well modeled by the FE analysis based on a push-out results of the demountable shear connector. The predicted bending stiffness and stresses are in a good agreement with test results. Maximum difference for effective bending stiffness is 13.3%. However, the development of the interface slip is predicted poorly by both numerical model and analytical solution (maximum deviation 34.1% and 42.0%, respectively).

- Apart from ensuring the slip resistant connections, it was shown that the resin injection procedure, in combination with accumulated concrete on top flange, contributed to the improvement of the serviceability performance of the composite beam.

- In the second life cycle, composite beam demonstrated a decrease in both bending and shear stiffness compared to the first life cycle. It was shown that the numerical model with a reduced shear connector stiffness by 40% demonstrates a good agreement with the test results for bending stiffness (maximum deviation 9.0%) and stresses.

- A decrease in bending and shear stiffness of the composite beam hypothetically occurred due to the change in longitudinal stress distribution across the slab width, which decreased the effective width or, alternatively, the initial stiffness of shear connectors got decreased by potential damages in the slab during re-assembly. More numerical and experimental investigations have to be carried out to identify the origin of this behavior.

- The development of the interface slip for elastic and plastic tests in the second life cycle had demonstrated highly unsymmetrical results for both ends of the beam. A high shear stiffness of 260.9kN/mm was observed for one end, whereas the other end demonstrated a stiffness of 38.7kN/mm for NonU-14 configuration. The high shear stiffness of the specimen potentially originated from the application of the wooden cantilever supporting structure, which might have been engaged in the unwanted transfer of longitudinal forces.

- The FE analysis had demonstrated that the load-mid span deflection development in second life cycle is relatively accurately predicted when the shear connector load-slip relationship is reduced by 40%. However, due to large difference in shear stiffness on both ends of the specimen, the prediction by FE model was not reliable.

- The measurement of the vertical separation of the slab and steel beam during tests have demonstrated discrepancy between obtained results. Therefore, a different method for recording the vertical separation has to be adopted to obtain more reliable data.

- The parametric study had demonstrated that the dimensions of the composite beam tested in the experiments represent the optimal solution for the first life cycle for an application in an office building. Based on FE analysis, the optimized shear connector arrangement can reduce the mid-span deflections by 3% compared to alternative uniformly distributed connector arrangement.

Based on the conducted experimental research, a number of recommendations is presented, which provide a framework for the future development and application of a demountable composite flooring system.

- An application of edge trims along the longitudinal joint should be adopted. It has potential to facilitate the cutting procedure and ensure the confinement of shear connectors. When used in combination with a full height timer separation and discontinuous reinforcement the re-assembly process can be facilitated due to clearances provided by full height timber piece. Nevertheless, the concrete cracking over the timber joist and durability issues have to be addressed and further investigated.

- The 26mm hole clearance in the steel beam flange is sufficient to successfully unmount and re-assemble the composite slab to its original position. However, to successfully re-use the composite slab in combination with an arbitrary steel beam, the hole clearance has to be increased in the second life cycle. Similar finding was confirmed in a feasibility study by Gîrbacea [14] on a demountable composite flooring system with large prefabricated decks.

- An alternative to the lifting procedure used in the experiments is potentially an application of a vehicle with a platform that can uplift a part of the slab from underneath or use of a vacuum lifter.

7.2. Future work

There is a need for a detailed study regarding the full execution process of the demountable composite slab floor system, which would involve longitudinal cutting, uplifting, storage, transportation and re-assembly stages.

The durability of longitudinal joint, which consists of timber separation, in the second life cycle has to addressed.

Large scatter between the measurements of relative slip was observed during tests. Therefore, more research has to be carried out in order to identify the source of those deviations and provide a reliable analytical model for perdition of interface slippage.

Similarly, more investigations on structural behavior of the composite beam in second life cycle have to be performed in order identify the reason of decreased bending stiffness and provide methods for its improvement.

Appendices

Analytical solutions for partial shear interaction

A.1. General data

$h_c = 70\text{mm}$

$h_p = 80\text{mm}$

$h_s = h_c + h_p = 150\text{mm}$

$h_a = 400\text{mm}$

$L = 8\text{m}$

$b_1 = 4\text{m}$

$b_{eff} = \min(L/8, b_1) = 2\text{m}$

$E_a = 210000\text{N/mm}^2$

$I_a = 23130 \cdot 10^4 \text{mm}^4$

$E_c = 33000\text{N/mm}^2$

$I_c = \dfrac{b_{eff}h_c^3}{12} = 5.717 \cdot 10^7 \text{mm}^4$

$r_c = h_p + \dfrac{h_c}{2} = 115\text{mm}$ Distance from centroid of the concrete slab to the interface

$r_s = \dfrac{h_a}{2} = 200\text{mm}$ Distance from centroid of the steel beam to the interface

$r = r_c + r_s = 315\text{mm}$ Distance between centroids of 2 elemetns

$EI_0 = E_a I_a + E_c I_c = 5.046 \cdot 10^4 \text{kNm}^2$ Bending stiffness in case of no composite action

$EI_{inf} = EI_0 + \dfrac{E_a A_a \cdot E_c A_c}{E_a A_a + E_c A_c} = 1.777 \cdot 10^5 \text{kNm}^2$ Bending stiffness in case of full composite action

A.2. Calculations according to Girhammar

A.2.1. Shear connectors placed every 300 mm

$k_{sc} = 2 \cdot 20 \dfrac{kN}{mm} = 40 \dfrac{kN}{mm}$ Initial stiffness of a pair of shear connectors

$s_{sc} = 300 mm$ spacing between shear connectors

$K = \dfrac{k_{sc}}{s_{sc}} = 1.333 \cdot 10^8 N/m^2$ Slip modulus of shear connection

$\alpha = \sqrt{\dfrac{Kr^2}{EI_0 \left(1 - \frac{EI_0}{EI_{inf}}\right)}} = 6.051 \cdot 10^{-4} \dfrac{1}{mm}$ Partial composite action parameter

$EI_{c,eff} \approx \left(1 + \dfrac{\frac{EI_{inf}}{EI_0} - 1}{1 + \left(\frac{\alpha L}{\pi}\right)^2}\right)^{-1} \cdot EI_{inf} = 1.017 \cdot 10^5 kNm^2$ Effective bending stiffness for partially composite beam

Un-propped: deflection due to selfweight $g = 6.5 kN/m$:

$w_{unprop} = \dfrac{5gL^4}{384E_aI_a} = 7.14 mm$

Unpropped: deflection due to imposed service load of $q = 10 kN/m$:

$w_{inf,max} = \dfrac{5qL^4}{384EI_{inf}} = 3.0 mm$

$w_{exact} = w_{inf,max} + \dfrac{q}{\alpha^4 EI_{inf}} \left(\dfrac{EI_{inf}}{EI_0} - 1\right) \left(\dfrac{1}{\cosh\left(\frac{\alpha L}{2}\right)} + \dfrac{\alpha^2 L^2}{8} - 1\right) = 5.23 mm$

Or

$w_{appox} = \dfrac{5qL^4}{384EI_{c,eff}} = 5.24 mm$

$w_{total} = w_{unprop} + w_{exact} = 12.37 mm$

Propped: Deflection due to imposed service load of $q = 10 kN/m$ and selfweight $g = 6.5 kN/m$:

$w_{inf,max} = \dfrac{5(q+g)L^4}{384EI_{inf}} = 4.95 mm$

$w_{exact} = w_{inf,max} + \dfrac{q+g}{\alpha^4 EI_{inf}} \left(\dfrac{EI_{inf}}{EI_0} - 1\right) \left(\dfrac{1}{\cosh\left(\frac{\alpha L}{2}\right)} + \dfrac{\alpha^2 L^2}{8} - 1\right) = 8.63 mm$

Or

$w_{appox} = \dfrac{5(q+g)L^4}{384EI_{c,eff}} = 8.65 mm$

End slip calculation:

$$V = \frac{(q+g)L}{2} = 55 = kN$$ Shear force

$$V_{s,eff} = (1 - \frac{EI_0}{EI_{c,eff}}) \frac{V}{r} = 88 = kN/m$$ Shear flow

$$s = \frac{V_{s,eff}}{K} = 0.66 = mm$$ End slip

A.2.2. Shear connectors placed every 600 mm

$$k_{sc} = 2 \cdot 20 \frac{kN}{mm} = 40 \frac{kN}{mm}$$ Initial stiffness of a pair of shear connectors

$$s_{sc} = 600mm$$ spacing between shear connectors

$$K = \frac{k_{sc}}{s_{sc}} = 6.667 \cdot 10^7 N/m^2$$ Slip modulus of shear connection

$$\alpha = \sqrt{\frac{Kr^2}{EI_0 (1 - \frac{EI_0}{EI_{inf}})}} = 4.279 \cdot 10^{-4} \frac{1}{mm}$$ Partial composite action parameter

$$EI_{c,eff} \approx (1 + \frac{\frac{EI_{inf}}{EI_0} - 1}{1 + (\frac{\alpha L}{\pi})^2})^{-1} \cdot EI_{inf} = 8.254 \cdot 10^4 kNm^2$$ Effective bending stiffness for partially composite beam

Un-propped: deflection due to selfweight $g = 6.5kN/m$:

$$w_{unprop} = \frac{5gL^4}{384E_a I_a} = 7.14mm$$

Unpropped: deflection due to imposed service load of $q = 10kN/m$:

$$w_{exact} = w_{inf,max} + \frac{q}{\alpha^4 EI_{inf}} (\frac{EI_{inf}}{EI_0} - 1) (\frac{1}{\cosh(\frac{\alpha L}{2})} + \frac{\alpha^2 L^2}{8} - 1) = 6.45mm$$

Or

$$w_{appox} = \frac{5qL^4}{384EI_{c,eff}} = 6.46mm$$

$$w_{total} = w_{unprop} + w_{exact} = 13.59mm$$

Propped: Deflection due to imposed service load of $q = 10kN/m$ and selfweight $g = 6.5kN/m$:

$$w_{exact} = w_{inf,max} + \frac{q+g}{\alpha^4 EI_{inf}} (\frac{EI_{inf}}{EI_0} - 1) (\frac{1}{\cosh(\frac{\alpha L}{2})} + \frac{\alpha^2 L^2}{8} - 1) = 10.64mm$$

Or

$$w_{appox} = \frac{5(q+g)L^4}{384EI_{c,eff}} = 10.66mm$$

End slip calculation:

$$V = \frac{(q+g)L}{2} = 66 = kN$$ Shear force

$$V_{s,eff} = (1 - \frac{EI_0}{EI_{c,eff}}) \frac{V}{r} = 67.88 = kN/m$$ Shear flow

$$s = \frac{V_{s,eff}}{K} = 1.018 = mm$$ End slip

A.3. Calculations according to Leskela

A.3.1. Shear connectors placed every 300 mm

$$\alpha_i = \frac{r^2}{E_a I_a + E_c I_c} \frac{E_a A_a \cdot E_c A_c}{E_a A_a + E_c A_c} = 2.521$$ Composite stiffness parameter

$$k_{sc} = 2 \cdot 20 \frac{kN}{mm} = 40 \frac{kN}{mm}$$ Initial stiffness of a pair of shear connectors

$$s_{sc} = 300mm$$ Spacing between shear connectors

$$K = \frac{k_{sc}}{s_{sc}} = 1.333 \cdot 10^8 N/m^2$$ Slip modulus of shear connection

$$\mu = \frac{5}{16 \cdot 3}$$ For uniformly distributed load

$$r_\delta = \frac{\alpha_i(E_a I_a + E_c I_c)}{\alpha_i(E_a I_a + E_c I_c) + \mu_m KL^2 r^2(\alpha_i + 1)} = 0.291$$ Flexibility parameter

$$\alpha_{i,eff} = \frac{1 - r_\delta}{1 + \alpha_i r_\delta} \alpha_i = 1.032$$ Composite stiffness parameter

$$EI_{c,eff} = (1 + \alpha_{i,eff})(E_a I_a + E_c I_c) = 1.025 \cdot 10^5 kNm^2$$ Effective bending stiffness

Un-propped: deflection due to selfweight $g = 6.5kN/m$:

$$w_{unprop} = \frac{5gL^4}{384E_a I_a} = 7.14mm$$

Un-propped: deflection due to imposed service load of $q = 10kN/m$:

$$w_{appox} = \frac{5qL^4}{384EI_{c,eff}} = 5.20mm$$

$$w_{total} = w_{unprop} + w_{approx} = 12.34mm$$

Propped: Deflection due to imposed service load of $q = 10kN/m$ and selfweight $g = 6.5kN/m$:

$$w_{appox} = \frac{5(q+g)L^4}{384EI_{c,eff}} = 8.581mm$$

End slip calculation:

Un-propped:

$$M = \frac{qL^2}{8} = 80 kNm$$ Maximum moment at the mid-span

$$\delta = \frac{qL^3}{24} \frac{rr_\delta}{E_aI_a + E_cI_c} = 0.786 mm$$ End slip

Propped:

$$M = \frac{(q+g)L^2}{8} = 132 kNm$$ Maximum moment at the mid-span

$$\delta = \frac{qL^3}{24} \frac{rr_\delta}{E_aI_a + E_cI_c} = 0.786 mm$$ End slip

A.3.2. Shear connectors placed every 600 mm

$$k_{sc} = 2 \cdot 20 \frac{kN}{mm} = 40 \frac{kN}{mm}$$ Initial stiffness of a pair of shear connectors

$$s_{sc} = 600 mm$$ Spacing between shear connectors

$$K = \frac{k_{sc}}{s_{sc}} = 6.667 \cdot 10^7 N/m^2$$ Slip modulus of shear connection

$$\mu = \frac{5}{16 \cdot 3}$$ For uniformly distributed load

$$r_\delta = \frac{\alpha_i(E_aI_a + E_cI_c)}{\alpha_i(E_aI_a + E_cI_c) + \mu_m KL^2r^2(\alpha_i + 1)} = 0.45$$ Flexibility parameter

$$\alpha_{i,eff} = \frac{1 - r_\delta}{1 + \alpha_i r_\delta} \alpha_i = 0.649$$ Composite stiffness parameter

$$EI_{c,eff} = (1 + \alpha_{i,eff})(E_aI_a + E_cI_c) = 8.321 \cdot 10^4 kNm^2$$ Effective bending stiffness

Un-propped: deflection due to selfweight g = 6.5kN/m:

$$w_{unprop} = \frac{5gL^4}{384E_aI_a} = 7.14 mm$$

Un-propped: deflection due to imposed service load of q = 10kN/m:

$$w_{appox} = \frac{5qL^4}{384EI_{c,eff}} = 6.41 mm$$

$$w_{total} = w_{unprop} + w_{approx} = 13.55 mm$$

Propped: Deflection due to imposed service load of q = 10kN/m and selfweight g = 6.5kN/m:

$$w_{appox} = \frac{5(q+g)L^4}{384EI_{c,eff}} = 10.58 mm$$

End slip calculation:

Un-propped:

$$M = \frac{qL^2}{8} = 80\text{kNm}$$
Maximum moment at the mid-span

$$\delta = \frac{qL^3}{24}\frac{rr_\delta}{E_aI_a + E_cI_c} = 0.989\text{mm}$$
End slip

Propped:

$$M = \frac{(q+g)L^2}{8} = 132\text{kNm}$$
Maximum moment at the mid-span

$$\delta = \frac{qL^3}{24}\frac{rr_\delta}{E_aI_a + E_cI_c} = 1.632\text{mm}$$
End slip

Calculation case study car park

In this annex the calculation of composite car park is demonstrated. The verification of individual members are presented as well as the design and verification of joints. Figure B.1 shows the view plan of the car park and demonstrates the location of different structural elements.
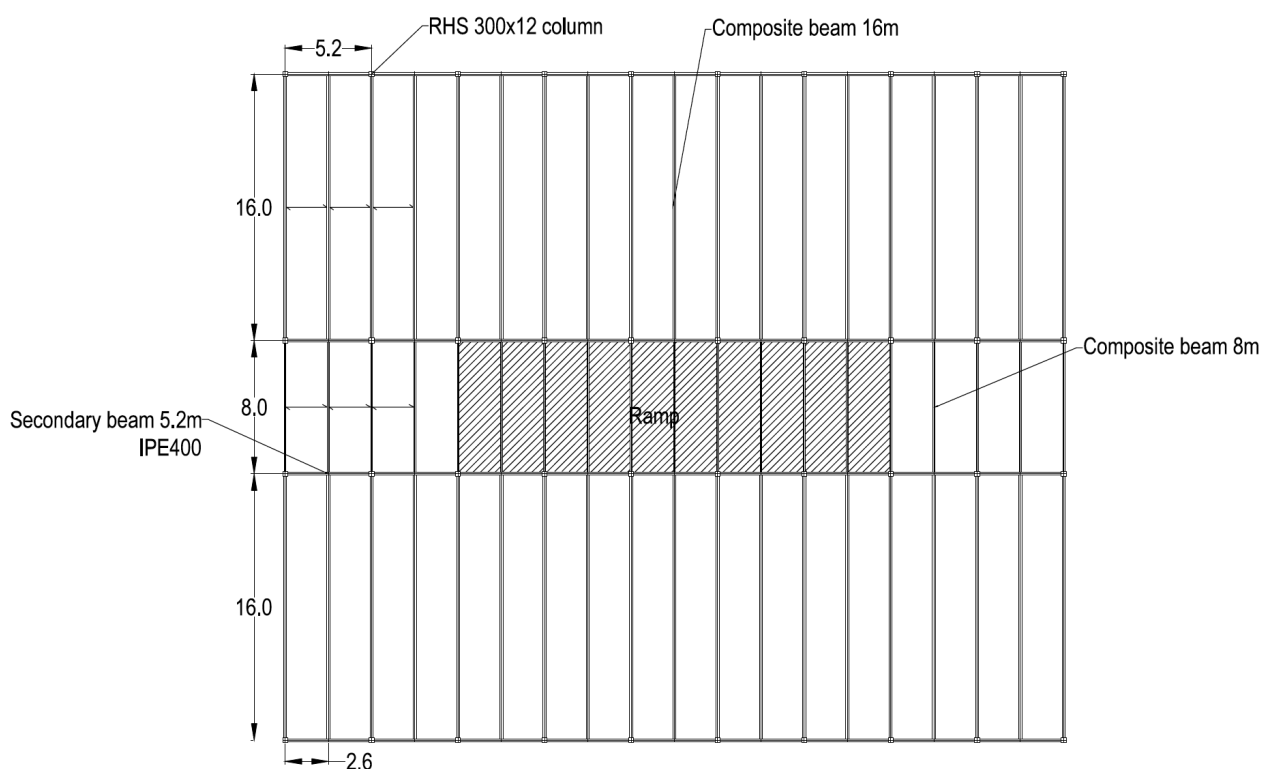
Figure B.1: Car park view plan

Composite beams of 16m and 8m are placed every 2.6 meters. The column spacing is 5.2 meters.

B.1. Composite beam 16 m

The cross section of the beam is shown on a fig. B.2.

B.1.1. Load actions on beam
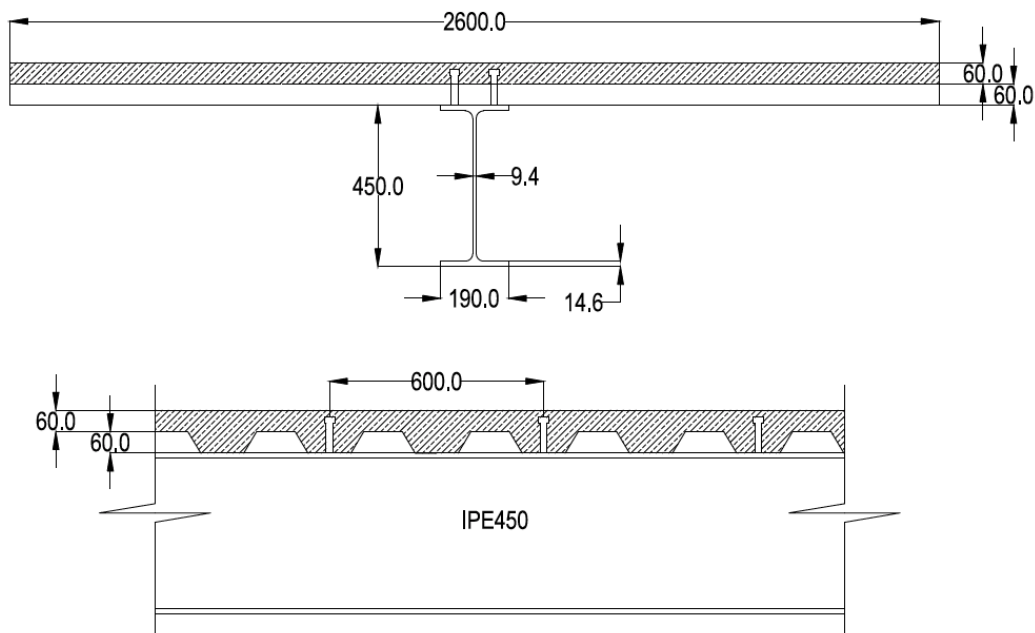
Figure B.2: Composite beam 16m

Selfweight:

$g_c = 5.7 \text{kN/m}$
$g_s = 0.9 \text{kN/m}$
$g_{tot} = 6.6 \text{kN/m}$

Imposed load:

$q_{var} = 3.0 \text{kN/m}^2 \cdot 2.6 \text{m} = 7.8 \text{kN/m}$

Design load:

$q_{ULS} = 1.2 \cdot g_{tot} + 1.5 \cdot q_{var} = 19.6 \text{kN/m}$

Resulting design section forces

$$M_{Ed} = \frac{q_{ULS}L^2}{8} = 628 \text{kNm}$$
$$V_{Ed} = \frac{q_{ULS}L}{2} = 157 \text{kN}$$

B.1.2. General data

$L = 16 \text{m}$ Beam length
$b_1 = 2.6 \text{m}$ Beam spacing
$b_{eff} = \min(2 \cdot \frac{L}{8}, b_1) = 2.6 \text{m}$ Effective width
$f_{yd} = 355 \text{N/mm}^2$
$E_a = 210000 \text{N/mm}^2$

IPE450:

$b_{fl} = 190mm$

$h_a = 450mm$

$t_w = 9.4mm$

$t_f = 14.6mm$

$r = 21mm$

$h_w = h_a - (2t_f + 2r) = 378.8mm$

$b_f = \dfrac{b_{fl} - t_w}{2} - r = 69.3mm$

$A_a = 98.8 \cdot 10^2 mm^2$

$I_a = 33740 \cdot 10^4 mm^4$

$W_{pl.a} = 1702 \cdot 10^3 mm^3$

$W_{el.a} = \dfrac{I_a}{0.5 \cdot h_a} = 1.5 \cdot 10^6 mm^3$

$M_{pl.a} = W_{pl.a} \cdot f_{yd} = 604.21kNm$

Concrete slab C30/37 with ComFlor75:

$f_{ck} = 30N/mm^2$

$f_{cd} = f_{ck}/1.5 = 20N/mm^2$

$E_c = 33000N/mm^2$

$h_c = 60mm$

$h_p = 60mm$

$A_c = h_c \cdot b_{eff} = 1.56 \cdot 10^5 mm^2$

$t_s = 0.9mm$ Thickness of ComFlor metal sheeting

$n_{ribs} = \dfrac{L/2}{300mm} = 26$ Number of available ribs

B.1.3. Cross section classification

Web (an internal part) in bending:

$\dfrac{c}{t} = \dfrac{378.8}{9.4} = 40 < 72 \cdot \varepsilon = 72 \cdot 0.81 = 58$

Flange (outstand part) in compression:

$\dfrac{c}{t} = \dfrac{69.3}{14.6} = 4.7 < 9 \cdot \varepsilon = 9 \cdot 0.81 = 7.3$

The cross section class is 1

B.1.4. Bending resistance of the beam

Headed studs:

$h_{sc} = 100mm$ Height of shear connector

$d_{sc} = 19mm$ Diameter of shear connector

$h_{sc} = 100mm > 3 \cdot d_{sc} = 57mm \rightarrow Ok$

$\dfrac{h_{sc}}{d_{sc}} = 5.263 > 4 \rightarrow \alpha = 1.0$

$f_u = 450N/mm^2$

$P_{Rd,s} = \min \left(\dfrac{0.8 f_u \pi (d_{sc}^2/4)}{\gamma_v}, \dfrac{0.29\alpha d_{sc}^2 \sqrt{f_{ck}E_{cm}}}{\gamma_v} \right) = 81.66kN$ Shear connector resistance in solid slab

Sheeting with rib transverse to the supporting beam

$n_r = 2$ Number of stud connectors per rib

$b_0 = 144$

$k_t = \dfrac{0.7 b_0}{h_p \sqrt{n_r}} \left(\dfrac{h_{sc}}{h_p} - 1 \right) = 0.792$

$k_{t,max} = 0.7$

$P_{Rd.kt} = k_{t,max} \cdot P_{Rd.s} = 57.2kN$

Bending moment resistance - partial interaction

$n_{sc} = 26$ Number of shear connectors per half span

$N_{sc} = n_{sc} \cdot P_{Rd.kt} = 1486kN$ Compression force in slab

$N_{a.Rd} = A_a \cdot f_{yd} = 3507kN$ Tension resistance of beam

$N_{c.Rd} = 0.85 \cdot b_{eff} \cdot h_c \cdot f_{cd} = 2652kN$ Compression resistance of concrete

$N_{w.Rd} = f_{yd} \cdot t_w \cdot h_w = 1486kN$ Tension resistance of web

$N_{f.Rd} = \dfrac{N_{a.Rd} - N_{w.Rd}}{2} = 1122kN$ Tension resistance of flange

$\eta_l = \dfrac{N_{sc.Ed}}{\min(N_{c.Rd}, N_{a.Rd})} = 0.56$ Degree of shear connection

$x_c = h_c \dfrac{N_{sc.Ed}}{N_{c.Rd}} = 33.6mm$ Height of concrete that contributes to the resistance

$z_{pl} = \dfrac{N_{a.Rd} - N_{sc.Ed}}{2 b_{fl} f_{yd}} + h_p + h_c = 135mm$

$a = \dfrac{N_{a.Rd} - N_{sc.Ed}}{2 b_{fl} f_{yd}} = 15mm > t_f = 14.6mm \rightarrow$ Neutral axis in the web

$M_{pl.c.Rd} = N_{sc.Ed} (h_a/2 + h_c/2 + h_p) + W_{pl.a} f_{yd} - \dfrac{1}{4} t_w f_{yd} \left(\dfrac{N_{sc.Ed}}{t_w f_{yd}} \right)^2 = 906.9kNm$ Bending moment resistance

$\dfrac{M_{Ed}}{M_{pl.c.Rd}} = \dfrac{628}{906.9} = 0.7 \rightarrow Ok$

B.1.5. Shear resistance

$A_v = 55.5cm^2$

$V_{pl.Rd} = A_v \cdot f_{yd}/\sqrt{3} = 1138kN$

$\dfrac{V_{Ed}}{V_{pl.Rd}} = \dfrac{157}{1138} = 0.14 \rightarrow Ok$

B.1.6. Deflections

Full composite stiffness:

$$n = \frac{E_a}{E_{cm}/2} = 12.727$$

$$I_c = \frac{h_c^3 b_{eff}}{12} = 4.68 \cdot 10^7 mm^4$$

$$I_{c.full} = I_a + \frac{I_c}{n} + \frac{A_a A_c}{n A_a + A_c} \left(\frac{h_c + 2h_p + h_a}{2}\right)^2 = 8.839 \cdot 10^8 mm^4$$

Delflection under selfweight: un-propped:

$$\delta_g = \frac{5 \cdot g \cdot L^4}{384 E_a \cdot I_a} = 79.5 mm$$

Delflection under imposed load:

$$\delta_c = \frac{5 \cdot q \cdot L^4}{384 E_a \cdot I_{c,full}} = 35.9 mm$$

$$\delta_{precam} = 55 mm$$

$$\delta_{tot} = \delta_g + \delta_c - \delta_{precam} = 61 mm < \frac{L}{250} = 64 mm \rightarrow Ok$$

B.2. Composite beam 8 m

The cross section of the beam is shown on a fig. B.3.
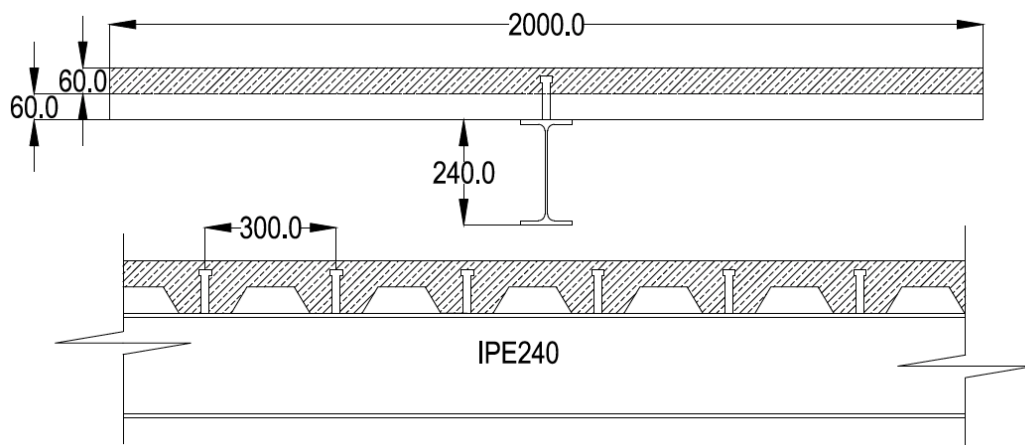
Figure B.3: Composite beam 8m

B.2.1. Load actions on beam

Resulting design section forces

$$M_{Ed} = \frac{q_{ULS} L^2}{8} = 156.8 kNm$$

$$V_{Ed} = \frac{q_{ULS} L}{2} = 78.4 kN$$

B.2.2. General data

L = 8m   Beam length
$b_1 = 2.6$m   Beam spacing
$b_{eff} = \min(2 \cdot \dfrac{L}{8}, b_1) = 2.0$m   Effective width
$f_{yd} = 355$N/mm^2
$E_a = 210000$N/mm^2

IPE240:

$b_{fl} = 120$mm
$h_a = 240$mm
$t_w = 6.2$mm
$t_f = 9.8$mm
$r = 15$mm
$h_w = h_a - (2t_f + 2r) = 190.4$mm
$b_f = \dfrac{b_{fl} - t_w}{2} - r = 41.9$mm
$A_a = 39.1 \cdot 10^2$mm^2
$I_a = 3890 \cdot 10^4$mm^4
$W_{pl.a} = 366.6 \cdot 10^3$mm^3
$W_{el.a} = \dfrac{I_a}{0.5 \cdot h_a} = 324 \cdot 10^3$mm^3
$M_{pl.a} = W_{pl.a} \cdot f_{yd} = 130.14$kNm

Concrete slab C30/37 with ComFlor75:

$f_{ck} = 30$N/mm^2
$f_{cd} = f_{ck}/1.5 = 20$N/mm^2
$E_{cm} = 33000$N/mm^2
$h_c = 60$mm
$h_p = 60$mm
$A_c = h_c \cdot b_{eff} = 1.2 \cdot 10^5$mm^2
$t_s = 0.9$mm   Thickness of ComFlor metal sheeting
$n_{ribs} = \dfrac{L/2}{300\text{mm}} = 13$ Number of available ribs

B.2.3. Cross section classification

Web (an internal part) in bending:
$\dfrac{c}{t} = \dfrac{190.4}{6.2} = 30.7 < 72 \cdot \varepsilon = 72 \cdot 0.81 = 58$

Flange (outstand part) in compression:
$\dfrac{c}{t} = \dfrac{41.9}{9.8} = 4.3 < 9 \cdot \varepsilon = 9 \cdot 0.81 = 7.3$

The cross section class is 1

B.2.4. Bending resistance of the beam

Sheeting with rib transverse to the supporting beam

$n_r = 1$ Number of stud connectors per rib

$b_0 = 144$

$k_t = \dfrac{0.7 b_0}{h_p \sqrt{n_r}} \left(\dfrac{h_{sc}}{h_p} - 1\right) = 1.12$

$k_{t,max} = 0.85$

$P_{Rd.kt} = k_{t,max} \cdot P_{Rd.s} = 69.4 kN$

Bending moment resistance - partial interaction

$n_{sc} = 13$ Number of shear connectors per half span

$N_{sc} = n_{sc} \cdot P_{Rd.kt} = 902.2 kN$ Compression force in slab

$N_{a.Rd} = A_a \cdot f_{yd} = 1388 kN$ Tension resistance of beam

$N_{c.Rd} = 0.85 \cdot b_{eff} \cdot h_c \cdot f_{cd} = 2940 kN$ Compression resistance of concrete

$N_{w.Rd} = f_{yd} \cdot t_w \cdot h_w = 833.7 kN$ Tension resistance of web

$N_{f.Rd} = \dfrac{N_{a.Rd} - N_{w.Rd}}{2} = 277.2 kN$ Tension resistance of flange

$\eta_l = \dfrac{N_{sc.Ed}}{\min(N_{c.Rd}, N_{a.Rd})} = 0.65$ Degree of shear connection

$x_c = h_c \dfrac{N_{sc.Ed}}{N_{c.Rd}} = 26.5 mm$ Height of concrete that contributes to the resistance

$z_{pl} = \dfrac{N_{a.Rd} - N_{sc.Ed}}{2 b_{fl} f_{yd}} + h_p + h_c = 125.7 mm$

$a = \dfrac{N_{a.Rd} - N_{sc.Ed}}{2 b_{fl} f_{yd}} = 5.7 mm > t_f = 9.8 mm \rightarrow$ Neutral axis in the flange

$M_{pl.c.Rd} = N_{sc.Ed} (h_a/2 + h_c + h_p - x_c/2) + \dfrac{N_{a.Rd} - N_{sc.Ed}}{2} (h_a - a) = 261.5 kNm$ Bending moment resistance

$\dfrac{M_{Ed}}{M_{pl.c.Rd}} = \dfrac{156.8}{261.5} = 0.6 \rightarrow Ok$

B.2.5. Shear resistance

$A_v = 23.5 cm^2$

$V_{pl.Rd} = A_v \cdot f_{yd} / \sqrt{3} = 482 kN$

$\dfrac{V_{Ed}}{V_{pl.Rd}} = \dfrac{78.4}{482} = 0.16 \rightarrow Ok$

B.2.6. Deflections

Full composite stiffness

$n = \dfrac{E_a}{E_c/2} = 12.727$

$I_c = \dfrac{h_c^3 b_{eff}}{12} = 3.6 \cdot 10^7 mm^4$

$I_{c.full} = I_a + \dfrac{I_c}{n} + \dfrac{A_a A_c}{n A_a + A_c} \left(\dfrac{h_c + 2 h_p + h_a}{2}\right)^2 = 1.636 \cdot 10^8 mm^4$

Delflection under selfweight: un-propped

$$\delta_g = \frac{5 \cdot g \cdot L^4}{384 E_a \cdot I_a} = 43.1 \text{mm}$$

Delflection under imposed load

$$\delta_c = \frac{5 \cdot q \cdot L^4}{384 E_a \cdot I_{c,full}} = 12.1 \text{mm}$$

$$\delta_{precam} = 30 \text{mm}$$

$$\delta_{tot} = \delta_g + \delta_c - \delta_{precam} = 25.2 \text{mm} < \frac{L}{250} = 32 \text{mm} \rightarrow \text{Ok}$$

B.3. Secondary beam

B.3.1. Load actions on beam

(a) Maximum bending moment

(b) Maximum shear force
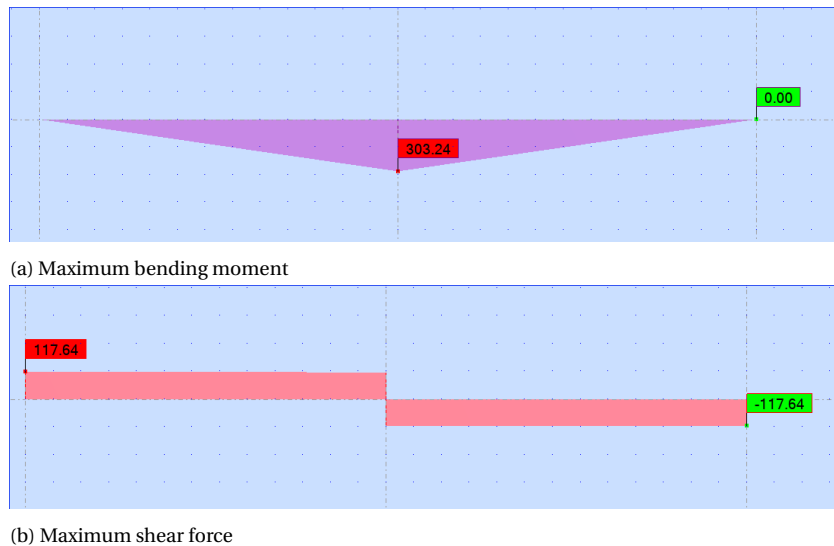
Figure B.4: Internal forces for 5.2m steel beam

Resulting design section forces

$$M_{Ed} = 303.24 \text{kNm}$$
$$V_{Ed} = 117.64 \text{kN}$$

B.3.2. General data

$$L = 5.2 \text{m}$$
$$f_{yd} = 355 \text{N}/\text{mm}^2$$
$$E_a = 210000 \text{N}/\text{mm}^2$$
$$G = 80769 \text{N}/\text{mm}^2$$

IPE400:

$b_{fl} = 180mm$

$h_a = 400mm$

$t_w = 8.6mm$

$t_f = 13.5mm$

$r = 21mm$

$h_w = h_a - (2t_f + 2r) = 331mm$

$b_f = \dfrac{b_{fl} - t_w}{2} - r = 71mm$

$A = 84.5 \cdot 10^2 mm^2$

$I_y = 23130 \cdot 10^4 mm^4$

$I_w = 492149 cm^6$

$I_t = 50.267 cm^4$

$I_z = 1317.8 cm^4$

$W_{pl.y} = 229 \cdot 10^3 mm^3$

$W_{el.y} = 146 \cdot 10^3 mm^3$

$M_{pl.y} = W_{pl.a} \cdot f_{yd} = 464kNm$

B.3.3. Cross section classification

Web (an internal part) in bending:

$\dfrac{c}{t} = \dfrac{331}{8.6} = 38.5 < 72 \cdot \varepsilon = 72 \cdot 0.81 = 58$

Flange (outstand part) in compression:

$\dfrac{c}{t} = \dfrac{71}{13.5} = 5.26 < 9 \cdot \varepsilon = 9 \cdot 0.81 = 7.3$

The cross section class is 1

B.3.4. Bending moment resistance

$M_{y.c.Rd} = W_{pl.y} \dfrac{f_{yd}}{1.0} = 464.34 kNm$

$\dfrac{M_{Ed}}{M_{y.c.Rd}} = \dfrac{303.24}{464.34} = 0.648 \rightarrow Ok$

B.3.5. Shear resistance

$A_v = 48.6 cm^2$

$V_{pl.Rd} = A_v \cdot f_{yd} / \sqrt{3} = 996.1 kN$

$\dfrac{V_{Ed}}{V_{pl.Rd}} = \dfrac{117.64}{996.1} = 0.11 \rightarrow Ok$

B.3.6. Lateral torsional buckling

$\dfrac{h}{t_w} = 46.5 < 75 \rightarrow k_{red} = 1.0$ Coefficient taking into account deformability of the section

$L_g = 5.2m$ Length of the beam between the points with torsional restraints

$L_{kip} = 2.6m$ Length of an equivalent laterally unrestrained beam

$C_1 = 1.75$ Coefficient taking into account the loading and boundary conditions

$C_2 = 0.0$ Coefficient taking into account position of the load

$S = \sqrt{\dfrac{E_a I_w}{G I_t}} = 1.595m$

Coefficient taking into account lateral restraints, support and boundary conditions, and type of loading:

$C = \dfrac{\pi C_1 L_g}{L_{kip}} \left[\dfrac{\pi C_2 S}{L_{kip}} + \sqrt{1 + \dfrac{\pi^2 S^2}{L_{kip}^2}(C_2^2 + 1)} \right] = 23.88$

$M_{cr} = k_{red} \dfrac{C}{L_g} \sqrt{E I_z G I_t} = 1628.3 kNm$

$\lambda_{LT} = \sqrt{\dfrac{W_{pl.y} f_{yd}}{M_{cr}}} = 0.549$ Beam slenderness

$\alpha_{LT} = 0.34$ Imperfection factor for buckling curve b

$\varphi_{LT} = 0.5 \left[1 + \alpha_{LT}(\lambda_{LT} - 0.2) + \lambda_{LT}^2 \right] = 0.71$

$\chi = \dfrac{1}{\varphi_{LT} + \sqrt{\varphi_{LT}^2 - \alpha_{LT}^2}} = 0.75$

$M_{b.Rd} = \chi W_{pl.y} \dfrac{f_{yd}}{1.0} = 384.15 kNm$ Lateral torsional buckling resistance

$\dfrac{M_{Ed}}{M_{b.Rd}} = \dfrac{303.24}{384.15} = 0.865 \rightarrow Ok$

B.3.7. Deflections

Delflection under selfweight:

$g = 0.9 kN/m$

$\delta_g = \dfrac{5 \cdot g \cdot L^4}{384 E_a \cdot I_a} = 0.2mm$

Delflection under imposed point load:

$P = 231 kN$

$\delta_P = \dfrac{P \cdot L^3}{48 E_a \cdot I_a} = 13.9mm$

$\delta_{tot} = \delta_g + \delta_P = 14.1mm < \dfrac{L}{250} = 20.8m \rightarrow Ok$

B.4. Rectangular hollow section column

B.4.1. Load actions on column

The normal force diagram is shown on a fig. B.5.
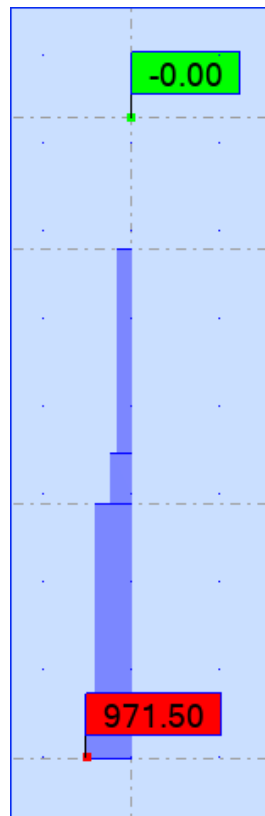
Figure B.5: Normal force diagram kN

Resulting design section forces

$N_{Ed} = 971.5$kN

B.4.2. General data

$L = 2900$m

$f_{yd} = 235$N/mm^2

$E_a = 210000$N/mm^2

RHS300x300x12

$b = 300$mm

$h = 300$mm

$t = 12$mm

$A = 143.75 \cdot 10^2$mm^2

$I = 19840$cm^4

B.4.3. Cross section classification

Web/Flange (an internal part) in compression:

$\dfrac{c}{t} = \dfrac{300 - 2 \cdot 12}{12} = 23 < 33 \cdot \varepsilon = 72 \cdot 1.0 = 33$

The cross section class is 1

B.4.4. Section axial resistance

$N_{c.Rd} = A \cdot f_{yd} = 3378 kN$

$\dfrac{N_{Ed}}{N_{c.Rd}} = \dfrac{971.5}{3378} = 0.3 \rightarrow Ok$

B.4.5. Buckling resistance

$N_{cr} = \dfrac{\pi^2 EI}{l_{cr}^2} = 48845.5 kN$

$\alpha = 0.13$

$\lambda = \sqrt{\dfrac{A \cdot f_{yd}}{N_{cr}}} = 0.26$

$\varphi = 0.53$

$\chi = 0.988$

$N_{b.Rd} = \chi \dfrac{N_{c.Rd}}{1.0} = 3034 kN$

$\dfrac{N_{Ed}}{N_{b.Rd}} = \dfrac{971.5}{3034} = 0.32 \rightarrow Ok$

B.5. Continuous ramp beam

B.5.1. Load actions on beam

UPE 400 steel section is chosen as a supporting beam for the ramp with steel grade S235. Ramp beam is an inclined continuous beam over four supports (5 spans). To determine design moment and shear, several load combinations have to be investigated. If all spans of the beam are loaded simultaneously with both permanent and live loads, the beam does not experience the largest shear or moment.

The largest moment in first span of the beam is achieved if first, third and fifth spans are loaded with live loads as shown on figure B.6.

The largest shear force and moment over second support are achieved when first, second and fourth spans are loaded with live load. The internal forces are displayed on a fig. B.7.

Therefore, the design moment is $M_{Ed} = 84 kNm$ and design shear force is $V_{Ed} = 55 kN$

B.5.2. General data

$f_{yd} = 235 N/mm^2$

B.5.3. Cross section classification
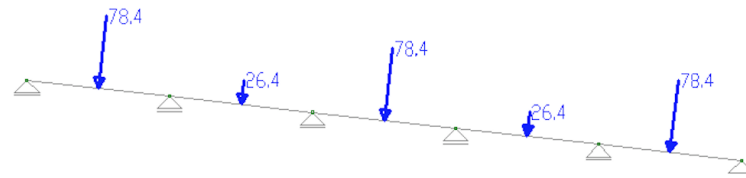
(a) Load case kN
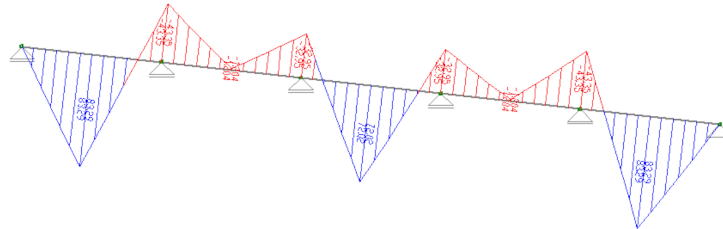
(b) Bending moment diagram kNm
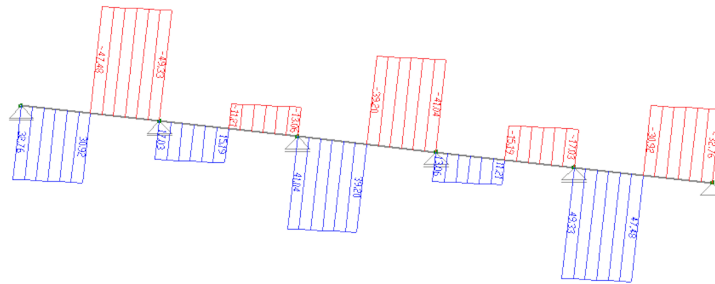
(c) Shear force diagram kN
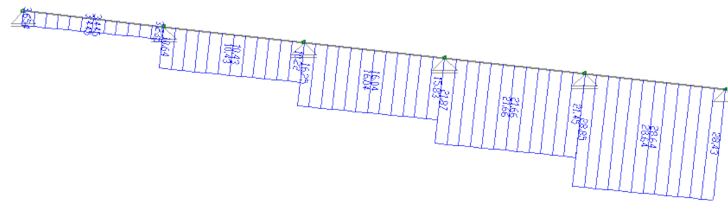
(d) Normal force diagram kN

Figure B.6: Internal forces for first load combination

Web (an internal part) in bending:

$$\frac{c}{t} = \frac{400 - 2 \cdot 18}{13.5} = 27 < 72 \cdot \varepsilon = 72$$

Flange (outstand part) in compression:

$$\frac{c}{t} = \frac{115}{18} = 6.4 < 9 \cdot \varepsilon = 9.0$$

The cross section class is 1
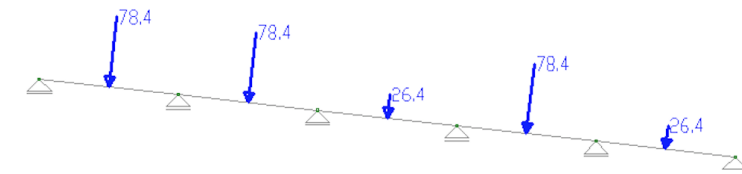
(a) Load case kN
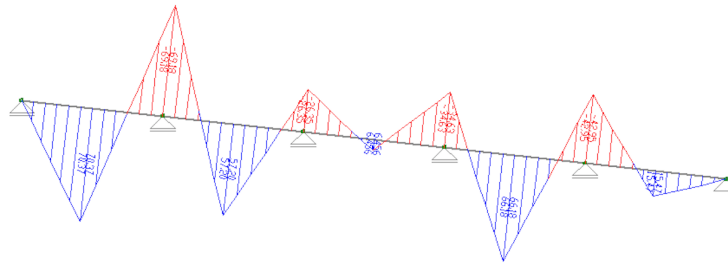
(b) Bending moment diagram kNm
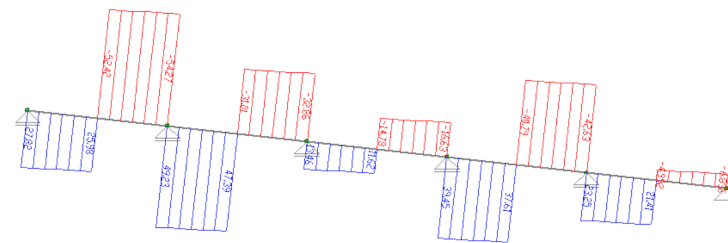
(c) Shear force diagram kN
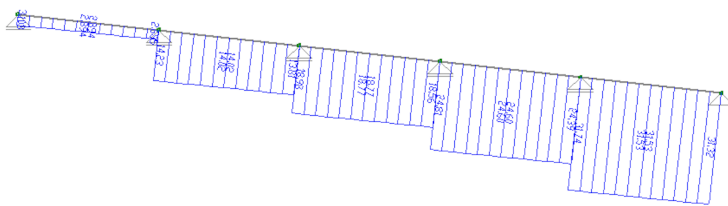
(d) Normal force diagram kN

Figure B.7: Internal forces for second load combination

B.5.4. Bending moment resistance

$$M_{y.c.Rd} = W_{pl.y} \frac{f_{yd}}{1.0} = 296 \text{kNm}$$

$$\frac{M_{Ed}}{M_{y.c.Rd}} = \frac{84}{296} = 0.3 \rightarrow \text{Ok}$$

B.5.5. Shear force resistance

$A_v = 56.2 \text{cm}^2$

$V_{pl.Rd} = A_v \cdot f_{yd} / \sqrt{3} = 762 \text{kN}$

$\dfrac{V_{Ed}}{V_{pl.Rd}} = \dfrac{55}{762} = 0.07 \rightarrow Ok$

In addition, the shear buckling resistance for webs without intermediate stiffeners should be checked according to section 5 of EN 1993-1-5, if:

$\dfrac{h_w}{t_w} > 72 \dfrac{\varepsilon}{\eta}$

η can be taken conservatively equal to 1.0

$\dfrac{h_w}{t_w} = \dfrac{400 - 2 \cdot 18}{13.5} = 27 > 72 \dfrac{\varepsilon}{\eta} = 72 \rightarrow$ Not necessary to verify shear buckling

Bending and Shear:

$V_{Ed} = 55 \text{kN} < 0.5 V_{Rd} = 0.5 \cdot 762 \text{kN} = 381 \text{kN} \rightarrow$ Not necessary to reduce the bending moment resistance

B.5.6. Lateral torsional buckling resistance

Here, the assumption is made that the normal forces resulting from the self-weight of the beam are small enough and can be ignored for the verification of the beam stability. The beam is laterally braced at the supports and laterally braced at the point of load application.

The formula used previously to calculate the elastic critical moment is only valid for symmetric cross sections, therefore the critical moment can not be correctly evaluated for UPE400 and more complex FE modeling is required for that purpose.

Based on an obtained eigenvalue from FE analysis, it can be derived that the elastic critical moment is equal to 434.3kNm. The initial imperfections and residual stresses were not accounted in the buckling analysis.

$\bar{\lambda}_{LT} = \sqrt{W_y \cdot f_y / M_{cr}} = X$

$\dfrac{h}{b} = \dfrac{400}{115} = 3.5 > 2 \rightarrow$ Buckling curve X $\rightarrow \alpha_{LT} = 0.49$

$\varphi_{LT} = 0.5 \left(1 + \alpha_{LT} \cdot [\bar{\lambda}_{LT} - 0.4] + 0.75 \cdot \bar{\lambda}_{LT}^2\right) = 0.55$

$\chi_{LT} = \dfrac{1}{\varphi_{LT} + \sqrt{\varphi_{LT}^2 - 0.75 \bar{\lambda}_{LT}^2}} = 1.01 > 1$

$M_{b,Rd} = \chi_{LT} W_y \dfrac{f_y}{\gamma_{M1}} = 1.0 \cdot 1260 \cdot 10^3 \text{mm}^3 \dfrac{235 \text{N/mm}^2}{1.1} = 269 \text{kNm}$

$M_{b,Rd} = \chi_{LT} W_y \dfrac{f_y}{\gamma_{M1}} = 1.0 \cdot 1260 \cdot 10^3 \text{mm}^3 \dfrac{235 \text{N/mm}^2}{1.1} = 269 \text{kNm}$

$\dfrac{M_{Ed}}{M_{b,Rd}} = \dfrac{226}{269} = 0.84 < 1$

B.6. Wind bracings

The car park is designed as an opened structure, however, for the calculation of the wind forces, the presence of the facade on all side of the car park was assumed.

Wind, which acts on the lower part of the car park is immediately transfered to the ground. The wind pressure acting on the middle and top part of the facades is accounted when calculation the design force in bracings. Wind brace is designed as a tension member only.

Design tension force in wind bracing is 100kN.

$$N_{c,Rd} = A \cdot f_y = 450kN$$

$$\frac{N_{Ed}}{N_{c,Rd}} = 0.22 < 1.0$$

B.7. IPE400 beam to IPE 450 beam fin plate connection

B.7.1. General data

Specific dimensions for fin plate connection are shown in fig. B.8.
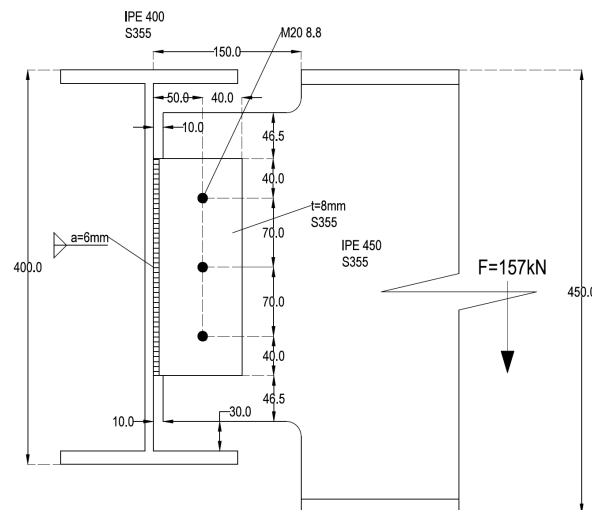
Figure B.8: IPE 400 beam to IPE 450 beam connection detail

$\gamma_{M0} = 1.0$

$\gamma_{M2} = 1.25$

M20 8.8 bolts

$A_s = 245mm^2$

$d = 20mm$

$d_0 = 22mm$

$f_{ub} = 800N/mm^2$

$f_{yb} = 640N/mm^2$

$n_1 = 3$

$n_2 = 1$

$\alpha_v = 0.6$

Plate

$t_p = 8mm$

$h_p = 220mm$

$f_{up} = 510N/mm^2$

$f_{yp} = 355N/mm^2$

$e_1 = 40mm$

$e_{1b} = 86.5mm$

$e_2 = 40mm$

$e_{2b} = 40mm$

$z = 50mm$

$p_1 = 70mm$

Beam IPE 450

$t_{bw} = 9.4mm$

$t_f = 14.6mm$

$h_w = 313mm$

$f_{ubw} = 355N/mm^2$

$f_{ybw} = 510N/mm^2$

B.7.2. Resistance to shear forces

Bolts in shear

$$F_{V.Rd} = \frac{\alpha_v f_{ub} A_s}{\gamma_{M2}} = 94.08kN$$

$$V_{Rd.1} = \frac{n_1 F_{V.Rd}}{\sqrt{1 + \frac{(6z)^2}{((n_1+1)p_1)^2}}} = 192.6kN$$

Fin plate in bearing

$\alpha = 1$

$$\beta = \frac{6z}{p_1 n_1 (n_1 + 1)} = 0.357$$

The vertical bearing resistance for a single bolt:

$$k_1 = \min(2.8\frac{e_2}{d_0} - 1.7; 2.5) = \min(2.8\frac{40}{22} - 1.7; 2.5) = \min(3.39; 2.5) = 2.5$$

$$\alpha_b = \min(\frac{e_1}{3d_0}; \frac{p_1}{3d_0} - \frac{1}{4}; \frac{f_{ub}}{f_{up}}; 1.0) = \min(\frac{40}{3\cdot22}; \frac{70}{3\cdot22} - \frac{1}{4}; \frac{800}{510}; 1.0) = \min(0.61; 0.81; 1.57; 1.0) = 0.61$$

$$F_{b,ver,Rd} = \frac{k_1 \, \alpha_b \, f_{up} \, d \, t_p}{\gamma_{M2}} = 98.9kN$$

The horizontal bearing resistance for a single bolt:

$$k_1 = \min(2.8\frac{e_1}{d_0} - 1.7; 1.4\frac{p_1}{d_0} - 1.7; 2.5) = \min(2.8\frac{40}{22} - 1.7; 1.4\frac{70}{22} - 1.7; 2.5) = \min(3.39; 2.75; 2.5) = 2.5$$

$$\alpha_b = \min(\frac{e_2}{3d_0}; \frac{f_{ub}}{f_{up}}; 1.0) = \min(\frac{40}{3\cdot22}; \frac{800}{510}; 1.0) = \min(0.61; 1.57; 1.0) = 0.61$$

$$F_{b,hor,Rd} = \frac{k_1 \, \alpha_b \, f_{up} \, d \, t_p}{\gamma_{M2}} = 98.9kN$$

$$V_{Rd.2} = \frac{1}{\sqrt{\left(\frac{\frac{1}{n}+\alpha}{F_{b,ver,Rd}}\right)^2 + \left(\frac{\beta}{F_{b,hor,Rd}}\right)^2}} = 202.5kN$$

Fin plate in shear: Gross section

$$V_{Rd.3} = \frac{h_p \, t_p}{1.27} \frac{f_{yp}}{\sqrt{3} \cdot \gamma_{M0}} = \frac{220 \cdot 8}{1.27} \frac{355}{\sqrt{3} \cdot 1.0} \cdot 10^{-3} = 284 \text{kN}$$

Fin plate in shear: Net section

$$A_{v,net} = t_p(h_p - n_1 d_0) = 8(220 - 3 \cdot 22) = 1232 \text{mm}^2$$

$$V_{Rd.4} = A_{v,net} \frac{f_{up}}{\sqrt{3} \, \gamma_{M2}} = 290 \text{kN}$$

Fin plate in shear: Shear block

$$A_{nt} = t_p(e_2 - d_0/2) = 8(40 - 22/2) = 232 \text{mm}^2$$

$$A_{nv} = t_p(h_p - e_1 - (n_1 - 0.5)d_0) = 8(220 - 40 - (3 - 0.5) \cdot 22) = 1000 \text{mm}^2$$

$$V_{Rd.5} = 0.5 \frac{f_{up} A_{nt}}{\gamma_{M2}} + \frac{1}{\sqrt{3}} f_{yp} \frac{A_{nv}}{\gamma_{M0}} = 252.3 \text{kN}$$

Fin plate in bending

$$h_p = 220 \text{mm} > 2.73z = 136.5 \text{mm} \rightarrow \text{Ok}$$

$$V_{Rd.6} = \infty$$

Buckling of fin plate

$$z = 50 \text{mm} < \frac{t_p}{0.15} = 53.3 \text{mm} \rightarrow \text{Ok}$$

$$V_{Rd.7} = \infty$$

Beam web in bearing

$$\alpha = 1$$

$$\beta = \frac{6z}{p_1 n_1 (n_1 + 1)} = 0.357$$

The vertical bearing resistance for a single bolt:

$$k_1 = \min(2.8 \frac{e_2 b}{d_0} - 1.7; 2.5) = \min(2.8 \frac{40}{22} - 1.7; 2.5) = \min(3.39; 2.5) = 2.5$$

$$\alpha_b = \min(\frac{p_1}{3d_0} - \frac{1}{4}; \frac{f_{ub}}{f_{ubw}}; 1.0) = \min(\frac{70}{3 \cdot 22} - \frac{1}{4}; \frac{800}{510}; 1.0) = \min(0.81; 1.57; 1.0) = 0.81$$

$$F_{b,ver,Rd} = \frac{k_1 \, \alpha_b \, f_{ubw} \, d \, t_{bw}}{\gamma_{M2}} = 155.4 \text{kN}$$

The horizontal bearing resistance for a single bolt:

$$k_1 = \min(1.4 \frac{p_1}{d_0} - 1.7; 2.5) = \min(1.4 \frac{70}{22} - 1.7; 2.5) = \min(2.75; 2.5) = 2.5$$

$$\alpha_b = \min(\frac{e_2 b}{3d_0}; \frac{f_{ub}}{f_{up}}; 1.0) = \min(\frac{40}{3 \cdot 22}; \frac{800}{510}; 1.0) = \min(0.61; 1.57; 1.0) = 0.61$$

$$F_{b,hor,Rd} = \frac{k_1 \, \alpha_b \, f_{ubw} \, d \, t_{bw}}{\gamma_{M2}} = 116 \text{kN}$$

$$V_{Rd.8} = \frac{1}{\sqrt{\left(\frac{\frac{1}{n} + \alpha}{F_{b,ver,Rd}}\right)^2 + \left(\frac{\beta}{F_{b,hor,Rd}}\right)^2}} = 266.9 \text{kN}$$

Beam web in shear: Gross section

$$A_{b,v} = t_b h_b = 9.4 \text{mm} \cdot 313 \text{mm} = 2942 \text{mm}^2$$

$$V_{Rd.9} = A_{b,v} \frac{f_{ybw}}{\gamma_{M0} \sqrt{3}} = 602 \text{kN}$$

Beam web in shear: Net section

$$A_{b,v,net} = A_{b,v} - n_1 d_0 t_{bw} = 2322 \text{mm}^2$$

$$V_{Rd.10} = A_{b,v,net} \frac{f_{ubw}}{\gamma_{M2} \sqrt{3}} = 546.9 \text{kN}$$

Beam web in shear: Shear block

$$A_{nt} = t_{bw}(e_{2b} - d_0/2) = 272.6mm^2$$

$$A_{nv} = t_{bw}(e_{1b} + (n_1 - 1)p_1 - (n_1 - 0.5)d_0) = 1612mm^2$$

$$V_{Rd.11} = 0.5\frac{f_{ubw}A_{nt}}{\gamma_{M2}} + \frac{1}{\sqrt{3}}f_{ybw}\frac{A_{nv}}{\gamma_{M0}} = 386kN$$

$$V_{Rd} = \min\{V_{Rd,i}\} = 192.6kN$$

$$\frac{V_{Ed}}{V_{Rd}} = \frac{157}{192.6} = 0.815 \rightarrow Ok$$

Elastic stresses in welds

$$\tau_{\parallel} = \frac{F_v}{2a \cdot l} = 59.5N/mm^2$$

$$\sigma_{\perp} = \tau_{\perp} = \frac{\sqrt{2}/2F_v z}{2al^2/6} = 57.3N/mm^2 < 0.9\frac{f_u}{\gamma_{M2}} = 367.2N/mm^2$$

$$\sqrt{\sigma_{\perp}^2 + 3(\tau_{\perp}^2 + \tau_{\parallel}^2)} = 60.3N/mm^2 < \frac{f_u}{\beta_w\gamma_{M2}} = 453N/mm^2$$

Requirement to avoid premature weld failure

$$a = 6mm > 0.55t_p = 4.4mm \rightarrow Ok$$

B.8. IPE400 beam to IPE240 beam fin plate connection

B.8.1. General data

Specific dimensions for fin plate connection are shown in fig. B.9.
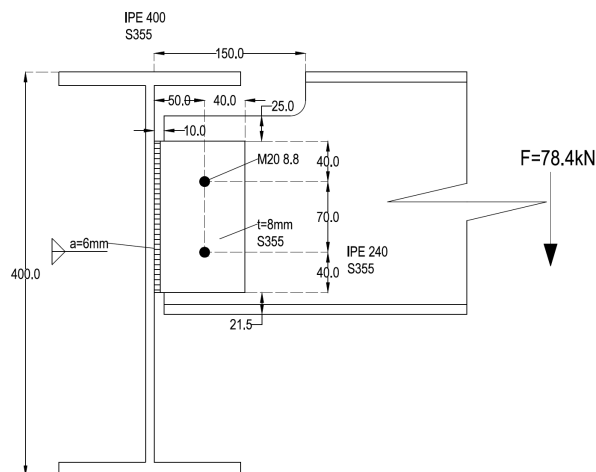
Figure B.9: IPE 400 beam to IPE 240 beam connection detail

M20 8.8 bolts

$A_s = 245mm^2$

$d = 20mm$

$d_0 = 22mm$

$f_{ub} = 800N/mm^2$

$f_{yb} = 640N/mm^2$

$n_1 = 2$

$n_2 = 1$

$\alpha_v = 0.6$

Plate

$t_p = 8mm$

$h_p = 150mm$

$f_{up} = 510N/mm^2$

$f_{yp} = 355N/mm^2$

$e_1 = 40mm$

$e_{1b} = 65mm$

$e_2 = 40mm$

$e_{2b} = 40mm$

$z = 50mm$

$p_1 = 70mm$

Beam IPE 240

$t_{bw} = 6.2mm$

$t_f = 9.8mm$

$f_{ubw} = 355N/mm^2$

$f_{ybw} = 510N/mm^2$

B.8.2. Resistance to shear forces

Bolts in shear

$$F_{V.Rd} = \frac{\alpha_v f_{ub} A_s}{\gamma_{M2}} = 94.08kN$$

$$V_{Rd.1} = \frac{n_1 F_{V.Rd}}{\sqrt{1 + \frac{(6z)^2}{((n_1+1)p_1)^2}}} = 107.9kN$$

Fin plate in bearing

$\alpha = 0$

$$\beta = \frac{6z}{p_1 n_1 (n_1 + 1)} = 0.714$$

The vertical bearing resistance for a single bolt:

$$k_1 = \min(2.8\frac{e_2}{d_0} - 1.7; 2.5) = 2.5$$

$$\alpha_b = \min(\frac{e_1}{3d_0}; \frac{p_1}{3d_0} - \frac{1}{4}; \frac{f_{ub}}{f_{up}}; 1.0) = 0.61$$

$$F_{b,ver,Rd} = \frac{k_1 \, \alpha_b \, f_{up} \, d \, t_p}{\gamma_{M2}} = 98.9kN$$

The horizontal bearing resistance for a single bolt:

$$k_1 = \min{(2.8\frac{e_1}{d_0} - 1.7; 1.4\frac{p_1}{d_0} - 1.7; 2.5)} = 2.5$$

$$\alpha_b = \min{(\frac{e_2}{3d_0}; \frac{f_{ub}}{f_{up}}; 1.0)} = 0.61$$

$$F_{b,hor,Rd} = \frac{k_1 \, \alpha_b \, f_{up} \, d \, t_p}{\gamma_{M2}} = 98.9 \text{kN}$$

$$V_{Rd.2} = \frac{1}{\sqrt{(\frac{\frac{1}{n}+\alpha}{F_{b,ver,Rd}})^2 + (\frac{\beta}{F_{b,hor,Rd}})^2}} = 113.4 \text{kN}$$

Fin plate in shear: Gross section

$$V_{Rd.3} = \frac{h_p \, t_p}{1.27} \frac{f_{yp}}{\sqrt{3} \cdot \gamma_{M0}} = \frac{150 \cdot 8}{1.27} \frac{355}{\sqrt{3} \cdot 1.0} \cdot 10^{-3} = 193.6 \text{kN}$$

Fin plate in shear: Net section

$$A_{v,net} = t_p(h_p - n_1 d_0) = 8(150 - 2 \cdot 22) = 848 \text{mm}^2$$

$$V_{Rd.4} = A_{v,net} \frac{f_{up}}{\sqrt{3} \, \gamma_{M2}} = 199.8 \text{kN}$$

Fin plate in shear: Shear block

$$A_{nt} = t_p(e_2 - d_0/2) = 8(40 - 22/2) = 232 \text{mm}^2$$

$$A_{nv} = t_p(h_p - e_1 - (n_1 - 0.5)d_0) = 8(150 - 40 - (2 - 0.5) \cdot 22) = 616 \text{mm}^2$$

$$V_{Rd.5} = 0.5 \frac{f_{up}A_{nt}}{\gamma_{M2}} + \frac{1}{\sqrt{3}} f_{yp} \frac{A_{nv}}{\gamma_{M0}} = 173.6 \text{kN}$$

Fin plate in bending

$$h_p = 150 \text{mm} > 2.73 z = 136.5 \text{mm} \rightarrow \text{Ok}$$

$$V_{Rd.6} = \infty$$

Buckling of fin plate

$$z = 50 \text{mm} < \frac{t_p}{0.15} = 53.3 \text{mm} \rightarrow \text{Ok}$$

$$V_{Rd.7} = \infty$$

Beam web in bearing

$$\alpha = 0$$

$$\beta = \frac{6z}{p_1 n_1 (n_1 + 1)} = 0.714$$

The vertical bearing resistance for a single bolt:

$$k_1 = \min{(2.8\frac{e_{2b}}{d_0} - 1.7; 2.5)} = 2.5$$

$$\alpha_b = \min{(\frac{p_1}{3d_0} - \frac{1}{4}; \frac{f_{ub}}{f_{ubw}}; 1.0)} = 0.81$$

$$F_{b,ver,Rd} = \frac{k_1 \, \alpha_b \, f_{ubw} \, d \, t_{bw}}{\gamma_{M2}} = 102.5 \text{kN}$$

The horizontal bearing resistance for a single bolt:

$$k_1 = \min\,(1.4\frac{p_1}{d_0} - 1.7; 2.5) = 2.5$$

$$\alpha_b = \min\,(\frac{e_2 b}{3 d_0}; \frac{f_{ub}}{f_{up}}; 1.0) = 0.61$$

$$F_{b,hor,Rd} = \frac{k_1\,\alpha_b\,f_{ubw}\,d\,t_{bw}}{\gamma_{M2}} = 76.7\text{kN}$$

$$V_{Rd.8} = \frac{1}{\sqrt{(\frac{\frac{1}{n}+\alpha}{F_{b,ver,Rd}})^2 + (\frac{\beta}{F_{b,hor,Rd}})^2}} = 95\text{kN}$$

Beam web in shear: Gross section

$$A_{b,v} = t_b h_b = 6.2\text{mm} \cdot 186.7\text{mm} = 1158\text{mm}^2$$

$$V_{Rd.9} = A_{b,v}\frac{f_{ybw}}{\gamma_{M0}\sqrt{3}} = 237.2\text{kN}$$

Beam web in shear: Net section

$$A_{b,v,net} = A_{b,v} - n_1\,d_0\,t_{bw} = 884.74\text{mm}^2$$

$$V_{Rd.10} = A_{b,v,net}\frac{f_{ubw}}{\gamma_{M2}\sqrt{3}} = 208.4\text{kN}$$

Beam web in shear: Shear block

$$A_{nt} = t_{bw}(e_{2b} - d_0/2) = 179.8\text{mm}^2$$

$$A_{nv} = t_{bw}(e_{1b} + (n_1 - 1)p_1 - (n_1 - 0.5)d_0) = 632.4\text{mm}^2$$

$$V_{Rd.11} = 0.5\frac{f_{ubw}A_{nt}}{\gamma_{M2}} + \frac{1}{\sqrt{3}}f_{ybw}\frac{A_{nv}}{\gamma_{M0}} = 166.3\text{kN}$$

$$V_{Rd} = \min\{V_{Rd,i}\} = 95\text{kN}$$

$$\frac{V_{Ed}}{V_{Rd}} = \frac{78.4}{95} = 0.825 \rightarrow Ok$$

Elastic stresses in welds

$$\tau_\parallel = \frac{F_v}{2a \cdot l} = 43.6\text{N/mm}^2$$

$$\sigma_\perp = \tau_\perp = \frac{\sqrt{2}/2 F_v z}{2al^2/6} = 61.6\text{N/mm}^2 < 0.9\frac{f_u}{\gamma_{M2}} = 367.2\text{N/mm}^2$$

$$\sqrt{\sigma_\perp^2 + 3(\tau_\perp^2 + \tau_\parallel^2)} = 144.5\text{N/mm}^2 < \frac{f_u}{\beta_w \gamma_{M2}} = 453\text{N/mm}^2$$

Requirement to avoid premature weld failure

$$a = 6\text{mm} > 0.55 t_p = 4.4\text{mm} \rightarrow Ok$$

C

Risk assessment of the lab testing

General Risk Assessment

TUDelft

Date	Assessed by:	Validated by:	Location	Review date:
24-08-18	A. Gritsenko	Ir. M.P. Nijgh	Stevin II Laboratory	20-08-18

Task: REDUCE 8m composite beam test

Determine Priority for Assessment

LIKELIHOOD X SEVERITY			CONSEQUENCE					
1. Extremely Unlikely	1. Minor injury with no lost time		LIKELIHOOD	1.Minor	2.Up to 3 days	3. 3 days	4. Major	5. Death
2. Unlikely	2. Up to 3 days lost		1. Ext.Unlikely	1	2	3	4	5
3. Likely	3. Reportable. Over 3 days lost		2.Unlikely	2	4	6	8	10
4. Very Likely	4. Major injury		3. Likely	3	6	9	12	15
5. Almost Certain	5. Death		4.Very likely	4	8	12	16	20
			5. Almost certain	5	10	15	20	25
				SIGNIFICANT		HIGHEST PRIORITY		
				NEEDS NO FURTHER ASSESSMENT				

What is the hazard?	Who might be harmed?	How might people be harmed?	Existing risk control measures	Risk rating L	C	R	Additional controls	New risk rating (Residual) L	C	R	Action/monitored by whom?	Action/monitored when?
During installation or preparation process composite beam might fall from the supporting structure	Technicians, academics, researchers	Specimen falls from the supports/crane causing impact injury	Wearing of safety shoes, wearing of helmets is mandatory	2	5	10	Plates will be welded at the supporting beams to limit the movement of the composite beam in longitudinal direction\n\nNo person is allowed to be present in the vicinity of the test setup during installation or transportation	1	5	5	Lab supervisor	During installation
During installation or preparation process composite beam might tilt on the side and fall due to technicians working on top of the slab.	Technicians, academics, researchers	Specimen falls from the supports causing impact injury	Wearing of safety shoes, wearing of helmets is mandatory	2	5	10	Additional supports will be introduced at the 4 corners of the concrete slab to ensure the stability\n\nAlong the beam, on both sides the triangular (cantilever) wooden supporting structure will be installed, which will aid transferring the loads from the concrete directly to the beam	1	5	5	Lab supervisor	During installation

Hazard	Who	Consequence	Control	L	S	R	Further control	L	S	R	Responsible	When
							and ensure the stability No person is allowed to be present in the vicinity of the test setup during installation or transportation					
Bolts might fall unexpectedly during installation or transportation	Technicians, academics, researchers	Bolts fall causing an impact injury	Wearing of safety shoes, wearing of helmets is mandatory	3	2	6	No person is allowed to be present in the vicinity of the test setup during installation	3	1	3	Lab supervisor	During installation
Resin might get into contact with skin, eyes during injection of the bolts	Technicians	Resin may cause skin irritation, irritation of airways or allergy reaction due to the toxic fumes, blindness	Wearing of safety coat and gloves is mandatory	3	2	6	Wearing of the mask, glasses	3	1	3	Lab supervisor	During installation
During longitudinal cutting of the concrete slab, the slab might fall suddenly from the supporting structure	Technicians, academics, researchers	Sudden failure/movement of the concrete slab can cause an impact injury of person on top or underneath the setup The loud noise coming from the sawing might be damaging for the ears.	Wearing of safety shoes, ear protection, wearing of helmets is mandatory	2	5	10	Person, who will be involved into the cutting procedure has to be secured with the rope/wire system 4 props on both sides of the slab are placed, which are transferring the loads immediately to the ground. No person is allowed to be near specimen during cutting	1	5	5	Lab supervisor	During installation
During uplifting procedure of the half slab, since there is no mechanical connections between the supporting beam and the slab, the slab might slide off the beam	Technicians, academics, researchers	Sudden movement of the concrete slab from the supporting beam can cause an impact injury	Wearing of safety shoes and helmets is mandatory	2	5	10	The supporting beam was installed with additional plates to ensure the stability for the slab and the hoisting of the supporting beam was conducted using 4 point. The temporary props remain under the slabs the whole time. No person is allowed to be near specimen during uplift	1	5	5	Lab supervisor	During installation
When the slabs are cut, lifted, placed back and connected to beam with the bolts the half slabs are not interconnected by reinforcement and therefore the halves of the slabs can fall down under their own weight	Technicians, academics, researchers	During removing of temporary props the halves of the slabs might fall down and cause an impact injury	Wearing of safety shoes and helmets is mandatory	2	5	10	Along the beam, on both sides the triangular (cantilever) wooden supporting structure will be installed, which will aid transferring the loads from the concrete directly to the beam and ensure the stability Additional supports will be introduced at the 4 corners of the concrete slab to ensure the stability No person is allowed to be present in the vicinity of the test setup during installation or transportation	1	5	5	Lab supervisor	During installation
Two point loads are applied to beam. Beam may fail suddenly	Technicians, academics, researchers	Sudden failure of the specimen may cause parts of the structure to fall on the ground.	Use position control so that full load would not apply to specimen at failure	2	4	8	No person is allowed to be near specimen during loading The props are placed on both sides of the slab, but not fully in contact.	1	4	4	Project Supervisor	During testing

Bibliography

[1] https://www.steelconstruction.info/Composite_construction. [Online; accessed 11-08-2018].

[2] British Standards Institution (1990). Bs 5950: Structural use of steelwork in buildings, part 3 design in composite construction. section 3.1 code of practice for design of simple and continuous composite beams, 1990 including amendments 2010.

[3] NEN-EN 1990. Nationale bijlage bij nen-en: Eurocode: Grondslagen van het constructief ontwerp.

[4] EN 1991-1-1. Eurocode 1: Actions on structures - part 1-1: General actions - densities, self-weight, imposed loads for buildings.

[5] NEN-EN 1991-1-3. Eurocode 1: Belastingen op constructies - deel 1-3: Algemene belastingen - sneeuw-belasting.

[6] EN 1994-1-1. Eurocode 4: Design of composite steel and concrete structures - part 1-1: General rules and rules for buildings.

[7] NEN-EN 1994-1-1+C1/NB. National annex to nen-en 1994-1-1+c1 eurocode 4 design of composite steel and concrete structures – part 1-1: General rules and rules for buildings.

[8] Olugbenga O. Akinade, Lukumon O. Oyedele, Kamil Omoteso, Saheed O. Ajayi, Muhammad Bilal, Hakeem A. Owolabi, Hafiz A. Alaka, Lara Ayris, and John Henry Looney. Bim-based deconstruction tool: Towards essential functionalities. *International Journal of Sustainable Built Environment*, 6 (1):260 – 271, 2017. ISSN 2212-6090. doi: https://doi.org/10.1016/j.ijsbe.2017.01.002. URL http://www.sciencedirect.com/science/article/pii/S2212609016301030.

[9] Abdolreza Ataei, Mark A. Bradford, and Hamid Valipour. Sustainable design of deconstructable steel-concrete composite structures. *Procedia Engineering*, 145:1153 – 1160, 2016. ISSN 1877-7058. doi: https://doi.org/10.1016/j.proeng.2016.04.149. URL http://www.sciencedirect.com/science/article/pii/S1877705816301564. ICSDEC 2016 – Integrating Data Science, Construction and Sustainability.

[10] Dallam. High strength bolt shear connectors- pushout tests. *ACI*, 65(9):767–9, 1968.

[11] Chuck Eastman, Paul Teicholz, Rafael Sacks, and Kathleen Liston. *BIM Handbook: A Guide to Building Information Modeling for Owners, Managers, Designers, Engineers and Contractors*. Wiley Publishing, 2008. ISBN 0470185287, 9780470185285.

[12] International Organization for Standardization. Building information models - information delivery manual - part 1: Methodology and format.

[13] Ioan Andrei Gîrbacea. State of art in composite beams. partial interaction and its benefits, 2017.

[14] Ioan Andrei Gîrbacea. Assessment of demountable steel concrete composite flooring systems. Master's thesis, Technical university of Delft, Delft, 2018.

[15] Ulf Arne Girhammar. Exact static analysis of partially composite beams and beam-columns. *International Journal of Mechanical Sciences*, 49:239–255, 2007.

[16] Ulf Arne Girhammar. A simplified analysis method for composite beams with interlayer slip. *International Journal of Mechanical Sciences*, 51:515–530, 2009.

[17] G. Hanswille, M. Porsch, and C. Ustundag. Resistance of headed studs subjected to fatigue loading. part i: Experimental study. *Journal of Constructional Steel Research*, 63(4):475–484, 2007. doi: 10.1016/j.jcsr.2006.06.035. URL `https://www.scopus.com/inward/record.uri? eid=2-s2.0-33751424836&doi=10.1016%2fj.jcsr.2006.06.035&partnerID=40&md5= 424912c9c06827a27f71459b4b9ba7e6`. cited By 58.

[18] G. Hanswille, M. Porsch, and C. Ustundag. Resistance of headed studs subjected to fatigue loading part ii: Analytical study. *Journal of Constructional Steel Research*, 63(4):485–493, 2007. doi: 10.1016/j.jcsr.2006.06.036. URL `https://www.scopus.com/inward/record.uri? eid=2-s2.0-33751435060&doi=10.1016%2fj.jcsr.2006.06.036&partnerID=40&md5= 371f628f5cc48d13c002c7690e9bda66`. cited By 38.

[19] N. A. Jasim. Computation of deflections for continuous composite beams with partial interaction. *Proceedings of the Institution of Civil Engineers, Structures and Buildings*, 122:347–54, 1997.

[20] A Kozma, C Odenbreit, M Volker Braun, M Veljkovic, and M. Nijgh. Push-out tests on demountable shear connectors of steel-concrete composite structures, 2018.

[21] Dennis Lam. Capacities of headed stud shear connectors in composite steel beams with precast hollowcore slabs. *Journal of Constructional Steel Research*, 63(9):1160 – 1174, 2007. ISSN 0143-974X. doi: https://doi.org/10.1016/j.jcsr.2006.11.012. URL `http://www.sciencedirect.com/science/article/pii/S0143974X06002471`.

[22] Matti V. Leskelä. *Shear Connections in Composite Flexural Members of Steel and Concrete*. ECCS, 2017. ISBN 978-92-9147-137-9.

[23] Marshall, Nelson, and Banerjee. Experimental study of the use of high strength friction grip bolts as shear connectors in composite beams. *Struct Eng*, 49(2):171–8, 1971.

[24] Mirza, Uy, and Patel. Behaviour and strength of shear connectors utilising blind bolting. *Steel and Composite structures*.

[25] Muiris C. Moynihan and Julian M. Allwood. Viability and performance of demountable composite connectors. *Journal of Constructional Steel Research*, 99:47 – 56, 2014. ISSN 0143-974X. doi: https://doi.org/10.1016/j.jcsr.2014.03.008. URL `http://www.sciencedirect.com/science/article/pii/S0143974X14000807`.

[26] K. S. Naraine. Slip and uplift effects in composite beams, 1984.

[27] N.M. Newmark, C.P. Siess, and Viest I.M. Tests and analysis of composite beams with incomplete interaction. *Proc. Soc. Experimental Stress Analysis*, 9(1):75–92, 1951.

[28] Martin Nijgh. New materials for injected bolted connections. Master's thesis, TU Delft, 2017.

[29] Martin Nijgh, Mareike von Arnim, Marko Pavlović, and Milan Veljković. Preliminary assessment of a composite flooring system for reuse, 2017.

[30] Martin Nijgh, Ioan Andrei Gîrbacea, and Milan Veljkovic. Elastic behaviour of a reusable tapered composite beam. engineering structures (under review), 2018.

[31] Martin Nijgh, H Xin, and Milan Veljkovic. Non-linear hybrid homogenization method for steel-reinforced resin, 2018.

[32] Deric John. Oehlers and Mark A. Bradford. *Composite steel and concrete structural members : fundamental behaviour / by Deric J. Oehlers and Mark A. Bradford*. Pergamon Kidlington, Oxford, U.K. ; Tarrytown, N.Y, 1st ed. edition, 1995. ISBN 0080419194.

[33] Manual of Steel Construction. American institute of steel construction (2010), aisc 360-10, specification for structural steel buildings.

[34] J.G. Ollgaard and J.W. Slutter, R.G.and Fisher. Shear strength of stud connectors in lightweight and normal-weight concrete, 1971.

[35] V.A. Oven, I.W. Burger, R.J. Plankt, and A.A. Abdul Wali. An analytical model for the analysis of composite beams with partial interaction. *Computers Structures*, 62(3):493–504, 1997.

[36] Sameera Wijesiri Pathirana, Brian Uy, Olivia Mirza, and Xinqun Zhu. Flexural behaviour of composite steel–concrete beams utilising blind bolt shear connectors. *Engineering Structures*, 114:181 – 194, 2016. ISSN 0141-0296. doi: https://doi.org/10.1016/j.engstruct.2016.01.057. URL `http://www.sciencedirect.com/science/article/pii/S014102961600081X`.

[37] Marko Pavlović. Resistance of bolted shear connectors in prefabricated steel-concrete composite decks.

[38] Marko Pavlović and Milan Veljković. 08.08: Prefabricated demountable concrete and frp decks in composite structures. *ce/papers*, 1(2-3):1889–1898. doi: 10.1002/cepa.233. URL `https://onlinelibrary.wiley.com/doi/abs/10.1002/cepa.233`.

[39] G. Ranzi, F. Gara, and P. Ansourian. General method of analysis for composite beams with longitudinal and transverse partial interaction. *Computers Structures*, 84, 2006.

[40] Naveed Rehman, Dennis Lam, Xianghe Dai, and Ashraf Ashour. Testing of composite beam with demountable shear connectors. *Proceedings of the Institution of Civil Engineers - Structures and Buildings*, 171(1):3–16, 2018. doi: 10.1680/jstbu.16.00172. URL `https://doi.org/10.1680/jstbu.16.00172`.

[41] Dassault Systemes. Abaqus user manual, version 6.14, 2014.

[42] University of Bradford University of Luxembourg. Reduce deliverable d5.1 push-tests, 2018.

[43] Mareike von Arnim. Demountable composite steel-concrete flooring system for reuse. Master's thesis, Karlsruhe Institute of Technology, Karlsruhe, 2017.

[44] W. Xue, M. Ding, H. Wang, and Z. Luo. Static behavior and theoretical model of stud shear connectors. *Journal of Bridge Engineering*, 13(6):623–634, 2008. doi: 10.1061/(ASCE)1084-0702(2008)13: 6(623).   URL `https://www.scopus.com/inward/record.uri?eid=2-s2.0-54249170070&doi=10.1061%2f%28ASCE%291084-0702%282008%2913%3a6%28623%29&partnerID=40&md5=66e165ddaf12315589bfa2a1d7541d70`. cited By 42.

[45] Fei Yang, Yuqing Liu, Zhibo Jiang, and Haohui Xin. Shear performance of a novel demountable steel-concrete bolted connector under static push-out tests. *Engineering Structures*, 160:133 – 146, 2018. ISSN 0141-0296. doi: https://doi.org/10.1016/j.engstruct.2018.01.005. URL `http://www.sciencedirect.com/science/article/pii/S0141029617325762`.